Nitrogen Functionalization of CNFs and Application in Heterogeneous Catalysis

vorgelegt von
Diplom- Chemikerin

Rosa Arrigo
Messina

Von der Fakultät II - Mathematik und Naturwissenschaften
der Technischen Universität Berlin
zur Erlangung des akademischen Grades
Doktor der Naturwissenschaften
Dr.rer.nat.

genehmigte Dissertation

Promotionsausschuss:

Vorsitzender: Prof. Dr. rer. nat. T. Ressler
Berichter/Gutachter: Prof. Dr. R. Schlögl
Berichter/Gutachter: Prof. Dr. R. Schomäcker
Berichter/Gutachter: Prof. Dr. G. Centi

Tag der wissenschaftlichen Aussprache: 28. August 2009

Berlin 2009

D 83

Al mio piccolo, grande
Walter

Stickstoff-Funktionalisierung von CNFs und seine Anwendung in der heterogenen Katalyse

Rosa Arrigo

Die Notwendigkeit der Entwicklung selektiver und aktiver heterogenen Katalysatoren hat zur Suche nach neuen synthetischen Strategien geführt, um die sehr spezifische chemische Struktur von Bio-Systemen nachzuahmen. Durch ihre unvergleichliche Eignung für chemische Funktionalisierung, stellen nanostrukturierte Kohlenstoffe ein ideales organisches Substrat dar, dessen Oberflächenchemie entsprechend der spezifischen Bedürfnisse angepasst werden kann.

In dieser Arbeit wurde Stickstoff Funktionalisierung auf der Oberfläche von CNFs über eine Aminierungsreaktion durchgeführt um N-Komplexe an offenen Stellen und / oder Kanten der graphene Schichten einzubringen, die sich an die Struktur des Stickstoff-Einheiten wie sie in biologischen Systemen angetroffen werden, angleichen könnten.

Im Idealfall kann die hohe koordinative Fähigkeit der Porphyrin-Strukturen zur Herstellung von hoch dispergierten unterstützten Metall-Katalysatoren genutzt werden. Der Effekt der Temperaturbehandlung auf die Verteilung der O-und N-Funktionalitäten ist untersucht worden.

Durch TP-XPS wurde gezeigt, dass die Menge von O-und N-Spezies temperaturabhängig ist. Insbesondere bei hohen Temperaturen ist Stickstoff als Ersatzposition der Grafit-Struktur, wie heterozyklische Ringe, stabilisiert.

Funktionalisierungsbehandlung durchgeführt bei niedriger Temperatur erzeugt Stickstoff Spezies mit basischem Charakter die mit sauren O-Funktionalisierungen koexistieren. In diesem Zustand wird eine bi-funktionelle Säure-Basis Oberfläche mit hohem hydrophilen Charakter erzeugt. Die funktionalisierten CNFs wurden als Support für die Pd-Nanopartikel verwendet. Cs-korrigierte HRTEM Untersuchungen haben die Rolle der Oberflächenchemie der CNFs bei der Immobilisierung von Metall-Nanopartikeln aufgezeigt.

Das Vorhandensein von Stickstoff als hetero-zyklische Ringe auf der Oberfläche von NCNF673K und NCNF873K produzieren eine Ladungslokalisierung auf der Grafit-Oberfläche, die sich als Lewis basische koordinative Stellen für Metall-Nanopartikel verhält.

Makroskopisch betrachtet verringert sich die Metall-/ Support Schnittstellen Energie wobei Metallbenetzung begünstigt ist. Die Metall-Support Wechselwirkungen produzieren Reorganisation von Metallatomen an der Oberfläche der Nanopartikel, mit Änderungen der Gitterkonstanten und der Bildung von "raft" Metall-Partikeln mit niedrigem Koordinationsstellen und Metall-Atom Versetzungen wie in den HRTEM Bildern gezeigt wird.

Die bessere katalytische Leistung die für diese Katalysatoren (Pd/NCNF673K und Pd/NCNF873K) in der flüssigen Oxidationsphase von Benzylalkohol zu Benzaldehyd beobachtet wird, lässt sich durch die verbesserte reduktive Sauerstoff Adsorption erklären. Diese Hypothese wird durch die ähnlichen Tendenzen in der katalytischen Leistung der Katalysatoren in der Synthese von H_2O_2 untermauert.

Da die Reaktion durch die Bildung von Superoxid-Arten stattfindet, wurde die verbesserte reduktive O_2 Adsorptionsfähigkeit der Katalysatoren, die einen höheren Grad der Benetzung der Pd-Nanopartikel auf der Kohlenstoff-Oberfläche zeigen, bewiesen.

Dies wird durch das Einfügen von Stickstoff-Hetero-Zyklus Ringen an der Oberfläche der CNFs realisiert was dazu führt, dass es zu einer Ladungslokalisierung an den Grafitdomänen kommt, welche die Metall-Nanostrukturen auf der Oberfläche der Nanopartikel modifizieren.
Zusammenfassend lässt sich sagen, dass ein wertvoller Weg zur Synthese von N-funktionalisierten CNFs in dieser Arbeit beschrieben und diskutiert wurde. Dieses Funktionalisierungsverfahren erlaubt es, die chemischen Oberflächeneigenschaften von CNFs zu ändern. Die detaillierte Charakterisierung, die in dieser Arbeit durchgeführt wurde hat dazu geführt, eine Verbindung zwischen der chemischen Eigenschaften der Oberfläche durch die Funktionalisierung und die Möglichkeiten dieser Materialien in der Katalyse herzustellen.

Nitrogen Functionalization of CNFs and Application in Heterogeneous Catalysis

Rosa Arrigo

The need to develop highly selective and active heterogeneous catalysts has lead to search for new synthetic strategies which mimic the highly specific chemical structure encountered in bio-systems. For instance, the high coordinative capability of porphyrin-like structures can be exploited in the preparation of highly dispersed supported metal catalysts. Due to their incomparable feasibility towards chemical functionalization, nanostructured carbons represent an ideal organic substrate whose surface chemistry can be tailored according to specific needs. In this work, nitrogen functionalization of the CNFs surface was carried out via amination reaction with the purpose of introducing N-complexes at vacancies and/or edges of the graphene layers which might resembles the structure of the nitrogen units encountered in biological systems. Successively, the functionalized CNFs were used as supports for Pd nanoparticles. The effect of the treatment temperature on the distribution of O and N functionalities was investigated. It was found that the acidic oxygen species on the CNFs surface are necessary to achieve high nitrogen concentrations and thus they are involved in the nitrogen insertion pathway. TP-XPS investigations show that the population of O and N species is temperature dependent. In particular, functionalization treatment carried out at lower temperature, introduces nitrogen moieties with basic character, coexisting with acidic O functionalities. At this condition a bi-functional acidic and basic surface is obtained showing high hydrophilic character. At high temperature, most of the oxygenated acid species are decomposed, while nitrogen is stabilised in substitutional position of the graphitic structure, as heterocyclic-like moieties. Cs-corrected HRTEM investigations have highlighted the role of the CNFs surface chemistry in the immobilization of metal nanoparticles.

The presence of nitrogen as hetero-cyclic moieties on the surface of NCNF673K and NCNF873K produce charge localization on the graphitic surface which act as Lewis basic coordinative sites for metal nanoparticles. The metal-support interactions produce metal atoms reorganization at the surface of the nanoparticles and formation of “raft” metal particles with low coordinated site as shown in the HRTEM images. Macroscopically, the metal/support interface free energy decreases favoring metal wetting as observed in the HRTEM investigation. The better catalytic performance observed for these catalysts (Pd/NCNF673K and Pd/NCNF873K) in the liquid phase oxidation of benzyl alcohol to benzaldehyde is a consequence of the increased amount of highly active sites induced by the interaction with the support.

In conclusion, a valuable route to the synthesis of N-functionalized CNFs was described and discussed in this work. This functionalization procedure allows tailoring the surface chemical properties of the CNFs. The detailed characterization presented in this work has lead to establish links between the chemical nature of the surface moieties introduced by the functionalization treatments and the potentiality of those materials in catalysis.

Index

List of Acronyms

AC	*Activated Carbon*
NC	*Nanocarbon*
N-NC	*Nitrogen-containing nanocarbon*
CCVD	*Catalytic Chemical Vapor Deposition*
TP-XPS	*Temperature programmed X-ray photoelectron spectroscopy*
MS	*Mass spectrometer a/o mass spectrum*
WMSI	*Weak metal support interaction*
CNFs	*Carbon nanofibers*
CNTs	*Carbon nanotubes*
TPD	*Temperature programmed desorption spectroscopy*
SWCNTs	*Single-wall carbon nanotubes*
MWCNTs	*Multi-wall carbon nanotubes*
DOS	*Density of states*
LDOS	*Local density of states*
E*f*	*Fermi level*
VB	*Valence band*
CB	*Conduction band*
HOMO	*Highest occupied molecular orbital*
LUMO	*Lowest occupied molecular orbital*
SE	*Secondary electron*
BSE	*Backscattered electron*
HRTEM	*High resolution transmission electron microscope*
FWHM	*Full width half maximum*
BE	*Binding Energy*
UHV	*Ultra high vacuum*
HOPG	*Highly oriented pyrolitic graphite*
GL	*Gaussian-Lorentzian line shape*

1

Introduction

This chapter aims to introduce some background ideas on which the scientific relevance of this thesis is based. Several aspects about the role of carbon material in catalysis are discussed, with more emphasis on the functional chemistry of nanocarbons. Finally a short overview of the thesis content is presented.

Carbon materials have been used for decades in heterogeneous catalytic reactions. Pioneering research in the field has been dedicated mainly to activated carbon (AC) which was used as early as 1963 as a catalyst or as well as catalyst support[1]. In the AC crystallites, the deviation from the characteristic order of graphene layers encountered in graphite, due to both vacant lattice sites and the presence of built-in hetero-atoms, together with a chaotic mutual arrangement of these crystallites by a cross-linked network of aliphatic carbon, assure a well developed porosity, and define the structural, electronic and chemical properties. The ability to disperse metal particles as well as the adsorption and catalytic features are due to a synergistic effect of the above mentioned properties. Soon AC has earned the reputation of offering incomparable flexible physical-chemical behavior and the deep characterization of the chemical-physical structure and the understanding of the impact of each property at "*working condition*" were considered to be the key point for tailoring the catalytic properties to specific needs. In fact, current research in heterogeneous catalysis aims at the design of highly efficient, safer and cleaner catalytic processes. Thus a catalyst with high catalytic activity, but especially

with high selectivity would lead to a series of advantages such as reducing waste and by-products, lower the cost of products separation, atom economy *etc*. Such a noble target is reachable, in theory, through the rational design of the whole AC production cycle. Necessary considerations include the choice of raw material, the activation processes, and subsequent thermal and chemical treatments.

On one hand, the developed microporosity is synonymous with high reactivity, i.e. high number of unsaturated valences and unpaired electrons at the edge of graphene layers (*active sites*). However, on the other hand it is responsible for the low thermal stability of AC in high temperature processes especially under oxygen or hydrogen atmospheres[2]. This is due to the difficulties of selectively tailoring and controlling the properties of AC during the activation process. Nowadays, AC is predominantly used to disperse precious metal catalysts, which are widely used in the synthesis of high value added chemical products[3,4,5]. Since these reactions are carried out in liquid phase, it should be emphasized that such narrow micropores very often lead to mass transfer limitation of the substrate to the active species. In the last two decades research in the field of materials science has been characterized by a large volume of literature dedicated to the problem of diffusion in micropores. This was the driving force for the development of synthetic routes to mesoporous solid materials, worthy of mention here are the successful syntheses of mesoporous silica and silica-aluminates.

Since the discovery of allotropic forms of sp^2 carbon in tubular-like arrangements, new hope has invigorated research aimed at exploiting the potential of nanocarbon (NC) in heterogeneous catalysis. The family of nanostructures of carbon includes nanotubes and nanofilaments with different orientation of the graphene planes with respect to the tube axis[6] as shown in Fig.1.1. These polymorphic forms of carbon exhibit outstanding properties such as: high thermal conductivity, the highest observed Young's modulus, and high mechanical resistance. They offer a broad range of intrinsic properties depending on the diameter, chirality and microstructure. The "*relatively higher chemical inertness*" of nanostructured carbon, with respect to AC, is expected to allow a better control of the surface chemical properties induced by chemical treatments. With respect to their applications in heterogeneous catalysis, NCs strike a good compromise in term of the concentration and type distribution of defective sites that affect the reactivity, selectivity and the thermal stability.

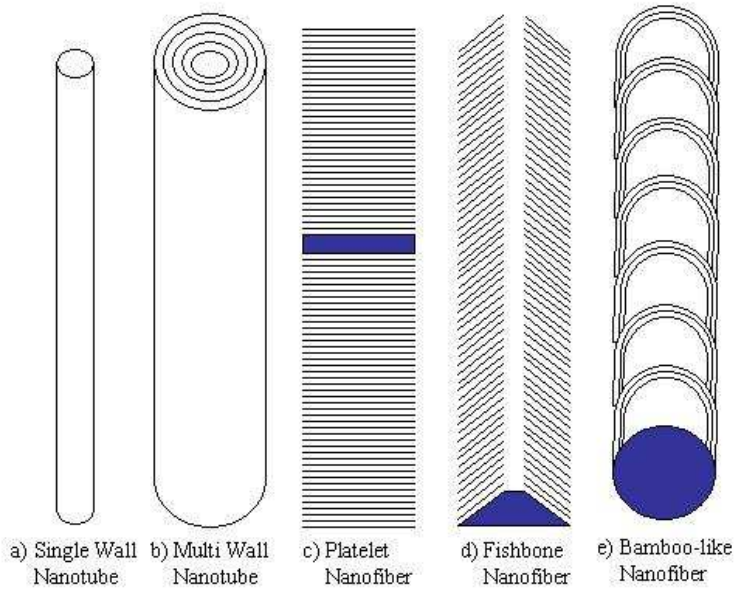

Fig.1.1: Schematic representation of ideal structures of NC.

1.1 N-containing NC: generality and aim of the work

The nitrogen functionalization is a well-known route in heterogeneous catalysis for inducing basic properties on the surface of a certain material and it was applied to different materials (Zeolite[7], Silicate[8], AlPO[9] and MOF[10]) including carbon material[11]. In the last three decades, after Boehm[12] has reviewed about the peculiar chemical properties of NH_3-treated AC, several groups investigated the catalytic behavior of AC treated by NH_3 in different catalytic reactions such us in the liquid phase oxidation of pollutants in water[13], liquid phase and gas phase oxidation of SO_2[14], NO_x abatement[15,16], H_2S oxidation[17], in fuel cell[18] *etc*. The common observation was the improved catalytic activity of N-containing carbon with respect to the N-free counterpart. This fact was explained in terms of improved ability of the nitrogen-containing carbon in the reductive oxygen adsorption and formation of superoxide-anions radicals (O_2^-). These species are considered the active oxygen species determining the catalytic activity of carbon in liquid phase oxidation[12,19]. However, no correlation between catalytic activity and amount of N was established[12]. One of the sources of uncertainty was the modification in the textural properties of the AC during the thermo-chemical treatment in NH_3. Development of microporosity due to the etching effect of NH_3 treatment was observed[12]. Recently, the interest of the scientific community is shifted to the nanostructured forms of carbon.

Several works have been dedicated to the application of nitrogen-containing nanostructured carbon (fullerene and nanofibers) in heterogeneous catalytic reactions. Among these are the applications in fuel cells[20,21], hydro-desulfuration reaction[22], and in oxidation of pollutants from water[13]. In analogy to the biological systems, nitrogen atom can improve the metal dispersion providing preferential sites (Lewis basic sites) for the adsorption of metal. One of the most recent and interesting applications of nitrogen-containing nanocarbon (N-NC) is as support for metal nanoparticles[23]. N-NCs have shown beneficial effect for a uniform assembly and stabilization of metal nanoparticles. Nitrogen atom influences also the metal catalytic activity[21], through weak metal support interaction (WMSI). Those interactions WMSI modify the structure of the metal particles by favoring specific crystallographic plane and defects such as steps, kinks, atom dislocation.

However, establishing a structure-activity correlation is complicated by the possible coexistence of different factors, which might have a synergistic effect on the catalytic performance. These factors include huge variety of possible surface chemical configurations of nitrogen on defect structures, the coexistence of other structural defects; presence of metal impurities, different texture and topological nanostructure. Another problem hindering the understanding of the "*nitrogen effect*" is the limited resolution of the analytical methodology, which is not yet sufficiently developed to analyze all occurring surface groups with suitable chemical resolution.

On the basis of the properties of N-containing carbon materials reported in literature, it is expected that compared with the N-free carbon, the application of nitrogen-containing carbon materials as support for noble metal should lead to catalysts more active towards the oxygen activation in liquid phase selective oxidation. To our knowledge no reports are available up to date on the use of N-containing carbon as support for metal nanoparticles and the application in the liquid phase oxidation of alcohol.

In the attempt to find correlation between the chemical configuration of the N atom on the surface of graphite-like materials, the surface reactivity, and the potentiality of this material in heterogeneous catalysis, the nitrogen functionalization is explored in this work as a way to tailor the surface chemistry of NC. Furthermore, the impact of the surface chemistry of the NC support in the catalytic performance of the metal supported catalysts was studied as well.

The thesis is split in two parts: in the first part the experimental procedure for nitrogen functionalization and the detailed characterization of the material is presented. In the second part the N-NCs are used as support for Pd nanoparticles and applied in liquid phase selective oxidation of benzyl alcohol to benzaldehyde. We use a post-synthesis treatment of commercial carbon nanofibers (CNFs) with NH_3, as suitable route for incorporating nitrogen functionalities on the surface. This chemical route, with respect to the most commonly used catalytic chemical vapor deposition (CCVD), allows efficient insertion[24] of nitrogen functionalities in a more homogeneously manner – depending on the homogeneity of the nanostructure of the starting NC material – and untying from the problems related to the control of the filaments nanostructure. The questions arising during the study on which the investigations have been addressed are:

- How does the distribution of nitrogen functionalities change by modifying the thermo-chemical treatment?
- Which is the thermal stability of the different nitrogen functional groups?
- How do the different thermo-chemical treatments mirror the surface chemical properties of nitrogen-containing CNFs?

Characterization techniques suitable for carbon are limited and the data reported in literature for the assignment of oxygen and nitrogen species are controversial.

One of the questions to be answered is if it is possible to assess precisely the nitrogen and oxygen functionalities. Application of temperature programmed X-ray photoelectron spectroscopy (TP-XPS) coupled by on-line mass spectrometer (MS) supply a phenomenological approach for assessing oxygen and nitrogen functionalities.

The second part of the thesis is aimed at the understanding of the role of the surface chemistry of the carbon support in the catalytic performance of the Pd on N-CNFs catalysts. Thus, in this section we will try to answer the following questions:

- How does the surface chemistry (acid/base and hydrophobic/ hydrophilic character) of the support affect the nanoparticles morphology?
- Does the metal-support interaction influence the catalytic performance of the Pd nanoparticles?
- Does the experimental condition influence the catalytic performance of the catalysts?

1.2 Overview of the thesis

The thesis is organized as follow:

Chapter 2 gives a literature survey on the nitrogen functionalization of NC, with emphasis on the experimental and theoretical studies focused on the influence of the nitrogen functional group on the electronic structure and chemical properties of the NC surface.

Chapter 3 discusses the experimental procedure for the functionalization, catalyst preparation and liquid phase oxidation reaction conditions. Furthermore an introduction of the characterization techniques used in this work is presented.

Chapter 4 is focused on the characterization of the nature of the surface species introduced by the thermo-chemical treatments. XPS and TPD characterizations of the functional groups are reported.

In **Chapter 5** is discussed the functionalization procedure as route for tuning the acid/base properties of NCs. Characterization of the basic sites by liquid phase titration and by microcalorimetry is presented.

Chapter 6 includes the characterization of the Pd-based catalysts and the screening of these catalysts in the liquid phase oxidation of benzyl alcohol to benzaldehyde. The catalytic tests have been performed partially at the department of inorganic Chemistry of the Fritz-Haber institute in Berlin and partially at the university of Milano in Laura Prati' s group. In order to establish structure-activity relationship, further results about the application of those catalysts in the liquid phase synthesis of H_2O_2 are presented. The catalytic tests in the H_2O_2 synthesis have been performed within the framework of ELCASS and IDECAT at the University of Messina in Prof. Gabriele Centi and Prof. Siglinda Perathoner's group.

Chapter 7 provides the summary and some outlook.

The carbon nanofilaments used in this work present an inner cavity, and walls with two differently structured sections: the most inner layer has “herringbone” structure and the outer layer present the typical no long range order of pyrolitic carbon black. The structure of pyrolitic carbon is referred as turbostratic[25,26] graphite lattice. The turbostratic lattice is defined as a series of graphene layers with random orientation, random stacking[25,26] and expanded lattice constant with respect to graphite. In virtue of the “special” structure not easily classifiable, the NC used in this work will be referred following in the text as a general term “carbon nanofiber”.

According to Zhou[27]:

“The overwhelming majority of the carbon material is better described as a “paper Mache” of small graphitic sheets, rather than a nested Russian doll. This model has been proposed for carbon black.

2

N-containing NC: a literature survey

As the thesis is dealing with nitrogen functionalization of carbon nanofibers and the application in heterogeneous catalysis a literature survey about the concepts related to the nitrogen functionalization is presented in this chapter. The emphasis is on the understanding of the effect that the presence of nitrogen and oxygen functionalities has on the physical and chemical properties of NCs.

The extraordinary properties of NC materials have led to the birth of an entirely dedicated branch of the scientific research. Historically, the pioneering work on the growth process of CNFs was carried out in 1976[28] by Endo and coworkers. However, the beginning of the *carbon nanotubes era* is usually dated back to the investigations of the microstructure of multi-wall carbon nanotube (MWCNT) by Ijima[29] in 1991, followed a few years later by the discovery of single-wall carbon nanotubes (SWCNT)[30].

Since then, *carbon nanotubes science* has become one of the most active fields of research. A large volume of literature is dedicated to the subject, much of it towards understanding of the structure and physical property of nanostructured carbon, but also the development of economic and high-yielding synthetic methods.

The intrinsic properties of NC materials vary within a wide range depending on the structure, morphology and topological characteristics on the nanometer scale. For this reason nanostructured carbon materials are suitable for use in a variety of applications in materials science and nanotechnology, such as nano-hetero-junctions, diode interconnectors, nanotransistors, sensors and nanocomposites.

Particularly, research in materials science has been heavily devoted to studying the outstanding physical properties of SWCNTs and MWCNTs, such as high tensile strength, elastic properties, high thermal conductivity, as well as topologically controlled electronic and field emission properties.

Recently, interest has been focused on the chemical properties of the NC surface, paving the road for CNTs and CNFs into heterogeneous catalysis. The lack of an economic large scale production and the low selectivity in controlling the physical properties are the factors limiting the commercial application of CNTs. Specifically, the growth of CNTs exhibiting homogeneous chirality has to date not been demonstrate, thus limiting the electronic application to mixtures of metallic and semiconducting CNTs.

For this reason, new directions in nanotube science, utilizing the concept of structural defect[31] as a way to tailor the electronic, mechanical and chemical properties of CNTs[32,52,61,45,33,34] have arisen. Besides the direct synthesis of NC oriented at the introduction of doping impurities, a dominant role is played by the post-synthesis chemical functionalization, currently representing an *open window* in carbon nanotube science. Chemical functionalization is a fundamental step in the view of exploiting the properties of CNTs in any potential applications. It can improve solubility[35] and processability, and at the same time establish the physical-chemical properties of the final material.

It is clear that in these applications the material is applied with different purposes and different specific requirements. Thus, theoretical and experimental studies aimed at evaluating the effect of the defects on the physical-chemical properties of nanostructured carbon are important issues in order to predict how functionalization affects the potential for various applications. For example, the control of the structure defectiveness on the nanometer scale provides potentiality for a new class of material applicable as nano-sized hetero-junctions[47]. This can be realized by the introduction of Stone-Wales defects (pentagon-heptagon pairs) in the CNT structure, which induces changes in the helicity and thus, produces a semiconductor/metallic junction within the same tube[36].

The introduction of donors/acceptors by substitutional doping with N a/o B has been studied theoretically and experimentally imparting outstanding electronic properties when compared with pure carbon nanostructures[31]. In this way it is possible to overcome the problems related to the topological dependence of the physical properties in CNTs[63].

N-doped CNTs behave similar to n-type semiconductors, while B-doped CNTs similar to p-type semiconductors. This fact has several implications on the physical properties of the resulting doped material. N-doped CNTs have a lower work function than pristine CNTs, while the work function of B-doped CNTs is higher than that of pristine CNTs. As consequence, N-doped CNTs shows enhanced field emission properties, while boron doping has an opposite effect on the field emission properties of CNTs[37]. On the other hand, the introduction of localized defects reduces the conductance in N-SWCNTs[36,47]. However, N-doping of graphitic material occurs in different way than the most studied case of substitutional nitrogen. Different effects have been reported depending on the chirality and the type of nitrogen-containing defective site[33,65]. By a controlled N-doping it is possible to modulate the sensitivity of the material with respect to adsorbed gas molecules, for e.g. sensor applications.

In every nanotechnological application, the nitrogen atom should exercise a doping effect on the electronic structure of graphitic-like material. A very small amount of nitrogen (below 1%) is sufficient to this scope[31]. Substitutional doping, where nitrogen is incorporated directly into the CNT`s framework is the most desirable methods as it does not compromise the mechanical properties of the nanotubes.

From a chemical point of view, the introduction of functionalities containing hetero-atoms is a way of manipulating the surface chemistry of NC according to specific needs.

Research devoted to the application of N-containing carbon materials in catalysis has taken two different routes: in one case nitrogen functionalization is used as a means of introducing basic sites on the carbon surface.

The carbon material is considered as a carrier which can be used to introduce nitrogen functionalities by grafting of organic moieties containing nitrogen atom with an ion pair available as pyridine or amino group[38]. In this case the chemical reactivity is determined by the chemical nature of the organic moieties and the textural properties of the material play the main role driving the choice of the carbon material used.

Other research has focused on exploiting the intrinsic chemical properties of the graphitic structure which contains substitutional N-functionalities interacting with the π-electron system.

In fact, the introduction of *n*-type donor states by basic nitrogen in substitutional positions in the graphite structure is expected to improve the reactivity with electron

acceptor molecules[39]. *Vice versa* the introduction of acceptor states (*p*-type acceptor states) in the valence band, typically by introduction of substitutional boron atoms[43] , would lead to an improvement of the reactivity with donor molecules. In this case, the electronic structure at the surface of NC is the key point describing and explaining the reactivity of the NC surface. The electronic structure of the functionalized NC reflects the "defectiveness" of the carbon material which is also the factor determining the reactivity.

In this thesis, the interest is focused on understanding and exploiting the chemical reactivity of graphitic system containing nitrogen functionalities.

Following, the description of the influence of defects on the electronic structure of an ideal graphene will be reported, with more emphasis on the presence of nitrogen substitutional impurities, curvature and vacancy defects. These are the typical defects characterizing the nanostructured form of carbon used in this work. Finally, a literature survey about the surface chemical properties of CNFs and CNTs containing nitrogen will be presented.

2.1 Electronic structure of Carbon

Due to the aromatic chemical nature of the sp^2 bonding in an ideal graphite sheet, the basal planes at the surface manifest low reactivity, and act mainly as nucleophiles through the π-system toward weakly adsorbed species (dispersive interaction). Indeed, the surface chemistry of sp^2 carbon involving covalent bond formation is relevant at the prismatic face. However, the assumption of the inertness of the basal plane and the restriction of the reactivity to the prismatic face is not longer valid for realistic nanostructured carbon systems, whereas the role of defect became a key factor dominating the reactivity. The possible defective structures present in carbon material can be classified into four main groups: topological (introduction of rings containing more or less than six carbon atoms), curvature induced pyramidalization and π orbital misalignment (rehybridization ability of carbon atom to hybridize between sp^2 and sp^3), incomplete bonding (vacancies, dislocations) and doping with other elements such as N, B, P…..*etc*.

These features are present in every form of sp^2 bonded carbon network such as fullerenes, nanofilaments, nanotubes[45] and other non-crystalline carbon structures containing fullerene-like segments[40] also known as nanoporous carbon[58] (soot, glassy carbon, carbon black, charcoal, AC). The occurrence of these defects determines the atomic nanostructure and the electronic structure of the carbon material. In addition, realistic non-crystalline carbon materials are characterized by a mixture of tri-coordinated and tetra-coordinated atoms. The loss of long-range order produces smoothing of the density of states (DOS) features and tailing of the localized states below the band edge into the band gap[41,42].

Research in the field often suffers from the challenge of coupling experiment and theory. This is because realistic sp^2 carbon networks are characterized by a nanostructure of more complicated defectiveness than the model system described above. Theoretical calculations have shown that the population of point defects in SWCNT depends on the curvature[45] and on the topology[43,44,74].

The population of defects, e.g. vacancies, increases with the curvature of the graphitic planes resulting in a higher concentration of vacancies, which are binding sites for hetero-atoms. On the other hand, it was predicted by theoretical calculation that the introduction

of hetero-atoms during the growth of CNTs induces other defects such as pentagonal rings[62], structural corrugations and atom vacancies with consequent deviation from the planarity of the graphene layer[45].

Thus the surface of realistic functionalized NC is expected to be characterized by heterogeneously and energetically different defective sites co-participating in defining the surface electronic structure.

However, the theoretical predictions concerning the effect of point defects on model graphitic system on the electronic properties of these structures give useful information for understanding the impact of the defects on the reactivity of realistic carbon systems.

2.1.1 Influence of the defect on the electronic structure of the model carbon system

The pioneering theoretical calculations on the electronic structure of graphite were carried on by Wallace[48] in the early 1947. These studies have been extended to the case of SWCNTs by M. S. Dresselhaus and co-authors and reported in several textbooks[36,46,47]. A small graphene domain was used as model system to derive the electronic structure of graphite and SWCNT and to study the modification induced on the electronic structure by defects.

To describe the electronic structure of graphene, "π-orbital tight-binding" approach was used[48]. According to the "tight-binding approximation", the electrons are considered part of the atoms and overlapping of the electrons wave function between neighboring carbon atoms is possible. The linear combination of neighboring $2sp^2$ hybridized carbon atoms lead to σ bands formation and the linear combination of $2p_z$ atomic orbitals lead to the formation of π bands. The σ bonds form the hexagonal network, and the π bonds, pointing perpendicular to the surface, are responsible for the weak van der Waals interactions between graphene sheets.

The σ bonds are too far from the Fermi level to play a role in the electronic transport or optical adsorption properties. The *bonding* and *antibonding* π bands, in contrast, meet each other at the k-point of the *brillouin* zone (Fig. 2.1) exactly where the Fermi level (E_f) is Fig. 2.2.

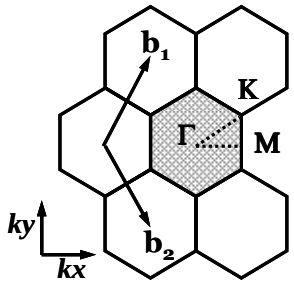

Fig. 2.1: Brillouin zone in graphene

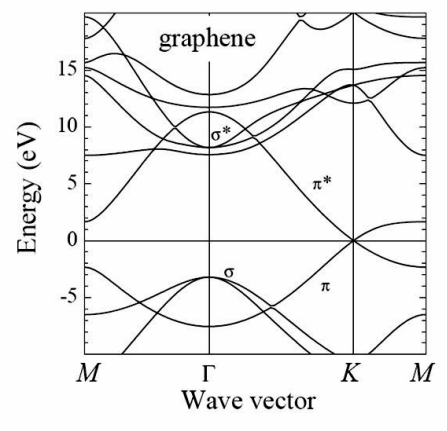

Fig. 2.2: Band structure of graphene

For this reason an individual graphene sheet is a zero-gap semiconductor. The interaction between the graphene layers in graphite causes the bands to overlap such that the bands are partially filled at the E_f. I.e., perfect graphite is actually a semimetal[49,50].

SWNTs can be imagined as a graphene sheet rolled up in such a way that the edges are joined together; concentrically cylinders are referred as MWCNTs.

For perfect tubes, the dependence of the electronic properties on the diameter and chirality of the CNTs[46,47] is well-known. This concept is usually depicted in the CNTs index map often reported in text books dealing with the topic[46,47] (not shown here).

Recently, more sophisticated theoretical studies based on *ab initio* calculations have been used to derive the electronic structure of graphitic systems[36,51] . One important issue in the study of CNTs is the effect of the curvature which is claimed to determine in part the higher reactivity of CNTs compared to flat graphite.

Very large CNTs can be approximated as a flat graphene layer. However, curvature induces rehybridization of σ and π states, which is especially pronounced for tubes with small diameter[45]. Such a rehybridization is enhanced by the local and inhomogeneous distributed deformations of the tube which are locally twisted and bent. These structural distortions modify the electronic structure of CNTs[52,107] locally at the distortion site. For metallic SWCNTs[52] it has been reported that due to the mixing of the π-σ states at the deformed region of the CNT structure, the LDOS near E_f increases and a shift of the valence band edge to a lower binding energy occurs.

With increasing local distortion, a broadening of the fine structure of the mixed π-σ states is observed near E_f. In addition, due to the π-σ rehybridization a charge polarization of the C–C bonds in the distorted regions is observed resulting in charge density localization (increased σ character). This fact has an implication on the electric transport and on the chemical reactivity.

In fact, scattering of the conduction electrons at the defect side leads to charge-carrier localization and the reduction of the conductance. On the other hand, the localized charge density induced by defects plays a role in electron transfer reaction[53] and facilitates the adsorption and dissociation of molecule.

Dynamic structural distortion is a feature of the nanotube surface in contact with a substrate. It was observed experimentally[54] and theoretically[55] that the nanotube surface in contact with a substrate (support or metal) tend to bend and to conform to the morphology of the substrate. Local bending is also present in other forms of graphite-like material and thus similar effects are expected on their local electronic structure.

Other types of defects of relevance and extensively studied in carbon material are the possibility to introduce n-type donor and p-type acceptor states within the same tube. This can be realised by B and N substitutional impurities in the carbon network. The effect of B impurities and N impurities on metallic SWCNT is depicted in Fig. 2.3 and Fig. 2.4, as was reported in literature[56] for a (10,10) CNTs.

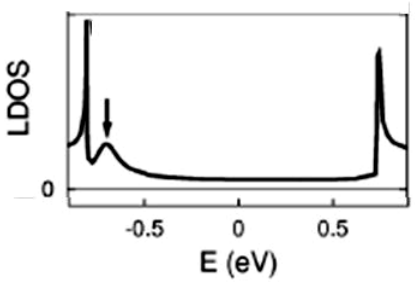

Fig. 2.3: Effect of B impurities on the LDOS for (10,10) CNTs[56]

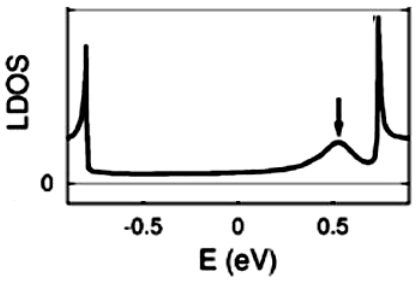

Fig. 2.4: Effect of N impurities in the LDOS for (10,10) CNT[56]

The presence of nitrogen or boron impurities generates quasi-bound states close to the conduction band and valence band, respectively, as in typical semiconductor or semi-conducting nanotubes.

The quasi-bound levels associated with the nitrogen impurity behave as donor states with respect to the lower sub-band of the conduction band. In contrary, the quasi-bound states associated with boron behave as acceptor states with respect to the valence band. In both cases two quasi-bond levels are generated: one quite localized with stronger binding energy having s-like character and one more delocalized with weaker binding energy state having p-like character.

SWCNTs can become hole-doped in the presence of adsorbed oxygen because of oxygen's electron affinity[57]. Other types of defects often found in sp^2 carbon are vacancies and motifs derived from them[58]. The atoms in the neighbourhood of a vacancy rearrange to reduce the number of dangling bonds leading to the formation of motifs which are combinations of non-hexagonal rings. In addition, carbon atoms rearrange to reduce the bond strain by changing the bond angle and by bending the lattice.

Vacancies motifs can be classified in even defects (even number of missing atoms) and odd defects (odd number of missing atoms)[58]. In the even defects the carbon atom are totally bond saturated, while the odd defects have under-coordinated C atoms.

The absence of an atom perturbs the alignment of the p_z orbitals forming the π band. This will produce additional peak in the DOS close to the Fermi level. For vacancies formed by an odd number of missing atoms there will be a localized dangling bond. These odd vacancies are negatively charged[58] and are thought to be responsible for the chemical reactivity of sp^2 carbon materials. This is in agreement with the experimental observation that O_2 molecules preferentially dissociate at these sites[59].

Typical defects in graphitic material are the Stone-Wales defects characterized by a pair of heptagon-pentagon ring. The presence of this type of defects produces additional DOS above and below the E_f. For this reason the introduction of these types of defect offers interesting opportunity for the design of new nano-junction electronic devises.

In summary, the reactivity of carbon materials is correlated with the existence of localized quasi-bond states close to the Fermi edge which produce static charge localization around the defect site. Depending on the origin of these localized quasi-bond states, a different reactivity is expected: quasi-bond states generated from the valence

band (VB) are acceptor sites characterized by charge depletion around the defect site (seen as positively charged), thus they adsorb donor molecules. Quasi-bond states generated from the conduction band (CB) are donor sites characterized by charge localized around the defect site (seen as negatively charged) thus they adsorb and dissociate acceptor molecules.

2.1.2 Nitrogen chemical configuration in nanostructured carbon

The nitrogen insertion in the graphitic structure of NC surface dramatically influences the morphology, nanostructure and the electronic properties of the NC surface.

The way and the magnitude in which the physicochemical surface properties of NC are affected depends on different factors: type of nitrogen functionalities present, concentration and mutual organization of the nitrogen species in the graphene layer, topological localization of nitrogen site (i.e. armchair or zigzag termination), extension of the graphene domains and eventually the NC microstructure (i.e. curvature effect), and the coexistence of other type of structural point defects (vacancies, other hetero-atoms).

One important point in the view of the exploitation of the physical and chemical properties of N-functionalized NC is the establishment of "atomic structure-electronic structure" correlation. In simple words, it is important to understand the chemical configuration of the nitrogen responsible for the induced electronic properties discussed above. One approach often used to derive the chemical structure of nitrogen in graphitic nanostructures, is the comparison between the experimentally measured electronic structure and that theoretically calculated for complex model sp^2 carbon networks.

Nitrogen in the graphitic structure may be present as a substitutional atom (N1[33,56]), defect complexes composed by substitutional N and vacancies (N3+vac[31,33,63,64] and N4 +divac[33,65]) and as chemisorbed N moieties[56].

The effect of the presence of substitutional doping was studied in the literature on different model systems: graphene[61], small SWNTs[61], amorphous carbon nitrides[42,41,60] etc.

It was shown by Miyamoto[60] *et al*. that two different systems are expected to exist in a sp^2 bond configuration: C_3N_4 in which each N is bond to 2 C atoms in a pyridine-like configuration and CN in which N is bond to 3 C atoms. In that paper, it is shown that

both C_3N_4 and CN are not stable in planar forms at high nitrogen content. Out-of-plane atomic deformation results in the structure stabilization. Furthermore the development of three-dimensional covalently bonded CN_x structures are predicted to occur at very high nitrogen concentration.

Those results are in agreement with the theoretical calculation by dos Santos and Alvarez[61] on the nanostructure of nitrogen substituted in graphite clusters.

It is possible to distinguish two extreme situations regarding the coordination of the nitrogen atoms in the carbon atom network. The nitrogen coordination depends on the amount of nitrogen incorporated. In theory, at low concentration the nitrogen is substitutional in a 3-fold coordinated configuration. The additional electron fills the empty state in the conduction band while the planar structure is maintained. With increasing N concentration, the conspicuous excess of electrons coming from N atoms occupying the π^* anti-bonding states destabilize the planar geometry. As the energy increases, the configuration changes from planar to "out of plane" bonding and the additional electron occupies a non-bonding state on the nitrogen and produces a carbon-dangling bond. Such carbon-dangling bond is unstable and give arise to cross-linking with neighboring atoms, forming a three dimensional carbon nitride network.

In addition, another natural consequence of the corrugation induced by nitrogen doping is the rolling of clusters to form a tube. This is corroborated by experimental evidences of the effect of nitrogen insertion to induce curvature of the graphene layers[62].

Sumpter *et al.*[62] have tried to explain the growth process of N-doped CNTs. They found that nitrogen prefers to substitute carbon into smaller diameter tubes and stabilize neighboring pentagon ring responsible for the curvature and the compartments. Entrapments of a pentagon or a heptagon by hexagons, but not both contiguously (as in Stone-Wales defects), is a necessary condition for the growth of curved sp^2 structures. In this situation the structure is stabilized and no carbon-dangling bonds are present in the DOS[61,62].

In order to assign the donor states in the DOS of N-doped graphitic material to a specific N species, Terrones[63,64] et al. have investigated experimentally and theoretically the electronic structure of N-doped MWCNTs. The identification of the lattice defects was carried out by scanning tunneling microscopy (STM) and the theoretically calculated

LDOS using tight binding and *ab initio* calculations were compared with that obtained experimentally.

In order to explain this additional level, laying approximately 0.2 eV from E*f*, the authors proposed in virtue of the scanning tunneling microscopy investigations and the theoretical DOS, an alternative model where N incorporates into the graphite lattice in N rich cavities (3N+vac). In such a way, zig-zag semi-conducting tubes can be *n*-doped by insertion of nitrogen.

At the same time such a nitrogen configuration introduces vacancies, behaving as acceptor site in the valence bands. For this reason, these electron-rich structures could pave the way to real molecular hetero-junction devices. Rossi[65] et al. has studied by DFT the thermodynamic stability, the implication on the total DOS and charge localization of different N-complexes in armchair, zig-zag carbon nanotubes and in graphene. Beside the 1N (three-fold coordinated N) and the 3N plus vacancy proposed firstly by Terrones[63,64], in this paper the authors proposed a more stable configuration of N-defects characterized by the presence of four N atoms and two vacancies (4N+divac)[33,65]. These defects might exist in flat graphene; however they occur more easily in curved graphitic structures as reported in many other works[56,60,61,62,63]. It was reported that defects composed by the N1 substitutional N introduces donor state close to the conduction band in a more pronounced way for armchair (5,5) nanotubes than for (8,0) zig-zag nanotubes. The three pyridine-like rings surrounding a vacancy introduces midgap states in the semiconductor (8,0) tubes, whereas acceptor site close to the valence band in the metallic (5,5) tubes. The N4-divac does not introduce new gap states in semiconductor tubes, while in armchair tubes, p-type acceptor states and n-type donor states are introduced. The presence of these defects produces charge density around the N atoms, in a more pronounced manner for the N4-divac defective sites. Those defects site are involved in defining the chemical reactivity and the affinity towards the adsorption of different kind of molecules.

Beside the issue of substitutional nitrogen defects in graphite and graphite-like material, the effect of chemisorbed molecule has been studied as well.

The understanding of the effect of donating or withdrawing functional groups (oxygen and nitrogen) on the electronic properties of carbon was matter of intensively studies in

early time, owing to the tailoring of the red-ox properties of the carbon for the application in electro-catalysis in substitution to precious metal based catalyst[18,19,66,67,68].

The effect of the side functionalization with electron donating moieties such as NH_2 groups or withdrawing NO_2 groups on the ionization potential has been determined[66,67] by Strelko *et al.*

Oxygen-containing functional groups lower the electron-donor properties of carbon matrices. The functionalization with electron withdrawing moieties such as carboxylic and carbonyl groups significantly shift the energy of the HOMO to a lower value[67,66]. Since the energy of the HOMO reflects the ionizing potential of the specie in such a way that the lower the HOMO the bigger the ionizing potential, those types of functional groups produce a decrease in the electron-donating properties of the carbon material[69].

In particular, the carbonyl group shows a very low LUMO level which is an indication that this site would rather behave as electron-acceptor site. Nitrogen-containing functional groups produce an increase in the electron-donating properties of the carbon material.

Nitrogen heteroatoms in pyridine species increase significantly the electron-donor ability of the carbon matrix. More significantly than the introduction of an amino group. Those species influence the adsorption properties of the carbon surface occurring through π-π staking interactions[70]. For instance, the functionalities with a donating resonance effect on the π-system will improve the adsorption of organic molecules. The opposite behavior is expected for withdrawing functionalities.

2.2 Surface chemistry of NC

The reactivity of the graphite-like carbon material is determined by the relative amount of exposed edge of graphene layer (maximum in the case of fishbone structure), defects and in the case of tubular or fullerene forms also by the strain induced by the curvature of the graphene layer, which in turn induces a rehybridization of sp^2 bond with partial sp^3 character. Bending of graphene layer is possible when less-stable non six-member rings are present. Edges, corners, vacancies and bent sp^2 carbon atoms at the surface are potential binding site for hetero-atoms. Such hetero-atoms, generally oxygen or nitrogen, can exist on the carbon surface in a wide range of different chemical configuration, and together with the delocalized electrons of the graphitic structure, define the acid/base and hydrophilic/hydrophobic properties of the surface.

Thus, understanding the surface chemistry of carbon is fundamental for the understanding of the adsorption properties and the catalytic and electrochemical properties.

2.2.1 Nitrogen and oxygen functionalities in NC

Carbon materials are very often accompanied by the presence of hetero-atoms such as H, O, N, P, and S.

From a chemical point of view, the most studied functional groups contain oxygen and nitrogen atoms.

Those functional groups present in carbon material can originate from both the precursor used for the production or can be intentionally introduced by specifically addressed post-synthesis treatments.

For instance in the production of N-CNT by CCVD, N functional groups are introduced during the synthesis by using a nitrogen-containing hydrocarbon. In the case of other forms of carbon, i.e. AC or carbon fibers, functional groups can derive from the raw material used such us coal, melamine resins *etc*.

Oxygen functionalization is often carried out by means of oxidative treatment[76] in gas-phase by oxygen, ozone, carbon dioxide, nitrous oxide or liquid phase by nitric acid, hydrogen peroxide, chromate, permanganate etc. Those functionalities, especially carboxyl oxygen species, can be used as grafting sites for more complex moieties, for

example grafting of hetero-atoms-containing molecule by mean of the classic routes used in organic chemistry synthesis[71].

Nitrogen functionalities are often introduced by gas phase chemical treatment with ammonia[11,12,154,155] or hydrogen cyanide[12].

The extension of the functionalization depends on the treatment condition, the functionalization agent and the nanostructure defectiveness of the carbon material.

Obviously the same treatment will give a higher degree of functionalization in AC than in graphite.

However, it is important to point out that the same types of O and N functionalities occur in any kind of carbon material indistinctly from the microstructure.

Most of the studies reported in literature have focuses on the identification of the chemical structure of the species and their impact on the surface properties, with special regards to the characterization of acid/base properties.

However due to both the limited resolution of the analytical technique available and the high complexity of the carbon surface, a detailed description of the surface functional groups in carbon material is often very difficult.

Conceptually, one can imagine that all the possible chemical configuration of nitrogen and oxygen in organic molecule (i.e. amide, amine, nitrile groups etc…) could be found in the graphene layer of NC.

Those nitrogen and oxygen functional groups can exist in side terminations of the graphene layer in both aromatic and aliphatic character or at the bending site of the graphene sheets. Heteroatoms may be introduced also at vacancies sites[72] .

In Fig. 2.5 is reported the schematic representation of a graphene cluster with the various hetero-atom (oxygen and nitrogen) chemical configurations.

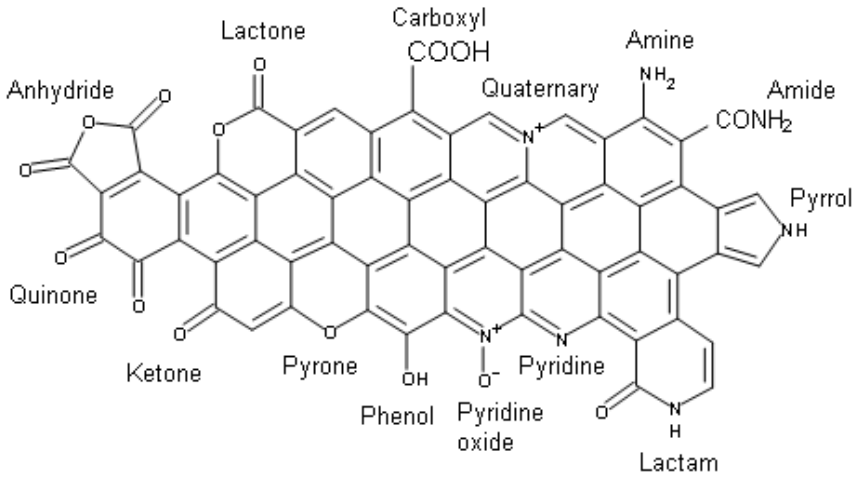

Fig. 2.5: Different oxygen and nitrogen species in carbon

In a deductive reasoning, the similitude of the reactivity of the functional groups in carbon material with the parent organic molecule is a good qualitative description of the system.

The temperature-programmed desorption of N and O is often used for determining qualitatively the acid/base strength of the species.

The less thermo stable species behave as acid in water solution, while the most thermal stable species are basic species. The thermal stability is related to the combination of the withdrawing or donor inductive and/or mesomeric effect of the functional groups on the π-electron system of graphite. The acidic functional groups exercise a withdrawing effect on the aromatic system which is a destabilization factor for the aromaticity, thus those acidic species has a low BE and decompose upon heating at lower temperature.

There is a general consensus that the acidic character of carbon material is due to the presence of oxygen structures like carboxylic acid, anhydride, lactone, and phenol[120,122,182-185].

In contrast, the structure and the strength of the basic oxygen species are not yet clarified. The proposed structures for basic oxygen species contain ketones group, ethers groups, quinones and pyrone-like structures. Among the N functional group, species like amine and pyridine are basic, while amide, lactam and nitrous species are considered to be

weakly acidic. However, the thermal desorption technique gives a chemical behavior feeling, but does not give a numerical scale of comparison as it is a pK_a value.

The pK_a value is determined experimentally by chemical titration, such as potentiometric titration and Boehm titration specifically developed for the acidic sites determination. However, it is not possible to deduce the structure of the functional group basing on the similitude between the experimentally determined acid/base reactivity (pK_a value) and that one of the parent organic aromatic molecules.

There are two motivations for this affirmation: first the experimental measured pK_a values are the resulting value among the different species present. The functional groups present on the carbon surface are not entities separated one another, but they can undergo to intra and inter- molecular interaction influencing each other the chemical behavior;

Secondly, assuming that one is able to characterize a single species, the pK_a value of certain acid/base specie substituted in the benzene ring is influenced by the number of member of poly-condensed aromatic hetero-cycle and the relative position of the hetero-atoms in the cluster (structural isomer)[75]. It is obvious how difficult would be to discriminate between the different kinds of species showing similar pK_a value.

In the attempt to identify the chemical configuration of the species inducing the strong basic character to the carbon surface, Montes-Morán[75] *et al*. have demonstrated by means of theoretical calculations that the pK_a value of pyrone-like species increase dramatically by increasing the number of poly-condensed aromatic hetero-cycle in a pyrone-like structure. Calculation on N species indeed, shown that no big variation on the pK_a value of the N species occurs among different structural isomers or by increasing the number of poly-condensed aromatic hetero-cycle. Also basal plane are considered as hydrogen bond acceptor, however the basic strength is much lower than that one of the functional groups, especially pyrone-like species.

In virtue of this fact, the authors propose a pyrone-like poly-condensed aromatic hetero-cycle cluster as plausible structure mainly determining the basicity of the carbon surface. However it is found experimentally that the amount of acid adsorbed on N-containing carbon is considerably higher than in the analogously prepared nitrogen-free carbon[73]. Thus, further studies are needed to elucidate the nature of the N species contributing to the basic character of nitrogen-containing carbon material.

In virtue of the peculiar surface chemical structure, carbon material can be used in application where proton transfer (acid/base reaction) or electron transfer (red-ox reaction) are involved.

2.2.2 Adsorption properties

The graphene network in carbon material can be considered as composed by hydrophobic domains coexisting with hydrophilic domains[74]. The graphitic basal planes represent the hydrophobic part while the functional groups induce hydrophilic character to the surface. In general nitrogen and oxygen functionalities in hetero-cyclic moieties which are stabilized by resonance with the π-electron system do not alter strongly the hydrophobic character of the carbon surface. The most important species of this class of functional groups are pyridine species which carry a double pair on the nitrogen atom and the species containing carbonyl and ethers oxygen atom. Those types of species produce partial charge localization of the π-electron system and infer Lewis a/o Brønsted basicity to the graphitic surface. They represent, in fact, reactive site for a further chemical attack. The hydrophilic character of the carbon surface is further enhanced from the subsequence chemical attack (usually oxidative) at the defective site leading to the local destruction of the extended electrons delocalization of the π-system.

By mean of oxidative treatments, Brønsted acid sites (carboxyl and phenol group) are introduced on the graphitic carbon surface. Those species can be converted basically in any types of moieties by grafting of functional organic molecules.

Thus once in aqueous solution, the surface of carbon material is amphoteric, and is characterized by the coexistence of both negatively and positively charged sites, in a given relative amount that depends on the pH of the aqueous solution. In the Fig. 2.6 is reported a schematic representation of the carbon surface depending on the pH of the aqueous solution.

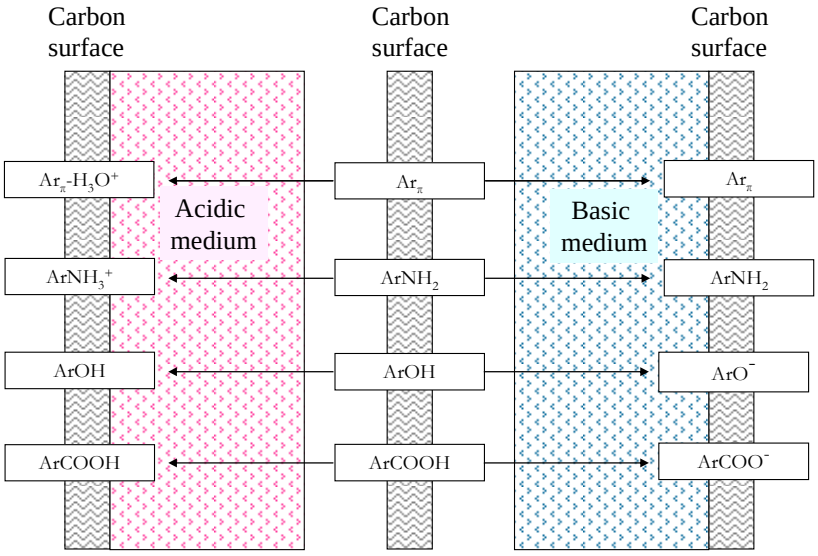

Fig. 2.6: Schematic representation of the carbon surface in aqueous media (adapted from ref.[231])

As shown in Fig. 2.6, the π-electron density of the carbon basal planes is considered as non-heteroatomic Lewis basic sites and undergo to protonation in aqueous solution[75,76].

The relative extension of the hydrophobic and hydrophilic domains a/o the acid/base properties can be tailored by thermo-chemical treatment according to the requirements of the application for which the carbon material is designated. For instance, through stronger oxidative treatment the extension of the hydrophilic part is increased, while by means of thermo-treatments the hydrophobicity restored.

In those application in which the electrostatic interactions play a fundamental role, for instance anions and cations adsorption, the proton exchange capacity must be maximized. This can be reached by increasing the hydrophilic properties of the carbon surface. In particular, for cations adsorption the functionalization must be addressed in such a way to develop a negatively charged surface (oxidative treatment) *vice versa* to adsorb anion the surface must be positively charged (basic carbon).

In opposition, the adsorption of organic molecules on the carbon surface, specially unsaturated molecules, occurs through π-π staking interactions which are hydrophobic in nature[70]. In such case all the functionalities with a donating resonance effect on the π-system will improve the adsorption of those molecules, specially those carrying electron with-drawing substitutes.

2.2.3 Electron transfer properties

The defects existing on the surface of sp^2-bonded carbon induce localization of the extended π-electron system with charge localization in the graphene plane. Those localized charges are artifice of the red-ox properties of the material. The electron transfer effect plays an important role in the oxidation reactions, electrochemical and electrocatalytic reactions.

Furthermore, the electron transfer process is responsible of the metal support interaction.

In the view of the application of graphite and graphite-like material as carrier, the electron transfer from the local site of the carbon surface to the metal is auspicial.

The nature and the strength of the metal support interaction have an influence on the atomic and electronic structure of the metal particles by inducing a preferential crystallographic structure and defects at the metal surface[77]. Flat particles have been found in catalyst with strong metal support interaction[77].

In particular, the electron donor functionalities, Lewis basic sites, such as oxygen and nitrogen atoms located at the edge of the graphite plane in hetero-cycle moieties, induce atom reorganization at the metal surface with changes in the lattice parameter, generation of low coordinated sites and probably charge accumulation at the metal surface.

On the other hand, electron deficiency on the metal nanoparticles can be originated from the interaction of the metal particles, with local acidic surface sites, Brønsted or Lewis acid sites. This effect became relevant for very small nanoparticles and for cluster.

The metal support interactions stabilize the metal nanoparticles and prevent them from sintering or leaching into the reaction media, and therefore prolonging the life-time of the metal supported catalyst. The effect of the metal-support interaction on the metal surface structure has an impact on the catalytic properties of the catalyst[78].

2.2.4 Reaction catalyzed by carbon

2.2.4.1 Carbon as catalyst

- Oxidative dehydrogenation (ODH) of organic substrate can be catalyzed by carbon at lower temperature than conventional catalyst. In the ODH of ethyl benzene to styrene, CNTs show higher long term stability than AC, with good selectivity and yield[2]. The selective introduction of functional groups, probably quinones species, on the surface of carbon material is a prerequisite for minimizing the unwanted total oxidation. ODH of n-butane to butadiene was carried on oxygen-functionalized CNTs. The selective blocking of acidic oxygen species by phosphate lead to an increase in the selectivity to butadiene[79].

- Dehydration of alcohol is catalyzed by carbon material containing oxygenated functional group with acidic character. In particular the activity was directly correlated with the amount of carboxylic acid group[76].

- SO_2 abatement can be realized by gas phase oxidation[80] into SO_3 and liquid phase oxidation into H_2SO_4 catalyzed by carbon material in the presence of molecular O_2[81]. The activity was directly correlated with the amount of certain basic groups as suggested by the enhanced catalytic performance of heat treated carbon material[82] or N-functionalized carbon material[Error! Bookmark not defined.].

- NO_x abatement is conduced by selective catalytic reduction with NH_3, in the presence or absence of O_2, by means of carbon catalyst[83]. In this reaction the coexistence of both acidic and basic site was the key point to assure a high catalytic activity[84]. Alternatively, the catalytic oxidation to NO_2 is used for the removal of NO from the effluent gas. Successively the NO_2 can be converted in nitrate by reaction with aqueous basic solution.

- H_2S can be adsorbed and catalytically oxidized by porous carbon into SO_2 or S. Important properties of the carbon material for this application are: developed microporosity of very small micropores and high concentration of nitrogen basic-sites[85].

- Oxidation of organic pollutants by H_2O_2 or O_2 can be catalyzed by carbon material. In this application the electron transfer capability of the basic site in the carbon material are claimed to be involved[86] in the formation of surface radicals species which are thought to be the oxidant species in liquid phase oxidation[12].

- Hydrodehalogenation of chlorinated of organic compound can be catalyzed by basic nitrogen functionalized carbon material[17].

- Knoevenagel condensation for the synthesis of fine chemicals was carried on recently by using N-containing CNTs as basic catalyst[108]. The pyridine-like species are suggested are active site for the reaction.

2.2.4.2 Carbon as catalyst support

- Hydrogenation reactions of different organic substrate have been carried on metal supported carbon material catalyst. Ni/B/CNT catalysts have been used for the selective partial hydrogenation of acetylene to ethylene. The treatment of the support with NH_3 improves high metal dispersion which turns out to have positive effect on the reactivity and selectivity. Liquid phase hydrogenation of cinnamaldehyde has been performed over Pd supported on CNF, CNT and AC. Pd/CNF catalyst are more reactive than Pd/AC catalyst. Pt/CNF has been also used in this reaction. The removal of oxygen-functional group by heat treatment leads to a substantial increase of the activity and selectivity to cinnamaldehyde. The hydrogenation of nitrobenzene into aniline in liquid-phase was carried out on palladium deposited inside MWNTs[87]. Slightly improved catalytic performances are observed with respect to the Pd/activated charcoal. This fact was explained in terms of mesoporous textural properties of the MWNT which by-pass the problem related to the mass-transfer of reactant and product occurring in microporous carbon.

- Liquid phase Oxidation of alcohol was carried on different noble metal supported catalysts[88]. For instance it was reviewed that Pt/C gives better catalytic performance in the cinnamyl alcohol oxidation than other noble metal catalyst supported on oxide. Recently, CNTs and CNFs have been used as support for

noble metal and used to catalyze the oxidation of glycerol to higher added value compounds.

- Fuel Cell electrocatalysis is one of the most relevant applications of CNFs and CNTs as support. Researches on the topic have shown that Pt supported on CNF are better electrocatalysts than commercial Pt /carbon black electrode in PEM fuel cell[89,90,91]. This was attributed to the CNF porous structure and to the better Pt–support interaction through the surface oxygen groups of the support. In other studies N-CNFs have been used as electrocatalyst for oxygen reduction in alkaline fuel cells[21]. With respect to the nitrogen free CNFs, N-CNFs shows better electro catalytic performance attributed to the presence of Fe-N-C surface complex in the nanotube structure which are thought as active sites. A recent study[20] has shown indeed that the realization of a metal-free electrocatalyst for the oxygen reduction reaction (ORR) in fuel cell as replacement of noble-metal based electrode is possible. Vertically aligned N-CNT_S, after the complete metal purification, have shown a much better electrocatalytic activity, long-term operation stability than conventional platinum based catalysts.

- The electrocatalytic conversion of CO_2 to fuel was carried on Fe and Pt nanoparticles supported on CNTs[92]. Although the catalysts suffer faster deactivation it is demonstrated that this difficult and challenging reaction could be realized with reasonable productivities.

- Liquid-phase synthesis of methyl isobutyl ketone MIBK from acetone and H_2 was carried on Hydrotalcites supported on CNFs with higher specific activity than that of unsupported catalysts[93].

- NH_3 decomposition was carried on successfully over commercial Fe- or Co-containing carbon nanotubes[94].

- Photocatalytic water splitting was carried on TiO_2 supported on carbon material. A significant increase in the photocatalytic activity was observed with respect to the unsupported TiO_2[95]. The facile reuse of the C-TiO_2 composite together with

the enhanced photocatalytic performance induced by the carbon material used open chance for the development of this technology.

2.2.5 Future prospective for N-containing NC

The need for developing highly selective and active catalysts has lead to the research of new synthetic strategy which mimics the highly specific chemical structure encountered in bio-systems. Biomimetic strategy offers large possibility in catalytic applications involving homogeneous transition metal catalysts and acid/base catalysts. The field of bio-catalysis is dominated by enzymatic catalytic systems made by polypeptides units. Such systems are very often composed by macromolecular N-containing heterocyclic units offering highly coordinative capabilities. For instance, the vast series of cytochromes are composed by porphyrin rings showing different properties depending on the type and oxidation state of the coordinated metal and on the ligand. On the other hand, strong bases with purine-like structure can find application in base-catalyzed reactions. Recently, it was reported that amine catalyze Diels−Alder cycloaddition between cyclopentadiene and dienes[96]. Furthermore, metal-free catalytic transfer hydrogenation of α,β-unsaturated carbonyl compounds was catalyzed by imines[97]. However, the strict environmental regulations on matter of waste disposal lead to a tendency of developing processes based on heterogeneous catalytic systems rather than homogeneous. Traditional approaches for combining the selectivity control of homogeneous catalysis and the easy separation and reuse of heterogeneous catalysis employ the anchoring of a metal complex at the surface of a support. For this purpose, zeolites and micro and mesoporous aluminosilicates have been the focus of research due to their shape selectivity which mimics the role of ligands in enzymes[98].

In analogy to the biological system, nanostructured carbons are a potential substrate with a surface chemistry that can be tailored to imitate the specific active site of the bio-molecules.

In this contest, N-containing NC plays a dominant role. N-containing NCs open possibilities for carrying out heterogeneous processes approaching homogeneous-like conditions. The chemical properties of N-containing NC embrace different fields of catalytic applications from redox catalysis to acid/base catalysis and bi-functional

catalysis. For instance, the introduction of a nitrogen complex at the vacancy or at the edge of the graphene layer in a pyridine-like fashion resembling the structure of the nitrogen units encountered in biological systems offers isolated sites for metal ion anchoring.

Another interesting aspect of N-NC is related to the application as basic catalyst. The use of basic heterogeneous catalysis is a branch of research in rapid development. Especially in fine chemistry synthesis, basic solid materials often show better performance than the acidic counterpart, either when used as catalyst[99] or as support for the active species[100]. The possibility to model at the atomic level the surface properties of NC by the introduction of nitrogen species in the aromatic ring in a conjugated situation that remark the structure of purine-bases is a very big challenge for obtaining super-strong basic material.

It should be noticed that the introduction of N species in the NC structure leads to improved redox properties of the material opening chances for the realization of metal-free catalysis[20]. Finally, N-NC can potentially be used to accomplish CO_2 fixation in analogy to the recently reported successful application of N-heterocyclic carbenes to CO_2 capture[101].

3

Experiments and characterization methods

The following chapter describes the experimental part and the characterization techniques used in this work. The first part is dedicated to the synthetic procedure for N-functionalization of NC. Following, the preparation of the Pd-based catalysts and the catalytic test condition are reported.

3.1 N-functionalization of NC

Various methods can be applied to introduce nitrogen in the structure of CNTs[102,103,104,105]: Magnetron sputtering[103], laser ablation[104,105], pyrolysis of nitrogen-containing organic molecules in the presence of organometallic catalyst[106,107], and CCVD of nitrogen-containing hydrocarbons over heterogeneous metal supported catalyst[108,109,110]. Most of the studies reported in literature have focused on CCVD of N-containing hydrocarbon. The main reason is that it is a high yielding process compatible with an economical scaling-up. Nowadays the state-of-the-art in N-CNTs synthesis by CCVD has not yet reached such level of knowledge as being able to control the process and there is a need for further investigation to understand the key factors driving the growth process. A wide range of catalytic systems have been tested in the CCVD. Basically, all systems active for growing CNTs can be used in the presence of nitrogen-containing hydrocarbons. In most of the literature studies, nitrogen insertion produces disordering due to a local bending of the planar graphitic structure and to the local

expansion of the π-π interlayer distance. Very often the incorporation of nitrogen affects the CNT growth leading to compartmentalization of the tubes in a typical *bamboo-like* fashion[107, 115].

However, systematic and detailed studies aimed at rationalizing the influence of the synthesis parameters are still missing in literature.

An attempt to discriminate between the synthesis condition chosen and the impact on structural properties was reported recently[111]. By investigation of several aspects of N-CNTs growth, i.e. the influence of the C/N source, type of catalyst and synthesis temperature, the authors were able to define some optimal parameter aimed to address the synthesis of N-containing CNTs to obtain a high amount of specific nitrogen functionalities.

However, the synthesis of N-CNTs with high concentration and uniform distribution of nitrogen sites is still challenging. Controlling simultaneously the localization of the nitrogen functional groups and the tube morphology is one of the main tasks. Literature reports high variability in the nitrogen concentration in different tubes within the same sample batch[112] and along the cross section of one single tube[113]. Theoretical calculations[114] are in agreement with the experimental evidences, which show that nitrogen is present with higher probability in the internal wall, and localized where the graphene layer is bent[107], or as molecular nitrogen encapsulated in the compartment of the bamboo-like structure of CNTs[115,116]. Controlling the growth process in the case of N-CNTs appears to be more complicated than for CNTs. Different morphologies are expected depending on the kind of nitrogen species and on the concentration[117]. In fact, depending on the type and concentration of nitrogen moieties, different degrees of disorder are obtained, i.e. bending, corrugation, edges and vacancies.

The important issue in N-CNT synthesis is the control of the process in such a way as to induce a specific chemical configuration of nitrogen, which must be located in an accessible position to be available for catalysis.

In order to introduce nitrogen in the structure of NC, other alternative routes can be taken into account. NC can be though as an extended system of condensed aromatic rings, thus all the reaction known in organic chemistry synthesis could be applied to. In fact a lot of work has been done in order to attach specific moieties on the surface of CNTs[118]. This

kind of approach is used for the development of CNT-based materials such as sensors and bio-sensors.

In analogy to AC[12], the surface of NC can be nitrogen-functionalized by post synthesis treatments, using N-containing molecules such as NH_3 and HCN. With respect to the CCVD synthesis, it is expected that better control of the type of nitrogen introduced functionalities may be achieved without affecting the textural properties and NC morphologies of the starting NC structure. If the starting NC presents fibers or tubes with homogeneous morphologies and nanostructure, a uniform degree of nitrogen functionalization is expected. Furthermore, such treatment introduces functionalities on the surface of carbon, which are accessible to the reactant once applied in catalysis. Such material could be considered a model system for investigating the "*nitrogen effect*" in catalytic or electro-catalytic application, without the uncertainty due to the different morphologies obtained with other synthetic methods.

3.1.1 Material and functionalization procedure

Commercial carbon nanofibers used in this study have been supplied by *Pyrograf Products*, Inc. The nomenclature used by the company, PR24PS, refers to the specific grade. PS stays for *Pyrolytically Stripping* which is the post-treatment applied to the as-produced fiber in order to remove the polyaromatic hydrocarbons from the surface. SEM images (Fig. 3.1) show heterogeneous morphology of the fiber with an average diameter

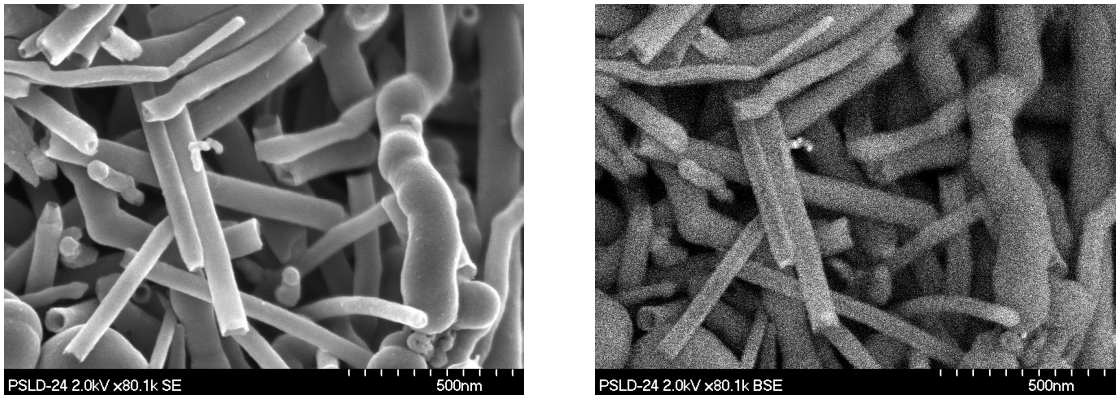

Fig. 3.1: SE and BSE images of the starting VGCNFs.

of 88 ± 30 nm. The presence of catalyst impurities was determined by X-ray fluorescence spectroscopy (XRF). They are composed mainly of catalyst traces (Fe, S) and traces of impurities such as Mg, Cl, Ca, Cr. HRTEM image (Fig. 3.2) shows the structure of these fibers which are made up of two differently structured layers.

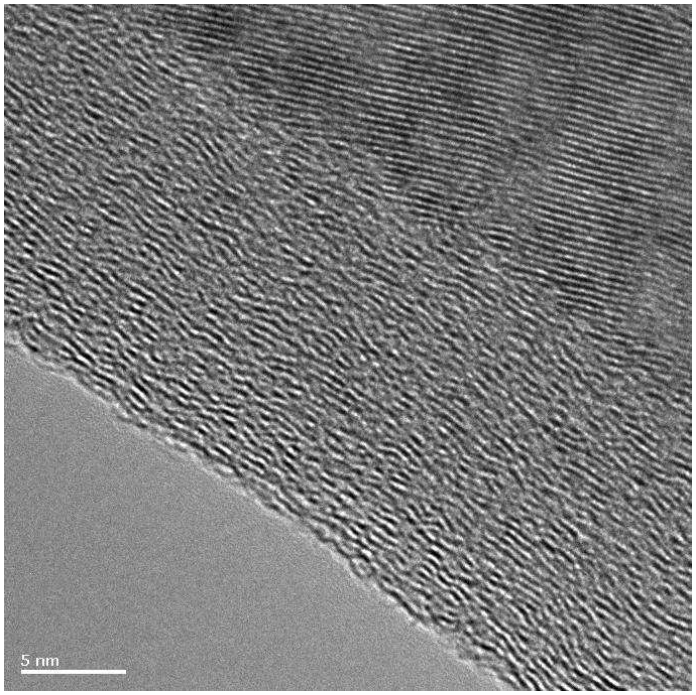

Fig. 3.2: HRTEM images for VGCNFs

The inner layer is composed of angled graphite sheets. This morphology, termed "stacked cup" or "herringbone", generates a fiber with exposed edge planes along the entire surface of the fiber. The second layer covering the CNF surface is due to deposited pyrolitic carbon so called turbostratic graphite. Detailed characterization of these nanofibers was conducted in within the working group and reported recently in literature[119]. The measured specific surface area is $55 m^2 g^{-1}$. N_2 isotherm (Fig. 3.3) shows a mesoporous texture with heterogeneous distributed pores diameter.

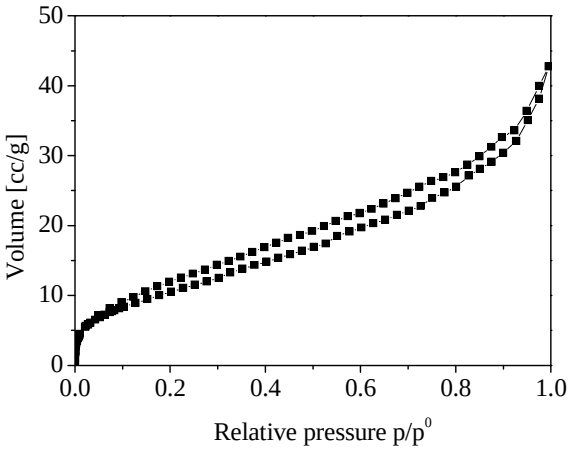

Fig. 3.3: N_2 isotherm of starting VGCNFs

Before the N-functionalization, the nanofibers were treated with HNO_3 in order to create oxygenated functional group that act as a reactive site for the nitrogen insertion. For this purpose the CNFs was suspended in concentrated HNO_3 (20 g of CNF per liter of HNO_3) and kept at 373 K for 2h under continuous stirring. Afterwards, the sample was filtered and washed with 1 liter distilled water and dried at 373 K overnight. During the oxidation the accessible metal impurities are largely dissolved. Aminated samples have been obtained by thermal treatment of pre-oxidized CNFs (10g for each batch) with NH_3 in the temperature range 473-873 K for 4 h. To gain detailed information regarding the importance of oxygen functionalities on the surface of CNFs, amination at 473 K have been performed in the oxidized CNFs on which a thermal treatment in He up to 973 K has been performed for 2 h. Samples notation is reported in Table 3.1.

Table 3. 1: Sample notation and details of correspondent functionalization procedure.

Sample	Characteristic
NCNF473K	CNFox functionalized by NH_3 at 473 K
NCNF673K	CNFox functionalized by NH_3 at 673 K
NCNF873K	CNFox functionalized by NH_3 at 873 K
NCNF873K*	CNFox annealed at 973K in He and then in NH_3 at 873 K
CNFox	CNF functionalized by HNO_3
VGCNF	Vapor Growth Commercial Carbon Nanofiber

3.1.2 Characterization techniques

Characterization techniques used to identify the nature of the functional groups in carbon materials can be classified, to a large extent, in analytical methods (wet- and gas-phase chemical methods) and in spectroscopic methods. The analytical methods have been mainly devoted to the characterization of acidic groups, and to lesser extent, to basic groups. Those techniques include: the liquid phase titration of acidic and basic sites, the more sophisticated Boehm[120] titration of acidic sites that allows to quantitatively discriminating between the different species present on carbon materials by mean of back titration with base of different strength. Less amount of literature is present for the determination of basic sites which is limited to the determination of the total amount of basic sites.

Potentiometric titration[202], gas phase titration by microcalorimetry[121], zeta potentials measurement, and a number of analytical tests used in organic chemistry for the functional group identification[122,123] are also characterization techniques widespread used for solid carbon material. These techniques test the behavior of the material in the medium investigated but do not give direct information about the individual chemical structure of the functionalities. The chemical methods are of practical relevance when the carbon material is used as adsorbent of ionic species and organic pollutants or as a support for a metal. These techniques are nevertheless important in view of the application in acid/base catalysis. The results of the characterization by potentiometric titration, microcalorimetry, and zeta potential are reported in chapter 5. The spectroscopic techniques lead to a description at atomic level of the functional groups. Among the spectroscopic methods, techniques such as FTIR[124,74], TDS[182-188], XPS[149-163], NEXAFS[74,125,126], EELS[127], UPS, ESR[76] have been employed in literature to identify the nature of the surface species in graphite and graphite-like materials. However, all the mentioned techniques present some limitations in assessing the chemical identity of the functional groups and this is the reason why they are often used in combination. In this work, X-ray photoelectron spectroscopy and TPD have been applied and reported in Chapter 4. The hydrophobic-hydrophilic properties of the VGCNFs and functionalized samples have been determined by means of contact angle measurements[128]. Following the description of the characterization techniques used in this work is presented.

3.1.2.1 XPS

X-ray photoelectron spectroscopy is a surface analysis technique widely used for obtaining information about the elemental composition, chemical state and electronic state of the elements present in the material under investigation. When a sample is irradiated by a beam of soft X-rays (200-2000 eV), atomic core electrons are emitted from the matter as consequence of the photoelectric effect. The kinetic energies of the emitted photoelectrons are related to their original electronic states through the following equation:

$$BE = h\nu - E_k - \Phi \quad \textbf{(1)}$$

where *BE* is the so called binding energy, which is designated as the energy needed to remove an electron from the ground-state to the vacuum level; *hν* is the energy of the incident X-ray photons, E_k is the kinetic energy of the emitted electron and Φ is the work function of the spectrometer. The variation of the BE of a certain atom, the so called chemical shift, depends on the chemical environment of the atom which is ionized (initial state effect) and on the hole relaxation processes following the primary electron photoemission process (final state effect). Thus the BE shift gives information about the chemical structure of the atom under investigation. Since for solids, photoelectrons can escape only from a depth on the order of nanometers (5-10 nm), XPS is a surface sensitive technique.

Experiments**:** The experiments have been performed at the synchrotron radiation facility BESSY (Berliner Elektronenspeicherringgesellschaft für Synchrotronstrahlung) located in Berlin using monochromatic radiation of the ISISS (Innovative Station for *In Situ* Spectroscopy) beam-line as a tunable X-ray source[129]. Additional XPS experiments have been performed using the high brilliance radiation of the undulator U49/2 as an X-ray source[130,131] as specified. XPS measurements have been performed in HV condition (pressure of 10^{-7} mbar) or in He at 0.5 mbar, according to the specification. In brief, the pellet of CNT samples is mounted inside a reaction cell onto a sapphire sample holder approximately 2 mm in front of the 1st aperture of a differentially pumped electrostatic

lens system. The homebuilt electron lens serves as the input system for a (modified) commercial hemispherical electron analyzer (PHOIBOS 150, Specs-GmbH). For the temperature programmed XPS experiments, heating is provided by a NIR laser at the rear of the sample and monitored by a thermocouple attached directly to the sample surface. The heating rate was fixed at 5 K/min or 10 K/min. The gas phase composition is monitored via a quadrupole mass spectrometer coupled to the spectroscopic characterization by XPS. For some experiments performed in "high pressure", helium was introduced to the cell with the pressure of 0.5 mbar in the XPS chamber.

The O1s, N1s envelopes were curve-fitted using mixed Gaussian–Lorentzian component profiles after subtraction of a Shirley background[132] using Casa XPS software[133]. In the spectra where the species abundance was close to the detection limit, a linear background has been subtracted. The number of peaks introduced has been determined by applying the difference methods[134,135] to spectra recorded sequentially during temperature programmed XPS experiments[24]. The fitting was done by fixing the peak maximum within ±0.1eV for all spectra and applying a full width half maximum (FWHM) of 1.4 -1.6 eV .

Energy shifts due to surface charging were corrected, when present, by calibration of the N1s and O1s XP spectra with the C1s BE for which the peak maximum was fixed at 284.6 eV[136].

The excitation energy for C1s/N1s/O1s core level spectra were 435/550/680 eV, respectively, resulting in a high surface sensitivity with an inelastic mean free path (IMFP) of the photoelectrons of about 0.86 nm. The spectra have been normalized to the impinging photon flux that has been determined by a cleaned Au foil and corrected for the fraction of higher order and the electron current in the storage ring. Quantitative XPS data analysis was performed by using theoretical cross sections[137] according to the following equation:

$$A = I/ \sigma^* r * n \gamma \quad \textbf{(2)}$$

where A is population of atom of the species A, σ is the theoretical cross section, r is the ring current in mA and n γ is the number of photon per mA ring current (photon flux).

3.1.2.2 TPD-MS

Temperature programmed desorption (TPD) is a technique used to characterize the chemisorbed species at the surface of a certain material. It also turns out to be very useful for the characterization of the functional groups present in a material.

When the sample is subjected to a temperature program in inert gas flow, and at atmospheric pressure, the thermal desorption of the species occur and the masses are simultaneously detected by a mass spectrometer.

The intensity of each mass as a function of temperature is the TD spectrum. The temperature at which the molecule starts to evolve is a measure of the BE of the molecule with the adsorption sites at the surface of the material under investigation. TDS does not directly characterize the chemical structure of the species, but by coupling the information of thermal desorption and mass spectroscopy is still possible to gain knowledge about the chemical nature of the species generating the mass fragments. The amounts of adsorbed molecules on the surface can be obtained from the intensity of the peaks, which preclude calibration of the mass spectrometer. When thermal desorption is used to study kinetics of adsorption and desorption, special equipment allowing operation in UHV conditions is required in order to minimize influence of contaminants. The TPD experiment may also be carried out in a thermo-gravimetric set-up, whereby the weight loss of the sample during temperature program can be recorded as function of temperature.

Experiments**:** Temperature programmed desorption analysis was done using a TPA instrument in the temperature range from 298 to 1423 K. In each experiment, about 15 mg of sample were placed in a tubular quartz reactor which was fed with 100 $mLmin^{-1}$ of He, with a heating rate of 5 K/min. The gas-phase products were transferred through a heated quartz capillary to a Balzers OmniStar quadrupole mass spectrometer operated in SIM mode.

3.1.2.3 Textural properties

The analytical methods for the determination of the textural properties, i.e. specific surface area and porosity of a solid material, are based on the physical adsorption of a gas at its condensation temperature, generally N_2 at 77 K. Among the different theories that have been developed to calculate specific surface area from an adsorption isotherm, the *Brunauer, Emmet and Teller* method[138] (BET) is the most widely used. BET theory is an extension of Langmuir model applied to multilayer adsorption. According to this theory the adsorption of the second layer starts when the first monolayer is complete. Thus from the measure of the amount of gas adsorbed to reach the monolayer, the surface area is obtained. The *Barrett-Joyner-Halenda* (BJH)[139] method is the most commonly used for calculating pore size distributions from the desorption branch of the N_2 isotherm.
The instrument used in this work is a Quantachrome Autosorb-6B KR sorptometer. The samples were previously outgassed at 473 K for 2 h under vacuum. The total surface area was calculated using the BET equation. Pore size distributions were determined using the BJH method.

3.1.2.4 Potentiometric titration

A potentiometric titration was carried out on the samples using a Mettler Toledo Titrator for the determination of the basic sites. Optimization of the procedure leads to the following conditions: about 0.2 g of sample were suspended in 50 ml of KCl $1*10^{-3}$ M, sonicated and equilibrated for several hours. Before each measurement, the suspension was continuously saturated with Argon to eliminate the influence of CO_2 until the pH was constant. Volumetric standard of HCl (0.01 M) was used as titrant, starting from the initial pH of the CNTs suspension. The pK_a value is calculated as the pH at a volume of titrant added corresponding to half of volume at the equivalent point (EQP).

3.1.2.5 Microcalorimetry

Adsorption microcalorimetry is used to evaluate the surface property of a solid by means of measuring the heat of adsorption of a specific molecule. Using this technique the

acid/base properties as well as the hydrophobic/hydrophilic properties of a solid can be determined. The differential heat of adsorption of a probe molecule, either basic (NH_3, pyridine etc.) or acid (CO_2, SO_2 etc.) measured as function of coverage, gives information about the strength and the distribution of the respective acidic and basic sites present on the surface. If coupled with other techniques (i.e. FTIR), it allows one to identify the nature of the adsorption sites.

Experimental: The heats of adsorption were measured in a MS 70, Setaram microcalorimeter of the Tian-Calvet type (C80 and HT from Setaram), combined with a house-designed high vacuum system, which enables the dosage of probe molecules within a range of 0.02 µmol. The pressure-controlled dosing system with calibrated volume allows for the detection of adsorbed amounts of molecules (adsorption isotherm) as well as differential heat of adsorption and gives the possibility to elucidate the distribution of the adsorption sites along the range of adsorption heats[140].
The samples were pretreated and activated under mild conditions to minimize thermal and mechanical stress. All samples were pressed under low pressures (125 MPa) and cut into small pellets, which were sieved to a diameter of 0.4 to 0.6 mm.
The activation was conducted separately in the calorimetric cell connected to a turbomolecular-pump (Balzers). The activation was performed for 17 h at 373 K with a heating rate of 2 K/min. The final pressure in the degassed cell was approximately 10^{-6} mbar. The cell was cooled down to room temperature, placed inside the calorimeter and connected to the micro calorimetric gas-adsorption system. Following this, CO_2 (4.5, Messer Griesheim) was dosed stepwise at 313 K. Pressures (mbar), adsorption temperatures (K) and the heat signals (V) were recorded.

3.1.2.6 Zeta potential measurement

The zeta potential is the electric potential at the interfacial double layer (DL) between the medium and the stationary layer of fluid attached to the dispersed particle in the medium. Zeta potential gives a quantitative indication of the magnitude of the electrical charge at the double layer, which is directly correlated to the surface charge of the dispersed particles. The experimental procedure used to determine the zeta potential is based on a

different physical principle. For instance, the zeta potential is calculated using theoretical models which are applied to the electrophoretic mobility of the particles determined experimentally in appropriates apparatus. In this work zeta potential measurements were performed using a Malvern Zetasizer. In practice, the Zeta potential of the particles dispersed in a suspension is measured by applying an electric field to the dispersion. Particles within the dispersion will migrate toward the electrode of opposite charge with a velocity proportional to the magnitude of the zeta potential. The velocity is measured using the technique of the Laser Doppler Anemometer.

The frequency shift or phase shift of an incident laser beam caused by these moving particles is measured as the particle mobility, and this mobility is converted to the zeta potential by the application of the Smoluchowski model. The mobility of the particles is measured as function of the solution pH in such way to determine the isoelectric point. The isoelectric point is defined as the pH value at which the zeta potential is zero. At this value, the sum of the positive charge compensates the negative charge so that the surface is neutral, therefore, at this pH no particle migration occurs. Before impregnation of metal ions on a polar support, it is convenient to determine the isoelectric point of the support and of the metal sol.

Briefly, since the ions adsorption on a surface occurs by electrostatic interaction[141] between the ionized species on the carbon surface and the ionic species present in the solution, the catalyst preparation must be optimized in order to realize an attractive interaction.

At pH below the pH_{IEP} the resulting surface charge is positive and will attract anions, above it, it is negatively charged and will attract cations. The experimental procedure used in this work for the determination of the zeta potential is the following: approximately 5 mg of CNFs were dispersed in 50 ml of $NaClO_4$ and sonicated for 10 min. Following the suspensions were kept at 298 K and the pH adjusted to a value of 12 by using 0.1 M sodium hydroxide. A titration was performed from pH 12 to pH 2 by addition of 0.1 M hydrochloric acid and the zeta potential was recorded as function of pH.

3.1.2.7 Contact angle

Hydrophobic or hydrophilic properties of solid surface are important in any application where wetting of solids by liquids plays a role, such as adsorption, or catalysis - especially in the case of multiphase reaction systems containing both gas and liquid phase together with a solid catalyst. The surface hydrophobicity or hydrophilicity of a solid determines the range of its prospective applications. The driving force of the adsorption of a substance on a solid surface can have an electrostatic or dispersive nature[141]. The electrostatic interactions contribute to the hydrophilic character of the surface, while the dispersive force to the hydrophobic character. In the majority of real solid surfaces, hydrophobic or hydrophilic sites coexist on the surface. Thus the relative contributions of those forces define the predominant character of the surface. The macroscopic observable parameter reflecting those interactions is the contact or wetting angle between the liquid phase and the solid phase. The same concept can be applied for the evaluation of the interaction of a metal particle with the solid surface through the wetting angle. The relation between the contact angle and the solid surface tension is given by the Young equation:

$$\text{Cos}\theta = (\gamma_{sg} - \gamma_{ms}) / \gamma_{mg} \qquad \textbf{(3)}$$

Where γ_{sg} is the surface free energy at the interface underlying solid-gas, γ_{ms} is the surface free energy at the interface sessile drop(particle)-underlying solid and γ_{mg} is the surface free energy at the interface sessile drop (particle)-gas.

A surface is considered hydrophilic when the contact angle of a sessile drop of water on the surface is less than 90°, and hydrophobic when greater than 90° as shown in Fig. 3.4.

In the same way, the particle shape depends on the balance of the surface free energy at the three interfaces. Between two extremes of not wetting (θ= 180°) and complete wetting (θ= 0°), situation of intermediate interaction exist as illustrated in Fig. 3.4.

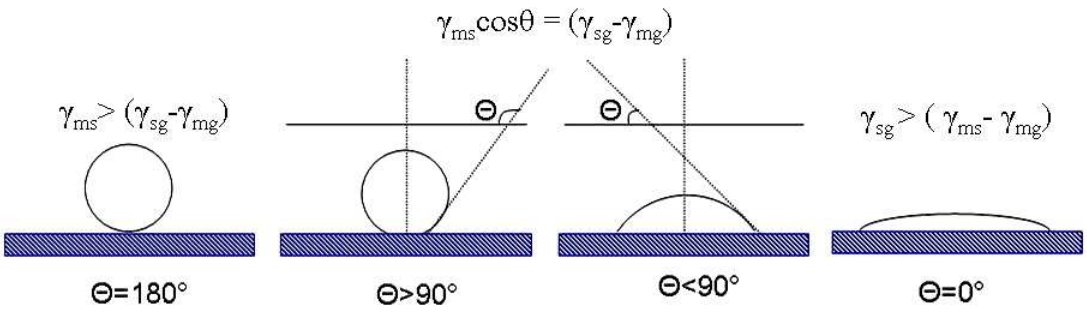

Fig. 3.4: The contact angle θ of a liquid drop over a solid surface[142]

3.1.2.8 Elemental Analysis

Overall nitrogen and oxygen contents were determined using a LECO TC-300 / EF-300 N/O analyzer (hot gas extraction). After thermal decomposition of the samples in a Ni/Sn/Pt-melt at ~3000 K under helium atmosphere (graphite-heated resistance furnace, graphite crucible), the oxygen content was determined by measurement of the CO_2 concentration (after oxidation of CO) with an IR-cell. Analysis of the nitrogen concentration was carried out measuring the thermal conductivity of the helium/nitrogen mixture after absorption of CO_2. The accuracy is ~2 % of the N/O present.
The Pd content was determined by XRF spectroscopy using a wavelength dispersive X-ray fluorescence (WDXRF) Bruker S4 Pioneer spectrometer. Typically, 0.5 g of sample were deposited inside a polystyrene holder (34mm in diameter) and covered with a 4 µm polypropylene foil. The measurements have been performed under He atmosphere.

3.2 Pd nanoparticles onto the surface of N-containing VGCNFs for the liquid phase selective oxidation of benzyl alcohol to benzaldehyde.

Metal nanoparticles have attracted a great interest in scientific research and industrial applications due to their uniquely large surface-to-volume ratios and quantum-size effects[143]. Because of these outstanding properties, differing from those of the bulk metal, metal nanoparticles mimic homogeneous catalytic systems leading to improved selectivity and efficiency in heterogeneous catalysis. For this reason they have been considered as promising materials for catalysis. In view of any potential application, one important issue is the control of the size and the shape of the metal nanoparticles.

Those directly observable characteristics of the metal nanoparticles are related to special structural features, which are the determining factors for the high selectivity. That is, the selectivity of the nanoparticles is size-dependent. For this reason, the target in the synthesis is to approach the ideal mono-dispersion.

Another issue is the stability of those nanoparticles in the application environment. In view of the catalyst recycling, metal nanoparticles–based catalysts are often assembled into macroscopic structures via immobilization or grafting onto inorganic or organic polymer supports. One of the approaches used to synthesize metal nanoparticles consists of the preparation of a colloidal solution of metal nanoparticles by reduction of metal salts in solution in the presence of a protective agent[144,145,146].

The protective agents, usually donor ligands, polymers, and surfactants, by means of different action mechanisms (steric, electrostatic or through ligand interaction[143]) have the role of controlling the growth of the initially formed nanoclusters and to prevent them from coalescence by wrapping around the nanoparticles. It forms a protective interface layer which also preserves the long term stability.

An obvious advantage of the metal colloid deposition with respect to the conventional salt-impregnation method is that both the size and the composition of the colloidal metal may be tailored independently of the support. The size of the nanoparticles is also determined by the kind of protective agent and by the strength of the reducing agent[146]. The stronger the reducing agent, the smaller the nanoparticle formed. Furthermore, it is not necessary to carry on any other thermo-reductive treatments to obtain the metallic

form, thus preventing the metal sintering or any chemistry modification of the support surface induced by the thermo-treatment.

However, the supports must have a suitable surface chemistry in order to optimize metal/support interactions during immobilization and thus to homogeneously distribute the metal nanoparticles all over the support surface. In the present work Pd nanoparticles have been synthesized by following this afore-mentioned route, which has been optimized and already reported in literature[144,145,146]. The colloidal solution was immobilized on the N-functionalized VGCNF described previously in section 3.1.1. The selective oxidation of benzyl alcohol to benzaldehyde is used as test reaction to explore the potential of functionalized CNFs in stabilizing metal nanoparticles in the reaction media a/o favoring preferential metal phase through metal support interaction. The work presented here is a comparative study on the influence of the surface chemistry of different NC supports on the catalytic properties of Pd-based catalyst.

3.2.1 Catalyst preparation: Immobilization of metal nanoparticles on VGCNFs

Na_2PdCl_4 from Aldrich (99.99% purity), $NaBH_4$ (>96% purity) from Fluka and polyvinylalcohol (PVA) (Mw = 13,000–23,000, 87–89% hydrolyzed) from Aldrich were used. Gaseous oxygen from SIAD was 99.99% pure. First, aqueous solutions of PVA (2%, w/w) and $NaBH_4$ (0.1 M) were prepared. The Pd sol $Na_2PdCl_4 \cdot 2H_2O$ (0.043 mmol) and PVA solution (880 μl) were added to 130 ml of H_2O. After 3 min, $NaBH_4$ solution (860 μl) was added to the yellow-brown solution under vigorous magnetic stirring. Successively the sol was immobilized by adding the CNFs and thus the suspension was acidified at pH 2 by sulphuric acid under vigorous stirring. The amount of support was calculated as having a final metal loading of 1 wt%.

3.2.2 Catalytic test: liquid phase oxidation of benzyl alcohol to benzaldehyde

The reactions were carried out in a thermostatic glass reactor (30 ml) equipped with an electronically controlled magnetic stirrer. The oxygen uptake was followed by a mass flow controller connected to a PC through an A/D board. The catalytic tests have been carried on in solventless condition and in aqueous solution fixing the metal/alcohol ratio

to 1/3000 mol/mol and the total volume at 10 ml. For the reaction in water, the alcohol concentration was 0.3 M. The reactor was pressurized at a pressure of O_2 of 2 atm and thermostated at 353 K. The reaction was initiated by stirring. When using the organic solvent, periodic sampling of the solution from the reactor was performed, whereas in the case of water as solvent, the product mixture was extracted with acetone at the end of reaction. Identification and analysis of the products were done by GC-MS and GC using a Dani 86.10 HT gas chromatograph equipped with a capillary column (BP21 30 m×0.53 mm, 0.5 μm film; SGE) Quantification of the reactant products was done by the external calibration method.

3.2.3 Catalytic test: liquid phase oxidation of H_2 to H_2O_2

Catalytic oxidation tests of H_2 to H_2O_2 were carried out in a stirred stainless steel reactor coated with Teflon (capacity 250 ml), containing 50 mg of catalyst in a fine powder form and 150 ml of anhydrous CH_3OH as a reaction medium. A gas mixture containing 7.5 vol% of H_2 with a H_2/O_2 ratio of 1:2 and CO_2 was bubbled continuously through the reaction medium under vigorous stirring at room temperature until the pressure reached the set value of 6.5 bar. The reaction products were analyzed by potentiometric titrations of H_2O_2 (*Metrohm, 794 Basic Trino*) and H_2O (*Metrohm, 831 KF Coulometer*), respectively.

3.2.4 Characterization of Pd/CNFs based catalysts by Electron Microscopy techniques

Electron microscopy techniques are powerful tools for the local investigation of the morphology, nanostructure, dispersion and size distribution of supported-.metal nanoparticles. The information is derived from the detection of the signal generated by physical processes occurring as consequence of the interaction of the electron beam with the matter. When electrons interact with a target material, they might scatter elastically or inelastically. The elastically scattered electron can be forwarded through the sample or backscattered. The inelastically scattered electrons transfer the energy to secondary processes such as Auger electron and x-ray emission. Those processes are reported in Fig. 3.5.

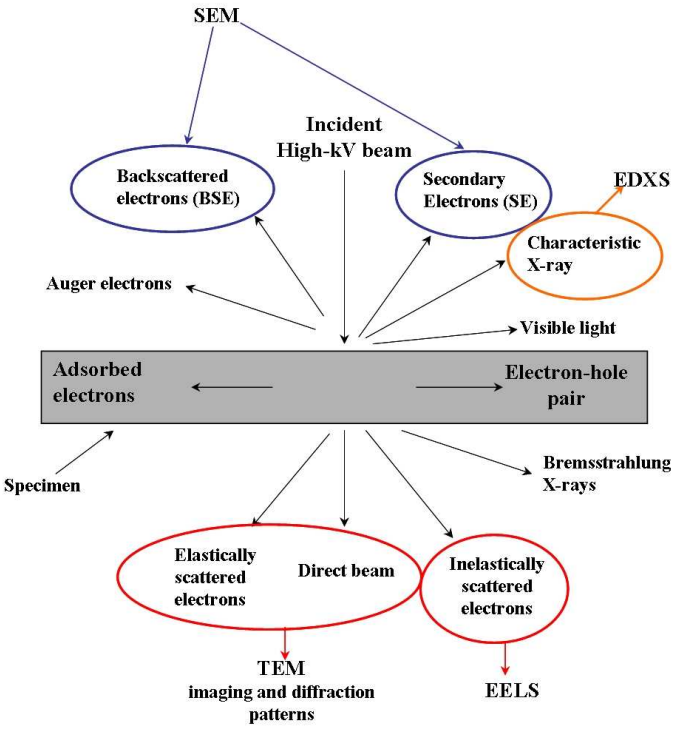

Fig. 3.5: Schematic representation of the Interaction of the electron beam with the matter (Adapted from[147]).

In the *Scanning Electron Microscope* (SEM), the images are formed by the detection of secondary electrons and elastically backscattered electrons. The secondary electrons have low energy so that they are emerging from the sample with a probing depth of few nanometers, depending on the acceleration voltage. For this reason secondary electrons give information about the surface morphology. The probability of back scattered electron (BSE) is proportional to the atomic mass of the elements, thus images in BSE mode give information about the elemental composition of a samples. Standard SEM instruments are always equipped with EDX detector, which gives information about the elemental composition by analyzing x-rays emitted in the relaxation process that follow the generation of the hole in the core shell due to the interaction with electron beam.

A *Transmission Electron Microscope* (TEM) operates in diffraction mode or in image mode. The diffraction mode produces the diffraction pattern of the sample when the electron beam is in Bragg condition. The transmitted electron beam forms an image, which is a two-dimensional projection of a three-dimensional object in the direction of the beam. Images formed by the large angle elastically scattered electrons are characterized by a contrast which is indicative of mass/thickness. The cross section for

high angle scattering is proportional to the thickness of the sample and the atomic mass of the elements composing the specimen. Thus, assuming the thickness constant, the HAADF give information about the element composition. A TEM might also be equipped with *Electron Energy Loss Spectroscopy* (EELS) detector.

The EELS is based on the detection of the inelastically scattered electrons. The inelastic scattering of the primary electron beam originates from interaction in which a part of the energy of the incident electron beam is transferred to the process of the ejection of an electron from the ground state to the valence band. Thus, the measure of the energy loss of the primary beam gives information about the electronic structure of the atoms and the bonding states of the elements in the specimen. The possibility of coupling all this information output in one instrument makes the electron microscopy techniques very powerful and established characterization techniques in catalysis. It should be however emphasized that due to the high resolution of the instrument they give only a local view of the system under investigation.

Different microscopes have been used in this work:

- A Hitachi S-5200 Scanning Electron Microscope (SEM) coupled with EDX detector for elemental analysis was used to investigate the surface morphologies of the nanoparticles and of the VGCNFs. The samples under investigation have been deposited on conduction carbon tape. All images were acquired using an acceleration voltage of 3 kV for better resolution of surface features, and 15 kV to investigate the inner cavity of the VGCNFs.

- The microstructure of the carbon samples and the supported catalyst was investigated by Transmission Electron Microscopy (TEM). HRTEM have been performed with a Philips CM200 TEM FEG equipped with a GATAN tridiem for EEL spectroscopy. The samples were dry-deposited or wet-deposited on a holey carbon film supported on a Cu grid. In order to investigate metal phase and structural defects of the nanoparticles and to get insight in to the immobilization process of metal nanoparticles through the understanding of the metal/support interface and the occurrence of the protective agent a FEI 80-300 Titan microscope equipped with Cs-corrector from CEOS has been used.

4

Characterization methods: XPS and TPD-MS

Nitrogen functionalities on the surface of CNFs are characterized by coupling two experimental techniques: Temperature programmed XPS with on-line MS. Information about the thermal stability of different N and O functional groups and the dynamic surface rearrangement of the functionalities are obtained. These measurements provide a phenomenological approach to the assessment of the nitrogen and oxygen species in the very broad N1s and O1s core level XP spectra.

In the introductory part of this thesis the importance of nitrogen and oxygen functionalities in determining the physic-chemical properties of the carbon surface, such as surface acidity-basicity, wetting and adsorption capability, red-ox properties, hydrophilic-hydrophobic properties, was emphasized. In order to induce specific properties on the NC surface, it is thus very important to introduce functionalities in a selective manner. The approach used in this work is tailoring the surface chemistry of oxidized carbon by means of thermal treatment in NH_3. The first question to answer is then: *how does the treatment temperature influence the distribution of N and O functionalities?* In order to answer to this question, deep characterization of the sample with high resolution analytical tools is necessary. When dealing with carbon material, the deep characterization of the surface functional groups is not an easy task. The characteristic high adsorption of light on carbon excludes the possibility of using IR spectroscopy, which is in principle the best technique for the characterization of functional

groups in organic chemistry. Indeed, XPS and TPD are the most suitable and applied techniques for the characterization of the chemical configuration of the species present on the surface of carbon materials. XPS studies the bonding configuration of the elements present in the sample, while TPD determines the thermal stabilities of the functional groups present on the carbon surface. Coupling the information from both the characterization techniques represents a valid approach in the attempt to assign the chemical nature of the measured XPS and MS signals. In particular, in this work the two characterization techniques are used in *tandem*. XPS measurements are performed sequentially during TPD experiments. When the sample is subjected to a thermal treatment, any occurring surface modification of the functional groups can be monitored by XPS and the gas release recorded by on-line MS. The experiments described following have two aims: on one side the more general and ambitious tentative to asses the BE of nitrogen and oxygen functionalities in graphite-like materials; on the other side to investigate the influence of the functionalization treatment conditions on the distribution of nitrogen and oxygen functionalities. The thermal stability and the surface rearrangement of the functional group are studied as well.

In order to describe and discuss the XPS data, it is necessary to establish the parameter for the fitting of the O1s and N1s spectra. The results of the difference spectra methods[148-134] applied to the XP spectra recorded during a TP-XPS experiment are reported in the Appendix. Literature assignment of the N1s and O1s envelopes and the thermal stability of the functional groups in carbon material determined by TPD are presented in this chapter. Finally, the chemical interpretation of the XPS is reported with emphasis on the influence of the functionalization temperature on the distribution of the N and O functionalities.

4.1 Assessment of N and O species in carbon by means of XPS and TPD

4.1.1 Surface analysis by XPS: Critical aspects

Although XPS is the most suitable analytical techniques for the characterization of the surface functional groups in carbon material, there are some limitations hindering the precise and unequivocal identification of those species. This is reflected in the large amount of literature dealing with XPS analysis of nitrogen a/o oxygen species in carbon materials and in a controversial assignment of the nature of the nitrogen and oxygen components in the N1s and O1s spectra among these data[153-173]. The controversy derives from the high heterogeneity of the carbon surface where a multitude of species are presents. Those species have nearly the same BE in the XP spectrum, not resolvable with the resolution of the analytical tool available nowadays. The peaks overlap with each other rending their assessment complicates. In addition, the surface of realistic nanostructured carbons obtained by CVD of a hydrocarbon, such as CNFs and CNTs, is very often characterized by the presence of a deposit of poly-cyclic aromatic hydrocarbon (PAH). The functional groups in the PAH contribute to the broadening of the XPS spectra. Conceptually, the XP spectrum of a model compound can be used as finger-print for the identification of the species on the surface of a carbon samples. Unfortunately, due to the intrinsic topological heterogeneity of graphite-like materials, it is also very difficult to prepare model system containing only one type of species. When the spectra are broad, the approach often used to solve the problem is the mathematical deconvolution of the very broad XPS peak in singular synthetic components. The main problems faced while analyzing XPS data concern the methods to fit the XP spectrum (number of peaks, peak shape, and type of background) and the assignment of the chemical identity of these peaks. Surface scientists have dedicated a lot of efforts in the understanding of the physic of the photoemission process resulting in the experimentally measured peaks. Although the problem of the peak deconvolution is still an open question, some fitting parameters have been settled nonetheless for comparison with literature work. In particular, N1s and O1s peaks are well described by a G-L curve after a Shirley background subtraction. Still the problems concerns the number of peaks used to fit the broad XP spectrum. In order to identify the different O or N species on carbon material, chemical, electrochemical and

thermal treatments have been applied to the carbon material with the aim of inducing surface modification that can be monitored by XPS[134,148,149,] Early literature has been mainly focused on the assessment of oxygen species in polymers or graphite fibers. In these papers[150,151], the authors analyzed principally the C1s core level and only in few cases there is an attempt to compare these data with the O1s analysis. Different values have been reported for a given species depending on the nature of the matrix in which they are present, if aliphatic[150] or aromatic[151]. Thus, the comparison of the measured BE to experimental BE of model organic molecule or to theoretical calculated for small graphitic domains, cannot be straightforward used to identify the species in graphite-like materials. In summary the scatter of the BE for certain functionalities can be due to the following situations[74]:

- The BE in condensed polyaromatic structure is expected to be smaller than the values obtained for not conjugated cycles.

- The accuracy for the position of the component is dependent upon the relative intensity of the peak. If the atom content is low, the uncertainty may be significant.

- The chemical shift is influenced by the extension of the interaction of the functionalities with the π-system. The size of the graphite domains and the charge redistribution in within the graphite domain due to relative presence of neighboring functionalities also influence the chemical shift for a given functionalities.

- The BE for a given functionality may slightly varies depending on the topology[152] of the termination in which it is located.

Another source of uncertainty in the assignment of the XP spectrum components arise from the presence of a film of adsorbed water, which is not removed in UHV. The relative interaction between neighboring species and the adsorbed water might produce a BE shift, which is not straightforward predictable. For all the listed above reasons, the absolute value of BE for a specified functionality cannot be established, but rather a BE region. It is thus clear than only coupling XPS with other experimental techniques allows the identification of the number and the chemical nature of surface species.

4.1.2 Surface analysis by XPS: literature assignment of nitrogen and oxygen functionalities in graphite-like material

Different nitrogen and oxygen functionalities on carbon with quite different chemical properties are reported[74] and illustrated in Fig. 2.5 (ref. see chapter 2).

Table 4.1 reports some literature data concerning the BE relative to the most common nitrogen and oxygen species in carbon materials[153-173].

Table 4.1: Literature assignments of the BE of the most common nitrogen and oxygen species present in carbon materials.

Type of N	pyridine	amine	amide	Pyrrol/ pyridone	Quarter.	N-oxide/Nitro	Material	Ref
BE [eV]	398.3			400.1/399.5	401.3	403.1	AC	153
	398.7±0.3			400.3±0.3	401.4±0.5	402-405	Char	154
	398.9±0.1			400.9		403.1±0.5	NC	155
	398.3 0.1			400.1± 0.1	401.3±0.1	403.1±0.1	Char	156
	398.7	399.9	399.9	400.7/399.7	402.5±0.5		AC	157
	398.7±0.3			400.4±0.3	401.4±0.3	402-404	Char	158
	398.6±0.1	399.4		400.3	401.5		Coal	159
	398.8±0.1			400.2±0.1	401.4±0.1	402-404	Coal	160
		400.2	399.4				CNT	161
		399.7					SWNT	162
						399.7-403.1	Model	163
						400.2/406	CNT	164
	398.4±0.1	399.4±0.1		400.1±0.1	401.1±0.1	406±0.1	CNF	This work

Type of O	Quinones	C═O	OH	C─O	NO_2	water	Mater.	Ref
BE (eV)	530.9					533.4	CNT	165
		531	534	532.5			CF	149
		531.7;532		533.3-533.8			CNT	166
		531.4				533.5	ACF	167
		530.6		532.3		536.3	AC	168
	531.1	532.3	534.2	533.3	534.3	535.9	AC	169
						533	Graphite	170
		531.6	533.6	532.4		535-536	CF	171
		531.1-531.8	532.6	533.5		535.2	CF	172
		530.3	533	531.6			Graphite	173
	530.7±0.1	531.4±0.1	533.7±0.1	532.4±0.1	533.1	535±0.1	CNF	This work

Acronyms: AC Activated Carbon; NC nanocarbon; SWNT single-walled nanotubes; CF carbon fiber; ACF AC fiber.

In the case of the N1s, the BE values reported in literature scatter slightly for a certain N species, but they are consistent with each other in the assignment to a specific bonding state. For instance, the BE of N in pyridine (to simplify is referred as N1) is well established in literature and can be used as reference for the shift of the other type of species. It lies between 113.7 eV and 114 eV higher than the maximum of C1s peak[136].

In agreement with the theoretical calculation[174], four different BE region have been individuated in the experimental N1s core level spectra of carbon material (Table 4.1): the first region ranging from 398-399 eV refers to the pyridine-like N atoms, considering any forms of nitrogen which contribute to the π system with one p-electron (N1); the second region between 400-400.5 eV refers to N atoms in pyrrol-like configuration donating two p-electrons to the π system (N3).

The N3 is composed of the contribution of pyridone, lactam and pyrrol functional groups; the pyridone functionality is the tautomeric form of the lactam functionality. It can be illustrated as a pyridine functionality having a phenol group in alpha position. Within the accuracy of XPS measurement, pyridone and pyrrol N cannot be distinguished[153-164].

The third BE region at around 2.5 eV higher than N1 (labeled as N4) is usually referred to any form of quaternary nitrogen (N4) including substitutional nitrogen[159], and quaternary N due to intra or inter-molecular hydrogen bond with pyridine or aniline functions. The chemical nature of the quaternary nitrogen, also known as “graphitic” nitrogen is still matter of discussion in literature. An exhaustive analysis about this species was carried out by Buckley[159]. The author argued on the inadequate assignment of this specie to an oxidized form of pyridine nitrogen. The argument was the lower thermal stability that an oxidized form of nitrogen species would have compared to the over mentioned quaternary form of nitrogen. The “graphitic” nitrogen is actually the highest thermal stable nitrogen species found in carbon material. A hypothetical structure of this functionality was derived by analogy of theoretical calculation carried out by Boutique[175] *et al.* on model compound as the one reported in scheme Fig. 2.5 in which nitrogen is incorporated in the graphitic structure replacing a carbon atom. In such configuration, the N atom forms three σ-bonds with neighboring C or H atoms and contributes with two electrons to the π-system. Thus, this nitrogen species carries a formal positive charge. The existence of the “graphitic” nitrogen is however not generally accepted.

In contrary, it is general accepted that the forth region above 402 eV is the region of oxidized forms of nitrogen. Pyridine oxide N5 is shifted to about 4.5 eV than pyridine[24, 153] and up to 6.5 eV there are the nitro functionalities N6[163].

The region between 399-400 eV is less documented in literature and it refers to functionalities in a chemical bonding state that is intermediate between pyridine-like and pyrrol-like configuration. This region is also referred to the region of the N-H bonds. There is a high uncertainty to define the nature of those species (referred here as N2) by mean of the XPS BE shift, since several are the candidates having nearly the same BE: amino group[161] attached to aromatic rings, amide group[176], nitrile groups and nitroso species[163]. The BE for amide and amine reference[161] are at 399.2 eV and 400.2 eV, respectively.

The assessment of the components in the O1s spectrum is even more controversial. As reported by some authors[74,177], the presence of a film of molecular water gives arise to a large O1s signal even in vacuum. This peak interferes with the peak of many oxygen functionalities and misguides the interpretation. Thus, there is no common assignment of the nature of the peaks composing the O1s spectra in graphite and graphite-like materials at the moment. The main disagreement regards assignment of the oxygen atom in carboxyl groups.

Previous study[148,134] has suggested that the C-O single bond in hydroxyl groups fall in the range of 532.3-533.3 eV regardless if due to phenol or carboxylic groups, while the ketone function in the range 531.1-531.8 eV.

By analogy to model acid compound, Desimoni[149,171] *et al.* assigned the peak at 534 eV to carboxylic acids.

Sherwood *et al.*[172] consider the two oxygen in carboxylic functionalities as XPS equivalent, with an intermediate situation between double and single bond, that give arise to the peak at around 532-533 eV. The most convincing description of the O1s XP spectrum consider the following BE regions[149,165-173]: O1 (530.7 eV) usually attributed to a highly conjugated form of carbonyl oxygen such as quinine or pyridone groups[165-136]; O2 (531.1-531.8 eV) is assigned to a carbon-oxygen double bond; O3 (532.6 eV) is the carbon-oxygen single bond; O4 (533.5 eV) refers to oxygen single bond in hydroxyl group. However from literature analysis is very hard to conclude which is the chemical structure of the two different peaks referred as C-O single bond. Note that the position of

water is quite debated in literature[167-172]. Exhaustive studies of adsorption of water carried on polycrystalline graphite have lead to the identification of very broad peak centered at 533 eV[170]. Furthermore, some authors assign the signal O5 above 535 eV to adsorbed water and/or oxygen.

4.1.3 Surface analysis by TPD: Oxygen functionalities

Surface oxygen functionalities on carbon materials decompose upon heating by releasing in gas phase CO_2 and CO at different temperature. These species can be detected in the mass spectrometer following the *m/z* 44 and *m/z* 28 signals.

The decomposition temperature is diagnostic of the chemical nature of the species decomposed. Unfortunately, thermal desorption peaks are quite broad.

In order to assign a chemical identity to the very broad TPD peaks, earlier work[178] has approached the problem by means of the analogy to the decomposition profile of model organic molecules. The thermal stability of organic acid molecules has been studied extensively in literature[179,180] as "finger-print" parameter to identify those molecules.

Furthermore, some authors investigated the influence of several substituents in the aromatic ring of benzoic acid[181] on the thermal decomposition of these species, proving that a shift in the decomposition temperature should be expected depending on the nature and mutual location of neighboring species. In a system where those species coexist, like in carbon material, this fact leads to the overlapping of fragments generated by the thermal decomposition of those species. In addition to that, realistic nanostructured carbons are characterized by a mixture of sp^2/sp^3 bonding configuration due to the presence of both aliphatic and aromatic fractions. The decomposition temperature of a functionality depends on the carbon chemical structure. There is other factors hindering the unequivocally assignment of the nature of the TPD peak to specific groups.

For instance, before the thermal decomposition, the species can undergo to rearrangement on the surface. Two adjacent carboxyl groups can undergo to dehydration and anhydride formation and decompose at higher temperature. Thus, this technique is not suitable for the characterization of species initially present on the sample, being itself a "destructive" technique in which the system can dynamically change. The broadening of the peaks is an indication of the occurrence of chemically different species but, it is also due to the presence of the same oxygen species on energetically different sites. For instance, it was reported[170] that functionalities present in different topological sites (*zigzag* or *armchair*) decompose upon heating at different temperature and thus broadening the TPD peak.

Other sources of controversy in the literature assignment of TPD peaks to specific surface groups are the porous texture of the material, the heating rate, and the geometry of the

experimental system used. These factors affect the re-adsorption of the decomposed species and the mass transfer of the species to the detection system.

Nevertheless some trends have been established[170,182-185]. It was found that oxygen functionalities with acidic character decompose giving arise to CO_2, while the basic species decompose upon heating releasing CO in gas phase. The stronger the acidic character (strongly oxidized species) the lower the decomposition temperature, *vice versa* the stronger the basic character, the higher the decomposition temperature. The temperature range of the thermal decomposition of some oxygen species in inert atmosphere are reported in Table 4.2.

Table 4.2: Literature data for the thermal stability of the most common oxygen species.

Surface group [product]	Carboxylic acid [CO_2]	Lactone [CO_2]	Anhydride [$CO+CO_2$]	phenols [CO]	Carbonyls in quinone-like species [CO]
Temp.	673 K[182] 550-590 K[183] 530- 654 K[184] 400-623 K[185]	900 K[182] 623-823 K[185] 463,573,693,903 K[170] (different sites) 706-792 K[183] 946 K[184]	673-850 K [182] 950 K[183] 770 K[184]	945 K[184] 873-973 K[182]	1070 K[184] 973,1093,1253 K[170] (Different sites) 1073 K[182]

According to the literature, CO_2 desorption appears at lower temperatures and proceeds from the decomposition of carboxylic to anhydride groups (acidic groups) and/or lactone. Those species can be distinguished by the fact that carboxylic anhydrides produce simultaneously to the CO_2 peak an equal amount of CO. On the other hand, CO desorption occurs at higher temperatures from the decomposition of several types of surface oxygen groups (i.e., phenolic, carbonyl, quinones and ether-like weakly acidic, neutral, and basic groups). Based on the value reported in literature, it is possible to quantify the different species by the deconvolution of the broad TPD peak[186,169]. However, in this thesis, the TPD measurements performed on the samples under study (Table 3.1) are reported and qualitatively discussed.

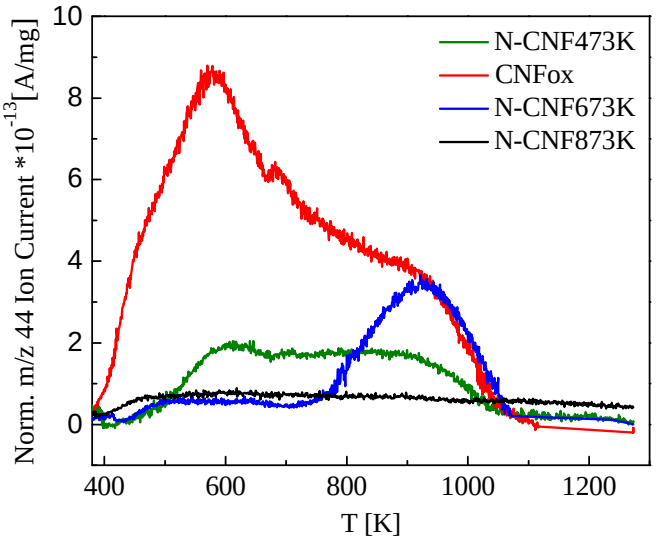

Fig. 4.1: *m/z* 44 traces for the CNFs samples during TPD

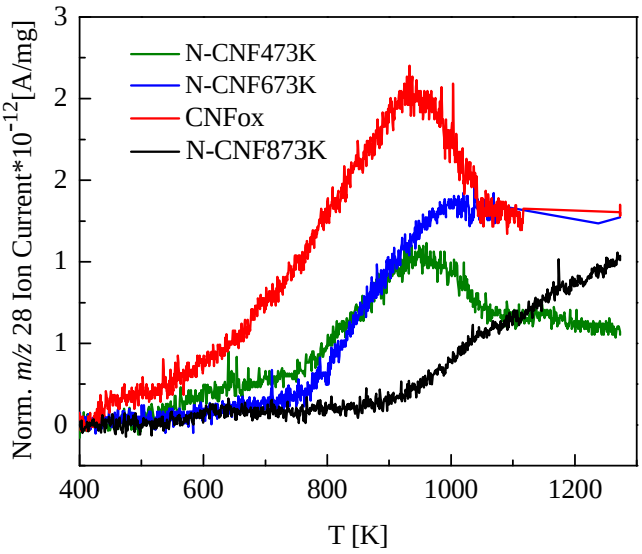

Fig. 4.2: *m/z* 28 signal for CNFox during TPD

Fig. 4.1 shows the evolution of *m/z* 44 during the TPD experiments for all the samples investigated. It can be seen that in the CNTox (red line), the CO_2 desorption is noticeable larger than in the others samples. Qualitatively the *m/z* 44 spectrum for this sample is composed by four components: the shoulder in the low temperature range of the spectrum

can be related to the lowest thermal stable species decomposing below 500 K; the peak II is in the temperature range 500-700 K with maximum at about 600 K. The number of peaks in the temperature range 600-800 K is more difficult to establish, nevertheless the shoulder in this range suggests for a peak III with maximum at about 750 K; clearly a peak IV with maximum at 900 K is present. The presence of those peaks is an indication of the existence of several kinds of oxygen species. The TPD of N-CNT473K (green line) shows *m/z* 44 traces evolving in a large range of temperature. The species (peak I) with thermal stability below 500 K are not present in the sample N-CNT473K while all the other oxygen species present in the CNFox are still retained after the NH_3 treatment at 473 K. However, the amount is drastically reduced (peak II with maximum at 600 K and peak IV with maximum at about 900 K). In the sample functionalized at higher temperature (NCNF673K blue line) only the high thermal stable oxygenated species decomposing through the formation of peak IV with maximum at 900 K in the TP spectra are present. According to data reported in table 4.2, those fragments are generated at that temperature by the thermal decomposition of lactone species. The sample NCNF873K gives arise to a negligible amount of CO_2 upon heating.

Fig. 4.2 shows the CO evolution (*m/z* 28) during the thermal decomposition of the surface functional groups for all the samples investigated. Although CNFox presents the evolution of CO in the low temperature range, for all the samples investigated, CO evolution occurs above 800 K. The samples CNFox, NCNF473K and NCNF673K are characterized by the main peak with maximum at 900 K. This peak is not present in the sample NCNF873K where the CO evolution occurs above 1000 K, indicating the presence of ultra stable OH[187] or quinone-like species. However, the amount of the high thermal stable species decreases while increasing the functionalization temperature. It is thus demonstrated that the thermal and chemical treatment in NH_3 produces on the CNFox surface, modification of the starting oxygen functionalities. In particular the most acidic functional groups such as carboxylic groups and anhydride, initially present on the CNFox, are thermally decomposed or converted in different kind of species by reaction with NH_3. This is clearly seen in the increase of the CO_2 evolution in the high temperature region for the sample NCNF673K with respect to the samples NCNF473K.

4.1.4 Surface analysis by TPD: nitrogen functionalities

It was reported[188] that nitrogen functional groups in carbon materials decompose upon heating by releasing in gas phase NH_3, HCN, N_2 and in the most oxidized samples NO.
In the samples investigated, nitrogen evolves mainly as NO (Fig. 4.3) in the samples CNFox and NCNF473K and, as CN radicals and HCN in the aminated samples (Fig. 4.4 *m/z* 27 for samples NCNF473K and Fig. 4.5 for the sample NCNF873K). For the CNFox sample, N evolves giving arise to the formation of NO (*m/z* 30) with a trend that highlights the decomposition of at least three species (Fig. 4.3).

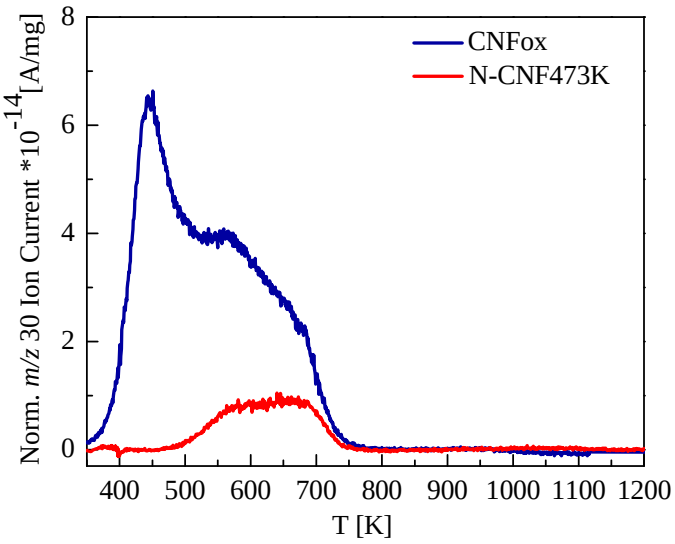

Fig. 4.3: *m/z* 30 traces for the sample CNFox (blue line) and for NCNF473K (red line) during TPD.

The two visible peaks start at 400 K with maximum at about 445 K and, the second maximum at about 550 K. Those peaks can be undoubtedly assigned to nitro functionalities[188]. The third peak has maximum at about 650 K. With increasing the desorption temperature, the acidic character of the species generating the fragments decreases. From a structural point of view, it is reasonable to imagine that the lower the number of O atom coordinated to the N atom, the higher the desorption temperature. In NCNF473K, the release of the NO regards the two higher temperature peaks but in smaller amount compared to the CNFox. Those NO species are introduced during the oxidative step and, being thermally stable at 473 K, they are still retained after the

amination step. The decomposition of N species in the NCNF473K occurs mainly by releasing in gas phase *m/z* 27 (Fig. 4.4).

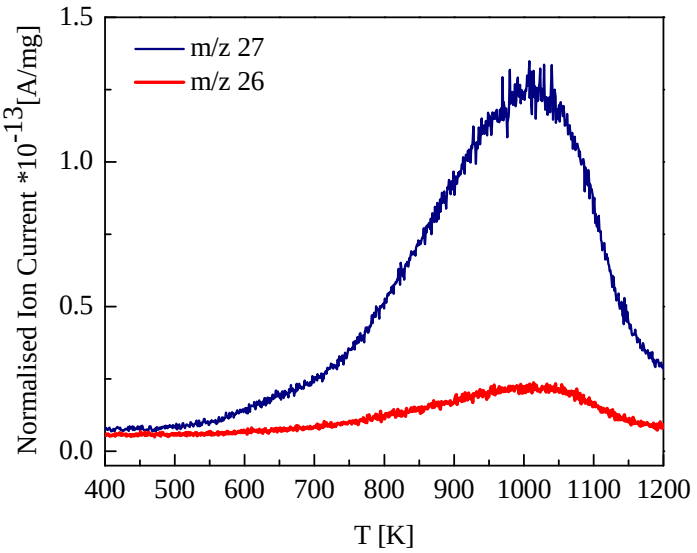

Fig. 4.4: Mass traces for the sample NCNF473K during TPD.

This is usually related to the formation of HCN as confirmed by the fact that the *m/z* 27 is always accompanied by the presence of the *m/z* 26 which is due to CN radicals. The origin of HCN is often referred in literature as a result of the reaction between nitrile radicals with water converted in HCN. The desorption temperature of HCN is indicative of the nature of the N species. It is reported[11] that formation of HCN below 1073 K is generated by decomposition of amide through a dehydration pathway or lactam through ring-opening followed by dehydration. Above 1073 K it was reported being generated by cracking of pyridine ring. In the sample NCNF473K, the evolution of HCN occurs in a large range of temperature. This is indication for the high heterogeneity of N species such as amide, lactam and pyridine. Nevertheless, the release of HCN above 1000 K due to pyridine species is very limited. In Fig. 4.5 are reported the signal generated during the thermal decomposition of the N species for the samples NCNF873K.

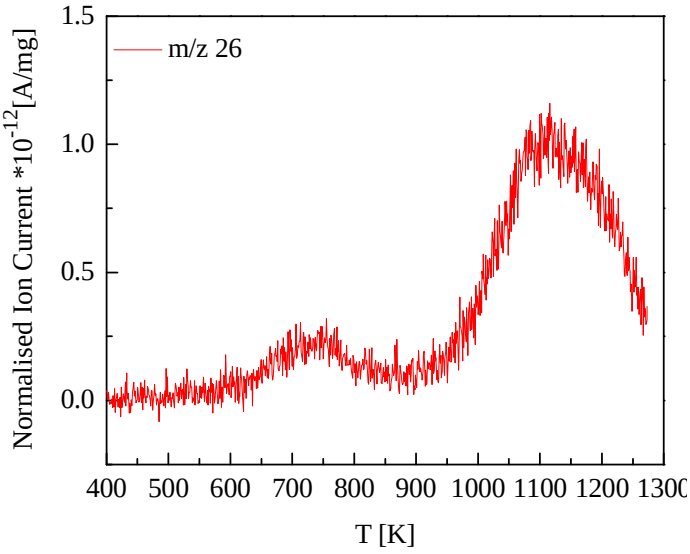

Fig. 4.5: *m/z* 26 for NCNF873K (red line) during TPD.

In contrary to the sample NCNF473K, the main MS signal for the sample NCNF873K is the *m/z* 26. The reason of the observed inversion in the relative amount of these two fragments (*m/z* 27 and *m/z* 26) for this sample might be related to the poor hydrophilic character of the sample NCNF873K with respect to the NCNF473K as shown later on in the O1s spectra of these two samples. The amount of water released during the TPD of the NCNF873K is quite limited (not shown) compared to NCNF473K. Although the idea reported in literature about the origin of HCN, it should be considered that in the case of lactam species, the N atoms has an sp^3 configuration and carries an H atoms, thus the break of the amidic C-N bond during the thermal decomposition leads obviously to the formation of HCN. Differently in the case of pyridine species the N atom has a sp^2 configuration and does not carry any H atoms, thus the thermal decomposition of these species certainly gives rise to nitrile radical formation as observed in our experiments. In Fig. 4.5 is possible to distinguish a small peak centered at 700 K due to amide species, and a very large peak centered at 1100 K which is probably due to the decomposition of pyridine species. In summary, the sample functionalized at lower temperature NCNF473K contains nitrogen functionalities as chain moieties on the surface which give arise to HCN formation through a very broad peak ranging from 800 to 1100 K centered at 1000 K. The sample NCNF873K is characterized by the thermal decomposition of species which give arise to the trace *m/z* 26 in the mass spectrum. A part for a small peak centered at 700 K, the CN radicals are generated above 1000 K. Thus, the

functionalization temperature has a strong impact on the nature of the nitrogen species introduced during the amination. In particular, when the functionalization is made at higher temperature (NCNF873K) the nitrogen moieties (stable at 473 K) can condensate in ring and eventually dehydrating during the treatment itself, and they evolve in the TPD mainly as *m/z* 26 at a temperature that depends on the degree of dehydration.

4.1.5 Dynamic Surface rearrangement and thermal stability of nitrogen and oxygen functional groups studied by temperature programmed XPS-MS

The mathematical treatment of the spectra recorded during TP-XPS (Appendix) offers a phenomenological approach to the fitting of the N1s and O1s envelopes. The critical analysis of the changes in the XP spectrum observed during the desorption process, the sequential thermal decomposition, the relative thermal stability and the type of fragment generated by the desorption process allows to identify the chemical nature of the species giving arise to the peaks observed in the XPS and TPD-MS spectra.

If the sample is subjected to a thermal treatment, either in inert atmosphere or in UHV, part of functional group will be decomposed and detected by on line MS. The remaining functionalities appear in the XP spectrum, allowing for a more constrained determination of the BE and the line shape, i.e. FWHM for these species. Once all the possible functional groups are well known, a consistent fit of all recorded spectra during the TP-XPS is done considering always the same contributions.

The temperature recorded in several runs might deviate due to a slightly different mounting of the temperature sensor. Shift in temperature are observed especially when the measurement are performed in UHV. Nevertheless, the MS traces are consistent with each other if one considers a rescaling of the recorded temperature.

Such kind of combined experiments are extremely useful to characterize the functional groups present on the surface of the carbon material and the species generated by their decomposition. Furthermore these combined experiments give information about the thermal stability of the functional groups present on the surface. This is of great importance in the view of the application of functionalized NC at elevated temperature, for instance in catalysis.

4.1.5.1 Temperature programmed XPS -MS on oxidized sample

The experiment described here aims at the comprehension of the nature of the functional groups introduced on the surface of VGCNF during oxidation by HNO_3.

The experiment is carried out in a high pressure in-situ XPS chamber (ISSIS beam-line) equipped with on-line MS in He at 0.5mbar and with heating rate of 10 $Kmin^{-1}$.

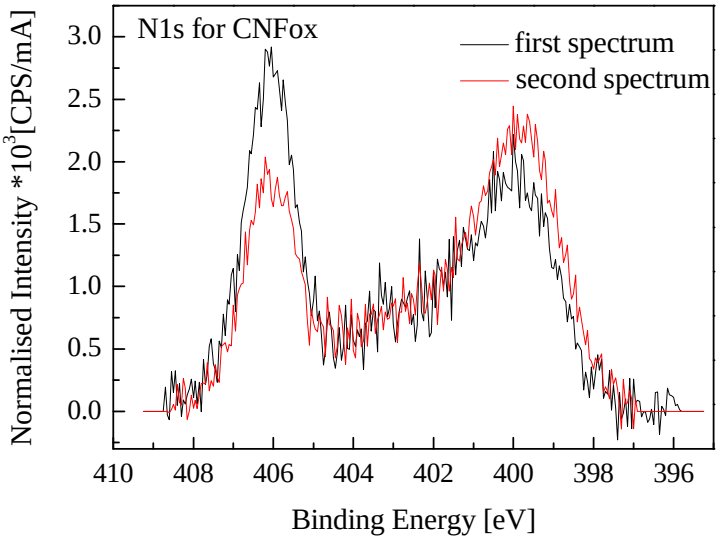

Fig. 4.6: Beam effect on the N1s for CNFox: first spectrum (black line); second spectrum (red line).

Fig. 4.6 shows XP N1s core level spectra for the CNTox at room temperature and after exposure to beam for a few second. Similar spectra have been already reported[189,192]. In agreement with literature data[189,190,191,192] the oxidative process by nitric acid introduces small amounts of nitrogen in the form of nitro functionalities, probably intermediate species further transformed in oxygenated functionalities. Those species referred as N6 are found in the XP N1s spectra at about 406 eV as discussed in section 4.1.2.

The chemical nature of the very broad peak between 398-400 eV with its maximum at 399.6 eV remains unclear, though it is a common feature reported in literature for nitric acid oxidation of carbon material[189,190,191].

In this binding energy region non oxidized nitrogen species are found, although some authors reported that nitroso functionalities can have BE within this region[163]. However, we observed that N6 species is beam sensitive, and that it is partially converted into this very broad peak upon exposure to the beam for few seconds (Fig. 4.6). Therefore, it is quite likely that the reductive effect of the X-ray beam converts those nitro species in reduced form of nitrogen having the chemical shift mentioned above.

This is accompanied by the simultaneous decrease in the O1s of the specie centered at 533.1 eV (FWHM 1.3) which is thus assigned to oxygen in N-O bond (Fig. 4.7).

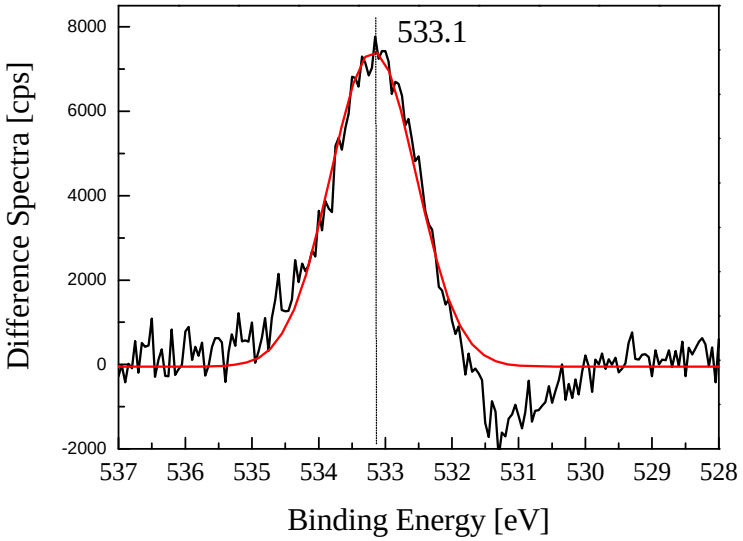

Fig. 4.7: O1s difference spectra before and after beam exposure for the sample CNFox.

Among the samples investigated only the CNTox has shown beam damage.

Fig. 4.8 and Fig. 4.9 reports the MS traces recorded during the temperature programmed desorption experiment.

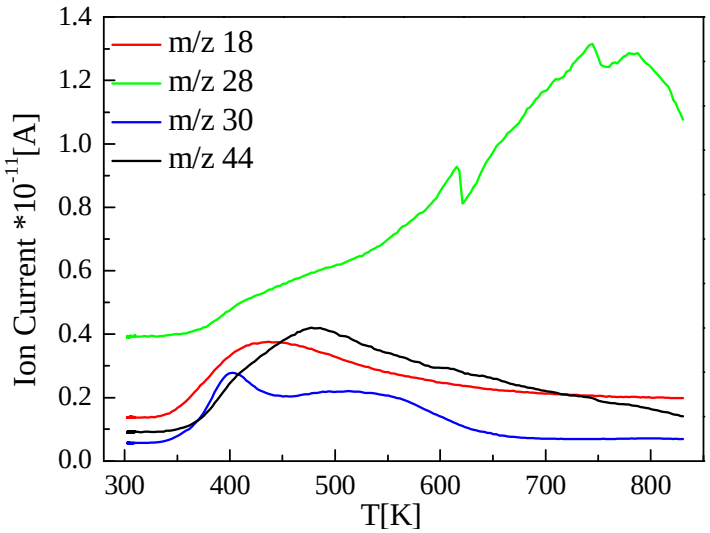

Fig. 4.8: MS traces recorded during TP-XPS experiments for CNFox.

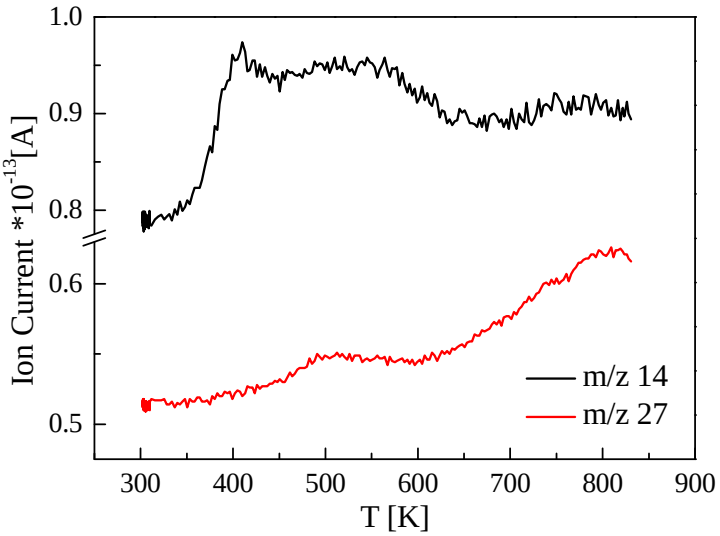

Fig. 4.9: MS traces recorded during TP-XPS experiments for CNFox.

Similarly to the TPD experiment, the nitrogen species decompose giving arise to NO detected as *m/z* 30.

Fig. 4.10 shows the modification of surface N species (N1-N6) while heating during TP-XPS experiment.

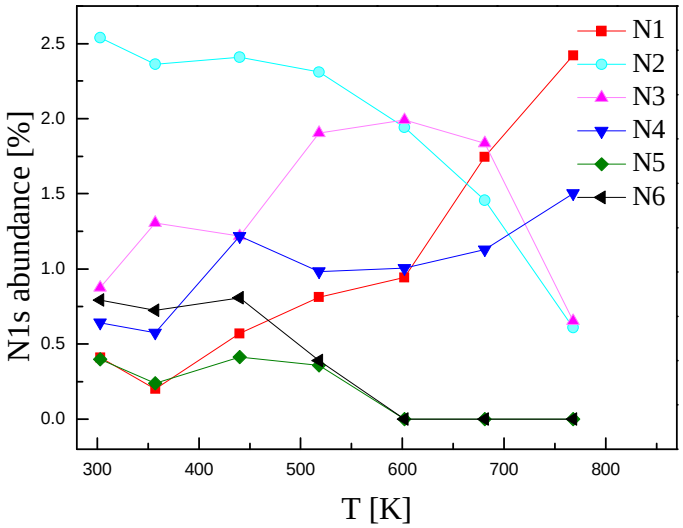

Fig. 4.10: N1s species abundances (±0.1 eV) versus T for CNFox during TP-XPS: N1(398.4 eV); N2 (399.6 eV); N3 (400.1 eV); N4 (401.1 eV); N5 (403 eV); N6 (406 eV).

At around 600 K the XP peak at about 406 eV (N6) is almost totally gone in the gas phase. It corresponds to the end of the evolution of the *m/z* 30 in the mass spectrum (Fig. 4.8). The evolution of the mass signals *m/z* 30 is attributed to the decomposition of nitro functionalities. Note that in this temperature range the *m/z* 14 has the same profile than *m/z* 30 (Fig. 4.9). The presence of the very broad m/z 30 peak between 398-400 eV in Fig. 4.6 justify the assumption that by HNO_3, apart of the oxidized nitrogen, others functionalities are introduced. This is proved by the evolution in gas phase of *m/z* 27 which is released when non oxidized N species in hetero-cycle moieties are decomposed. This is possible if one considers the reductive effect of the X-ray beam on the functional groups or if one assumes the presence of defects on the graphitic structure that can insert N atom in the graphitic structure. Thus, the spectrum is deconvolved as reported in the appendix. In the deconvolved spectrum the main peak is found at a BE of 399.6 eV (N2). This functional group decreases in the XPS N1s spectrum while increasing the temperature (Fig. 4.10) and might be related to the evolution of the *m/z* 27 in the MS (Fig. 4.9). Note that the *m/z* 14 evolves at lower temperature with a similar trend to *m/z* 30 and at higher temperature with a similar trend to the *m/z* 27 evolution. Later on, the N1s spectrum components at BE corresponding to pyridine (N1) and quaternary nitrogen (N4) at 389.4 eV and 401.1 eV respectively (Fig. 4.11). However, the intensity of these species is very low. It must be pointed out that for this sample the dynamic surface rearrangement of the N species follows the same trend as it is observed for the aminated samples. This phenomenon will be described and discussed in the next section dealing with the assignment of the N species. The modification of the oxygen species are analyzed by following the gas phase release of CO_2 and CO in the MS

The CO_2 evolution profile in the MS (Fig. 4.8) is characterized by the main peak centered at 500 K ending with a long tail.

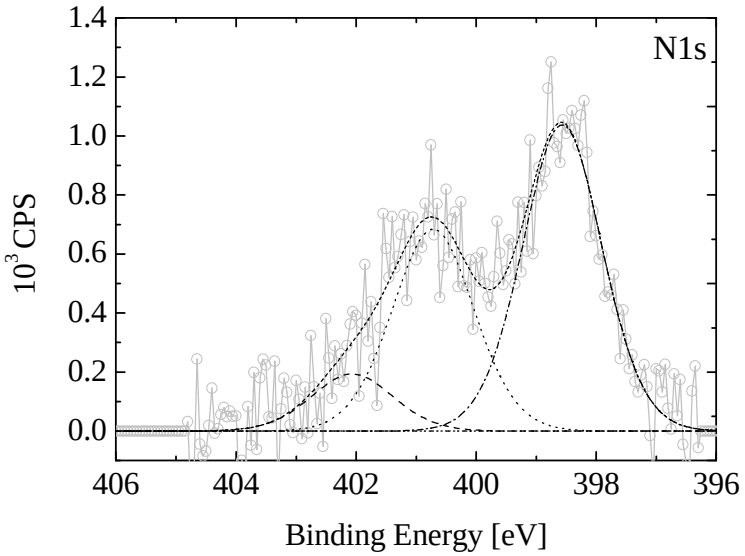

Fig. 4.11: N1s for CNFox at 770 K during TP-XPS.

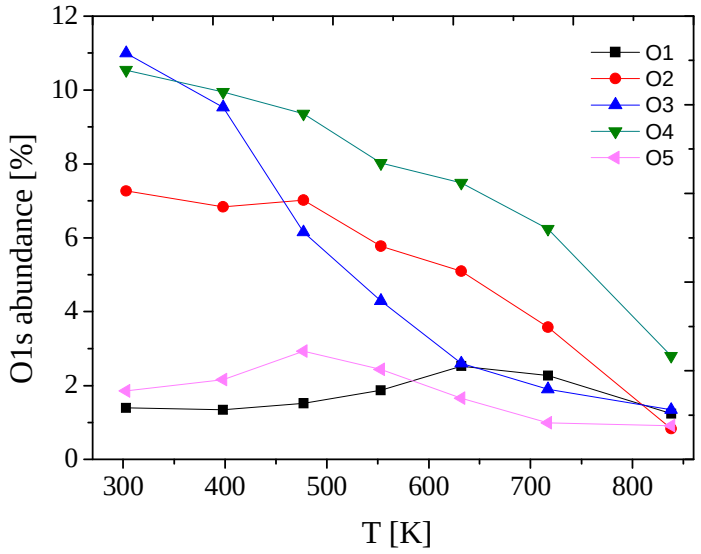

Fig. 4.12: O1s species abundances (±0.1 eV) vs temperature: O1 (530.6 eV); O2 (531.5 eV); O3 (532.5 eV); O4 (533.6 eV); O5 (535 eV).

The variation of the abundances of each species in the O1s during heating are reported in Fig. 4.12. In the fitting procedure of the O1s is shown that for the CNFox the O3 oxygen species at around 532.4 eV is the first species suffering modification induced by the thermal treatment (appendix Fig. A.5). Simultaneously, the release of CO_2 (*m/z* 44) and water (*m/z* 18) occurs in this experiment at about 373 K (Fig. 4.8).

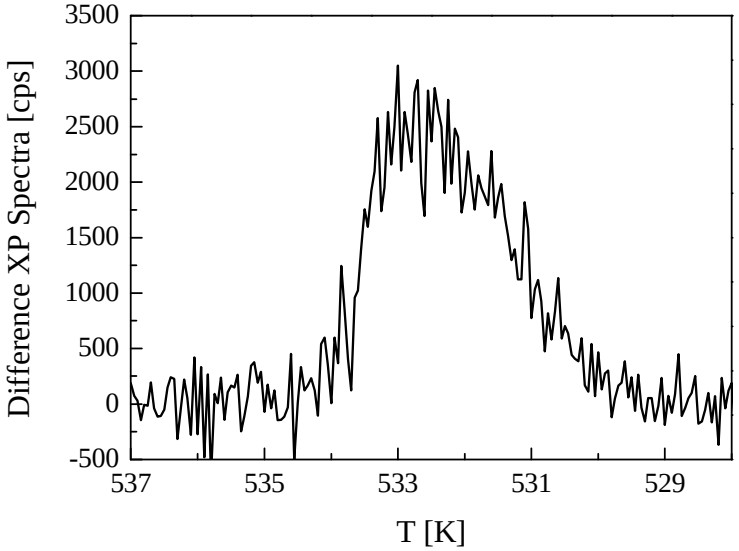

Fig. 4.13: Difference between O1s spectra recorded at 477 K and 553 K for CNFox.

The same trend is also observed for the sample NCNF473K. It was shown already in Fig. A.7 (Appendix) that between room temperature and 412 K a broad peak (FWHM 1.85 eV) centered at 532.4 eV decreases in the O1s spectrum. It was already reported in literature[170] that adsorbed water gives arise to a very broad peak covering a broad range of BE. The adsorbed water might interact with the functional groups present on the carbon surface producing a BE chemical shift. However, as reported in Table 4.1 the BE of the O3 species is referred to the region of the C-O single bond. During the thermal desorption the low thermal stable C-O single bond presents on the carbonate groups breaks firstly and this could explain the decreasing of the O3 (C-O single bond) as first species being thermally decomposed.

While increasing temperature, desorption of the species at 532.9 eV between 398 K and 477 K occurs for the CNFox as reported in Fig. A.8. This peak might be correlated to N-O species as observed during beam damage on the same sample (Fig. 4.7). Above 477 K the difference spectra reported in Fig. 4.13 shows broadening in the low BE side where the carbon-oxygen double bonds are found. The simultaneous and parallel decrease above 477 K of the surface abundances of O4 (533.6 eV) and O2 (531.5 eV) species observed in Fig. 4.12 suggests that these species might be inter-relatable The O4 species is found in

the region referred as the O-H bond region while the O2 species is the carbon-oxygen double bond. However, the O4 is always in larger amount than the O2 and it is the most abundant species at high temperature. The O1s XP spectrum recorded after the *m/z* 44 evolution shows a very low amount of oxygenated functionalities left, mainly present as O4 and O1(Appendix Fig. A.10). Considering that the less thermal stable O4 specie is found at a BE of 533.5 eV, while the high thermal stable species is found at higher BE 533.6 eV. The small shift in the BE of the O4, together with the different thermal stability of those species, is an evidence of at least two different chemical configuration of single O-H bond contributing to the O4 peak. The less thermal stable O4 species is identified as OH in carboxyl groups while the high thermal stable is identified as OH in ultra stable phenol groups. The O1 (530.6 eV) specie is present on the CNFox in very small amount. During the thermal desorption it slightly increases while above 700 K decreases again and reaches the initial value. The nature of this species is very difficult to establish. This region is referred as the metal-oxide region. However, metal was not detected in the survey spectra, although being the amount so small, it could be even not visible in the survey. Otherwise, the O1 species might be due to C-O double bond in highly conjugated quinine species. n summary, the amount of quinones-like species (O1) or ultra stable OH groups (O4) introduced by the HNO_3 treatment is very low and mainly by this way the carboxylic groups and anhydride are introduced. Finally, the O5 species at about 535 eV is still not well established. This feature is always present in the O1s spectra recorder during the thermal treatment. However, the abundance of this species increase and reaches a maximum (Fig. 4.12) in correspondence of the maximum observed in the *m/z* 18 in the MS (Fig. 4.8). Thus, in agreement with literature this feature might be assigned to adsorbed water.

4.1.5.2 Temperature programmed XPS -MS on NCNF873K

The experiment described here aims at the comprehension of the nature of the N species present on the surface of aminated CNFs.

The experiment is carried out in a XPS chamber (U49/2 undulator beam-line) equipped with on-line MS in HV (pressure 10^{-7} mbar) condition with heating rate of 5 $Kmin^{-1}$.

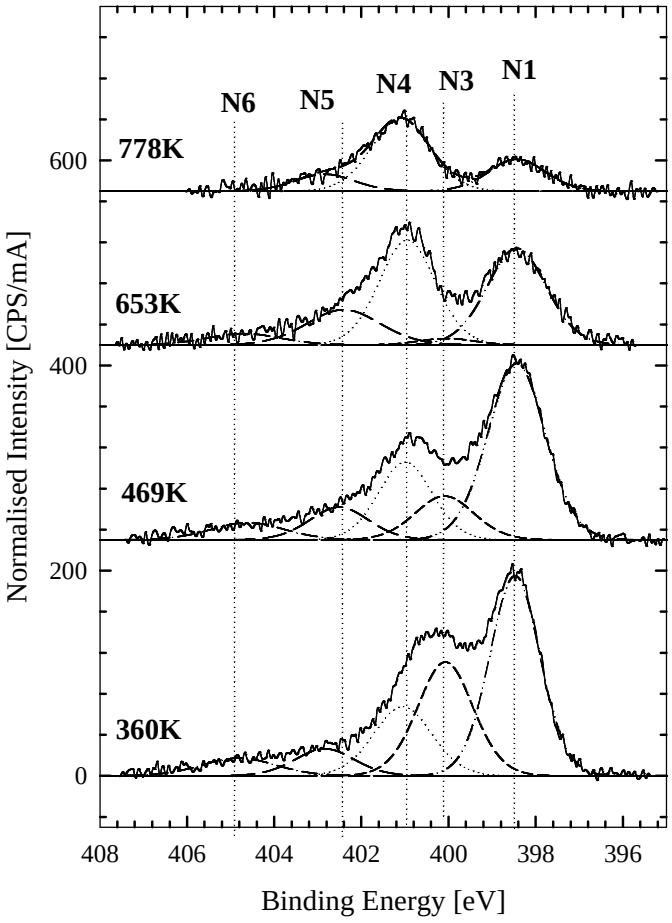

Fig. 4.14: Deconvoluted N1s core level spectra for sample NCNF873K during in-situ heating. N1at 398.5±0.1 eV; N3 at 400±0.1 eV; N4 at 401 ±0.1 eV; N5 at 403.4±0.1 eV.

The XPS N1s core level spectrum of the sample NCNF873K and its deconvolution is reported in Fig. 4.14. As described in section 4.1.2, three BE regions can be assigned to different nitrogen bonding in the N1s spectrum of model carbonaceous materials[174]: the pyridine nitrogen region (labelled as N1, at about 398.5 eV), referred to nitrogen

atom contributing to the π system with one p-electron; the pyrrol region (labelled as N3, at about 400.1 eV), referred to nitrogen atom contributing with two p-electrons to the π system. N3 composes the contribution of pyridone, lactam and pyrrol functional groups. The pyridone functionality is the tautomeric form of lactam functionality. The third region (labelled as N4, at 401-403 eV) is referred to the quaternary nitrogen, including protonated pyridine or the "graphitic" nitrogen when the nitrogen atom is incorporated in the graphene layer replacing carbon atom[158]. Furthermore, a peak labelled as N5 with a BE shift of about 5 eV to the high energy side compared to pyridine is assigned to pyridine oxide. No contribution of amine or amide between 399-400 eV has been found.

Fig. 4.15 displays the TPD-mass spectra during TP-XPS. The main detectable signals are HCN (*m/z* 27), NO (*m/z* 30) and N^+ (*m/z* 14). A part of the *m/z* 30, the species originated from the decomposition of the functional groups are the same observed in the TPD experiments. However the relative amount is different and temperature scale differs too. The *m/z* 27 signals (Fig. 4.15 dotted line) exhibit over all the temperature range several features corresponding two different functional groups. The oscillation of this signal between 400 K and 660 K indicates a dynamic change of the N-functional groups on carbon rather than a simple decomposition into gas molecules. In comparison with HCN, signal assigned to NO is relatively low, and its evolution characteristics differ too. In particular it is linked to the lower thermal stable nitrogen functionalities. The *m/z* 14 is strictly related to the nitrogen functionalities, since it comes from fragmentation of those species. In fact it presents the same oscillation than *m/z* 27, especially at high temperature. According to literature[11], decomposition of functional groups through formation of nitrile ion gives rise to HCN when water is present. At low temperature it is attributed to the decomposition of lactam groups, while to pyridine at higher temperature.

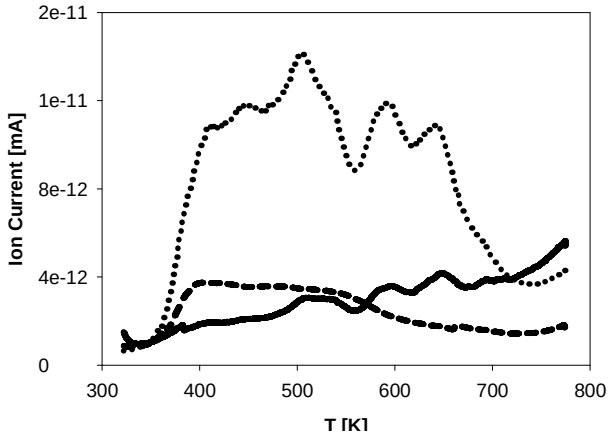

Fig. 4.15: Mass spectrum during *in-situ* TP-XPS for N-CNT873K: *m/z* 27 (dotted line); *m/z* 30 (dashed line); *m/z* 14 (full line).

Understanding the cause of NO formation is more complicate. It is probably due to dynamic surface rearrangement of moieties containing nitrogen and oxygen, e.g. lactam or pyridine oxide giving rise to NO in the mass spectrum. The fragments NO might be generated from the decomposition of the nitro species as well. From Fig. 4.14, it is clear that some of the nitrogen functionalities initially present in the sample are released in gas phase, with consequent decrease in the overall nitrogen content. However some functional groups are retained and undergo to dynamic surface rearrangement during heating. The evaluations of various components N1-N4 versus temperature are plotted in Fig. 4.16.

The N3 functionalities decrease continuously with increasing temperature. Since at the same time in the XP spectra, N1 and N4 components increase, lactam and pyrrol functional (N3) groups convert partly to these species.

Water trace is detected by MS while N3 component decrease, we assume that lactam species are present with a BE of 400.3 eV. However, the presence of pyrrol groups can not be excluded. Lactam can dehydrate to pyridine functionalities, or can be thermally decomposed through the breaking of the most strained amidic bond leading to the gas phase release of the *m/z* 27 signals. For this sample, the formation of *m/z* 30 in correspondence of the first main feature of the *m/z* 27 in the mass spectrum cannot be assigned to the initial presence of surface nitro groups as suggested by the absence of the N6 species in the N1s spectra. In part, the re-adsorption of the N species and/or the gas phase successive recombination of the decomposed N and O radical species can be

responsible for the NO formation. The pyridine total abundance reaches a maximum at 450 K and above this temperature starts to decrease (N1 curve in Fig. 4.16) while N4 still increase reaching a maximum at a higher temperature (600 K). Even in this case, a competition occurs between the structural transformation of pyridine into N4 and the decomposition in gas phase that give rise above 600 K to the second main feature in the *m/z* 27. Such processes occur in a wide range of temperatures so that the two pathways are overlapping each other. The N4 species is the most thermal stable species, it is generally referred in literature as quaternary nitrogen but the exact nature of this functionality is still poorly established. Early it was reported that a hypothetical structure of this functionality could be as reported in Scheme 4.1. The N5 and N6 species (NO_x species) are produced in small amount during the heating, however they are almost absent at high temperature.

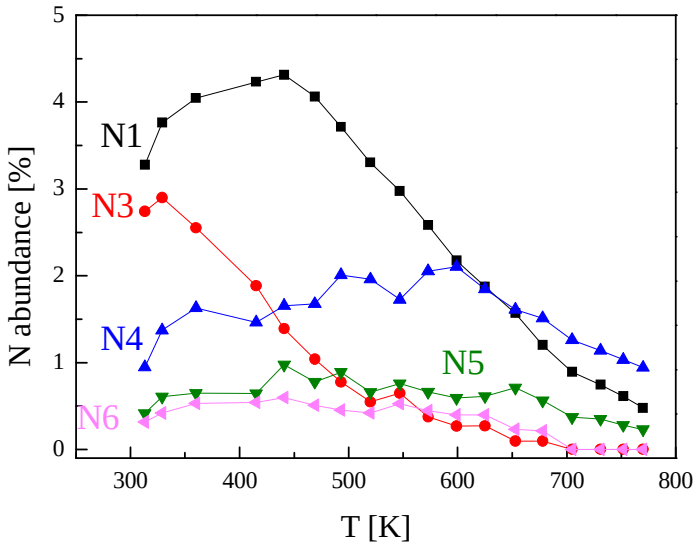

Fig. 4.16: Evolution of different N-species during TP-XPS for N-CNT 873:N1 (black curve); N3 (red curve); N4 (blue curve); N5 (green curve); N6 (pink curve).

4.1.5.3 Temperature programmed XPS -MS on NCNF473K

In order to corroborate the results discussed in the previous paragraph, TP-XPS N1s spectra of the aminated samples N-CNT473K is reported here following. The experiment is carried out in a XPS chamber at U49/2 undulator beam-line equipped with on-line MS in HV (pressure 10^{-7} mbar) condition with heating rate of 5 $Kmin^{-1}$.

The abundance of the different N species versus the temperature is plotted in Fig. 4.17.

The combined analysis of the Fig. 4.17 with the mass spectrum during temperature ramp

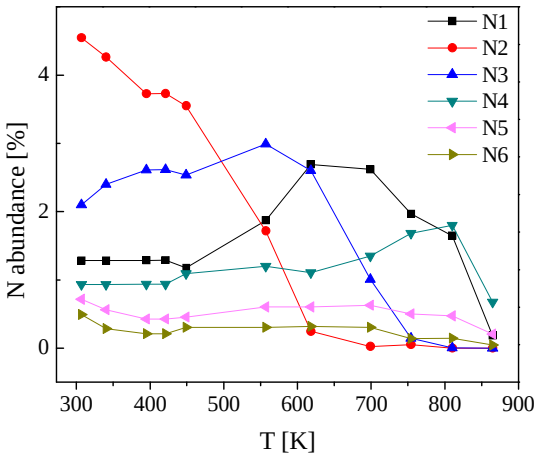

Fig. 4.17: N1s Abundance vs Temperature.

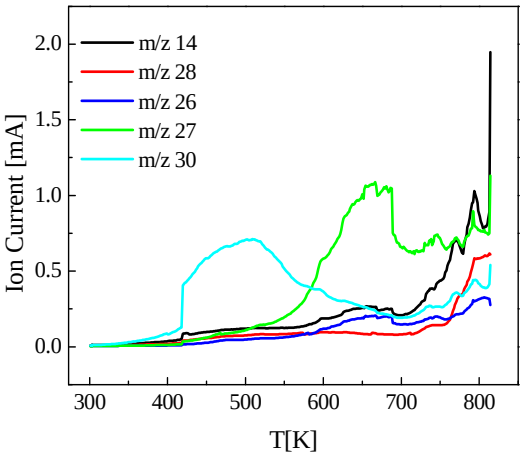

Fig. 4.18: MS during TP-XPS.

(Fig. 4.18) shows that in the high temperature region, the surface modification of the N functionalities in the XPS and the fragment generated by their decomposition and detected in the MS coincide with the previous experiments discussed above. In this experiment information concerning the lower thermal stable functionalities is obtained. In fact, below 400 K, N2 is converted in N3 and no evolution in gas phase was observed. Up to this temperature a further decrease in the N2 species correspond to NO evolution in the MS, and increase of N3 in the XPS is less pronounced. At about 550 K, N3 starts slightly to decrease. Fig. 4.18 shows *m/z* 27 traces evolving at 550 K with peak maximum at 650 K. Simultaneously N1 functionalities slightly increases and reaches the maximum at 650 K. Afterwards the N1 specie decreases and evolves in gas phase giving arise to a further increase of *m/z* 27. The *m/z* 27 signal is always accompanied by the evolution of *m/z* 26. In this sample (NCNF473K) the N1 and N3 species have the same behavior observed for the sample (NCNF873K) discussed in the previous paragraph. The N3 species can be

attributed to lactam or pyrrol groups since the contribution N3 in the XPS N1s spectrum with BE at 400.3 eV decreases in parallel with the evolutions of *m/z* 27 in gas phase.

The modifications of N1 species lead to the unequivocally attribution of this species to pyridine groups. Accordingly to the sample NCNF873K, the spectra recorded at the end of the experiment shows mainly the "quaternary" nitrogen. The nature of N2 is uncertain. In this experiment, the N2 species is the less thermal stable species and partially decomposes through the formation of the *m/z* 30. Thus, it is partially due to nitrogen oxide species still present from the oxidizing treatment. However, the N2 species is mainly due to not oxidized form of N species such amine or amide groups that converts into N3 while increasing the temperature. These results are in agreement with the experiments reported in section 4.1.4.

It is shown and discussed here the probable presence of amide and lactam groups on the surface of NCNF473K decomposing through the formation of *m/z* 27 and *m/z* 26 fragments in a broad range of temperature in the TPD-MS.

The difference in the relative amount of fragments generated in the two experiments (TPD and TP-XPS) mirrors the different condition in the experimental set-up. Those conditions influence the decomposition pathway of the N2 and especially the formation of NO in the gas phase. The re-adsorption of the primary decomposed species of the gas phase successive reaction might have an influence on the kind of fragments detected. Nevertheless, it has been shown that TP-XPS is a suitable tool for the understanding of the N1s spectrum and assessment of nitrogen functionalities. By correlating the mass signal, the decomposition temperature and the BE in the XP spectrum it is possible to assess the chemical nature of the functional groups present on the surface of the carbon materials. Although the decomposition of the functional group compete with the conversion to another functional group through a dynamic surface rearrangement that might depends on the heating rate and on the experimental pressure condition, a general trend was observed: initially N2 functional groups with a BE at 399.4 eV partly decompose through formation of NO, and partly convert into N3 species which have a BE of 400.1 eV (sample NCNF473K). With increasing the temperature those species N3 might decompose giving arise to HCN formation or convert into pyridine groups N1. Later on, pyridine (N1) is transformed into quaternary nitrogen (N4 401.1 eV) or decompose giving rise to further formation of HCN. Above this temperature the nitrogen

species so called quaternary nitrogen is the main species. In summary during the TPD experiments, as the temperature increases, the molecules covering the surfaces are successively desorbed according to the strength of the interaction with the surface sites. However, rearrangement of surface atoms also occurs during thermal treatment, which may change the number and nature of the starting species present on the surface. The results support the pathway for nitrogen insertion and modification during thermal treatment that was earlier proposed for aminated AC[158] and reported here in scheme 4.1.

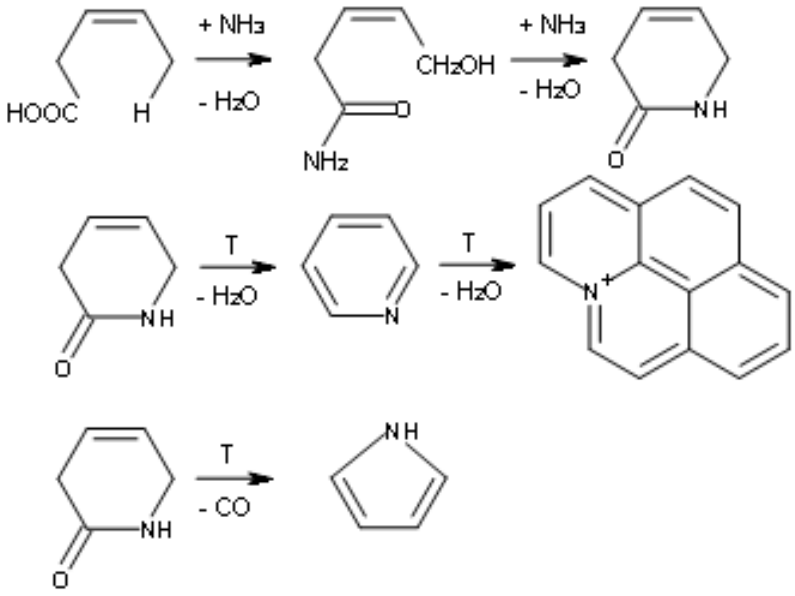

Scheme 4.1: Nitrogen insertion pathway in Carbon.

4.2 Influence of the treatment temperature on the distribution of N and O functionalities in VGCNF functionalized via amination

4.2.1 Surface analysis by XPS: C1s, N1s and O1s core level spectra

In the previous paragraphs, by means of literature analysis and specifically addressed experiments, the description of the N1s and O1s has been presented. In this paragraph the data are presented with emphasis on the influence of treatment temperature on the distribution of nitrogen and oxygen functionalities partly discussed in the previous paragraph.

Table 4.3: Elemental composition as determined by (a) XPS and (b) hot gas extraction.

Sample	N(at%)		O(at%)	
	Surface[a](5-10Å)	Bulk[b]	Surface[a]	Bulk[b]
NCNF473K	12.3	1.3	11.7	2.2
NCNF673K	18.8	1.5	11.7	1.2
NCNF873K	8	1.1	3.4	0.7
NCNF873K*	3	-	19	-
CNFox	5	0.6	23.3	5.6
VGCNF	1.3	-	6.7	-

Table 4.3 reports the surface and bulk elemental composition as determined by XPS and by hot gas extraction, respectively. The difference between the surface and bulk abundance is a clear evidence of surface enrichment of nitrogen and oxygen functional groups. According to the data, the presence of acidic oxygen functionalities introduced during the oxidative step by HNO_3, is crucial for the introduction of a high amount of nitrogen functionalities in the successive thermal treatment with NH_3 (samples: NCNF473K, NCNF673K, NCNF873K). The thermal decomposition of these oxygen functionalities with thermal stability below 973 K results in a considerable decrease of the amount of nitrogen bound to the CNFs surface (sample NCNF873K*). Beside the

oxygen species, in agreement with literature, the chemical treatment with nitric acid introduces also N functionalities[192]. As reported in Table 4.3, the concentration of N and O species is temperature dependent. The amount of N species depends on the kinetic of several competitive reactions: the reaction of NH_3 with the available acidic oxygen species at the CNFs surface, the thermal decomposition or the surface rearrangement of an oxygen species to another which affect the abundance of the reactive oxygen species and the thermal decomposition of NH_3. The increase of the temperature from 473K to 673K leads to the increase of the amount of N species. This is due to the fact that some heterocyclic oxygen species might undergo ring opening thus rending further acidic oxygen species available to react with NH_3. However after a certain threshold temperature (873 K), the thermal stability of both O and N functional groups and the competitive NH_3 thermal decomposition lead to a decrease in the overall N contents. At a certain temperature, the thermal stability of the different N species determines not only the total amount but especially the types of surface species. In fact, at high temperature the graphene layers have energy enough to rearrange the defective structure in the most thermodynamically stable graphene structure free of defects as hetero-atoms. For this reason more oxidizing species are less thermally stable and are firstly removed. This is also the reason why at high temperature the O content is smaller than the N content and, among all the temperature investigated, it is more difficult to introduce larger amount of N species at higher temperature. As reported later on, at high temperature N and O species in aromatic heterocyclic moieties are the most abundant species.

The effect of the functionalization on the XP C1s spectrum has been extensively studied earlier in the fields of polymer and graphite fibers science[148,149,150,151]. Although the fitting parameters have not yet been settled unanimously, it is general accepted in literature that the C1s spectrum in carbon material is composed by the main asymmetric peak attributed to carbon atom in extensively delocalized aromatic sp^2 configuration in the graphitic structure.

The asymmetry in the high BE side of the C1s peak of defect-free graphite is associated with the excitation of conduction electrons which occurs in metal or semimetals as consequence of the relaxation of the core-hole generated by the primary photoemission process [193,194]. The peak lineshape is well described by the Doniach-Sunjic function but the order of asymmetry depends on the structure defectiveness. Disruption of the HOPG

structure by ion bombardment produces a decrease of the intensity and the degree of asymmetry of the main C1s peak[195]. The BE of this peak may vary within few electron volts, usually the value reported for HOPG vary within 284.6 eV[196,197] and 284.4 eV[124]. Fig. 4.19 reports the C1s spectra for the samples investigated and compared with C1s of HOPG taken as reference after annealing at 873 K. The thermal treatment was performed on the HOPG with the aim of cleaning the surface from any traces of impurity. In such a way the C1s lineshape of almost pure, defect-free graphite with the smallest peak broadening for our setup is measured as a standard. Local

Immediately above the graphitic peak (above 285 eV), the peaks stemming from localized defects in the sp^2 graphitic structure and the sp^3 carbon species are found in the C1s. These peaks are not present in the HOPG spectrum.

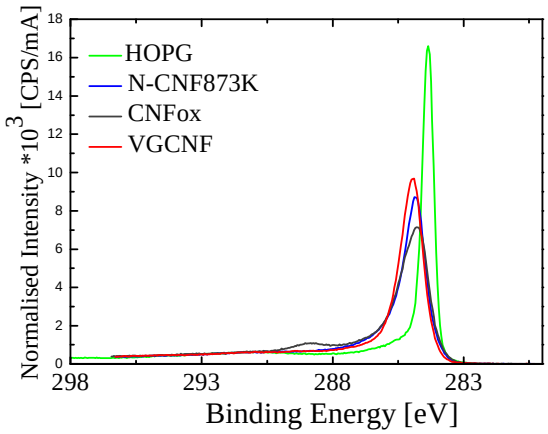

Fig. 4.19: C1s spectra for the CNF sample and for HOPG reference.

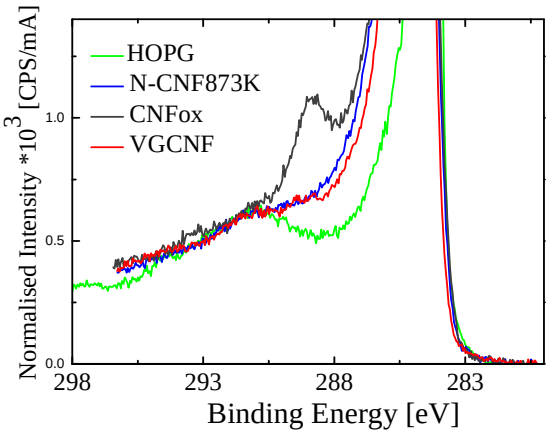

Fig. 4.20: C1s spectra for the CNF sample and for HOPG reference: zoom on higher BE region.

The shake-up satellite at about 291 eV gives also information about the degree of order characterizing the graphitic carbon sample. The higher the intensity of the peak, the higher the degree of order of the graphitic structure. Defects perturb the electron delocalization of the π-system reducing the weight of shake-up phenomenon which give arise to the tail in the main sp^2 peak and the satellite at 291 eV. At a further higher BE than the sp^3 carbon, all the carbon hetero-bonds are found.

In order to analyze the effects of functionalization it is necessary to refer the corresponding spectra to the HOPG reference (Fig. 4.19). The spectra have been normalized with the shake-up at 291 eV, assuming that these feature must be the same for carbon material with comparable graphitic order.

For all samples, the intensity of the maximum of the C1s peak is lower compared to HOPG. For both, the N functionalized (NCNF873K) and the O functionalized (CNFox) the intensity of the peak is even lower than the starting VGCNF. Furthermore, the apparent BE of the main peaks slightly differs for different samples. It is found at 284.4 eV for HOPG, at 284.7 eV for CNFox, at 284.8 eV for the NCNF873K and at 284.9 eV for VGCNF. Compared to HOPG, these shifts together with a broadening on the high BE side strongly suggest the presence of further components which we will address below.

In Fig. 4.20 the details of the high energy side region of the C1s is illustrated. With respect to HOPG, all samples exhibit a high intensity region between ~ 285 and ~ 291 eV. In the case of CNFox a distinct additional feature at about 288.8 eV is observed which is attributed to oxygen functional group[198,199]. A detailed analysis of the C1s region between ~ 285 and ~ 291 eV is beyond the scope of this work due to the highly heterogeneity of the surface. In this special case, it is very difficult to deconvolute the spectra, because of many possible contributions of both oxygen and nitrogen functionalities as illustrated in Fig. 2.5. However, useful information about the structural modification of the CNF subjected to the functionalization treatments can be extracted out of the C1s spectrum. The difference between the spectra of the C1s for the functionalized sample investigated and the HOPG after normalization with shake-up at 290.9 eV are reported in Fig. 4. 21.

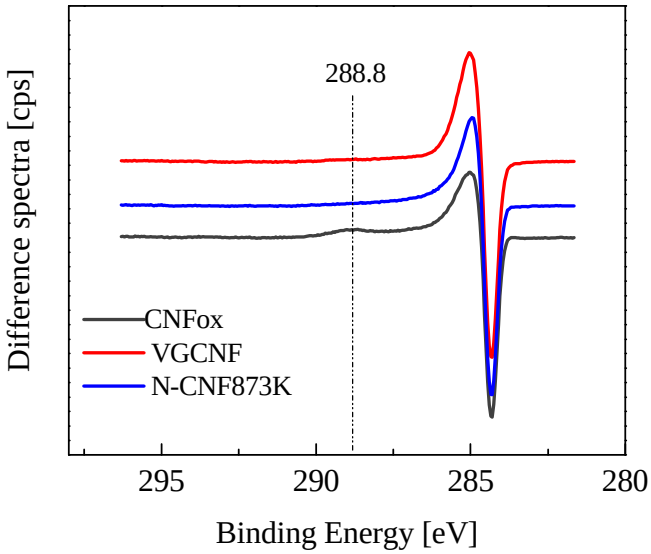

Fig. 4. 21: Difference C1s spectra of CNF samples and HOPG.

Apart from the feature at 288.8 eV directly related to oxygen, which is obviously most prominent in the CNFox spectrum, in this figure several distinct differences between HOPG and our sample series are visible. The samples present differences in the intensity of the contribution with its maximum at around 285 eV (see Fig. 4.20) compared to HOPG. In particular, the feature at this BE in the difference spectrum shows a long high BE tail for NCNF873K and VGCNF being more pronounced for the former, whereas the CNFox exhibits a smaller intensity in that region. This tail suggests further contributions of carbon hetero-bonds such as CO and N-related species. According to data reported in Table 4.3, the VGCNF has higher oxygen content on the surface whereas NCNF873K exhibits more nitrogen. Hence, we suggest that the broader tail may be related to N-C species rather than oxygen on NCNF873K. Oxygen and nitrogen functionalities can be analyzed by the O1s and N1s emission, respectively.

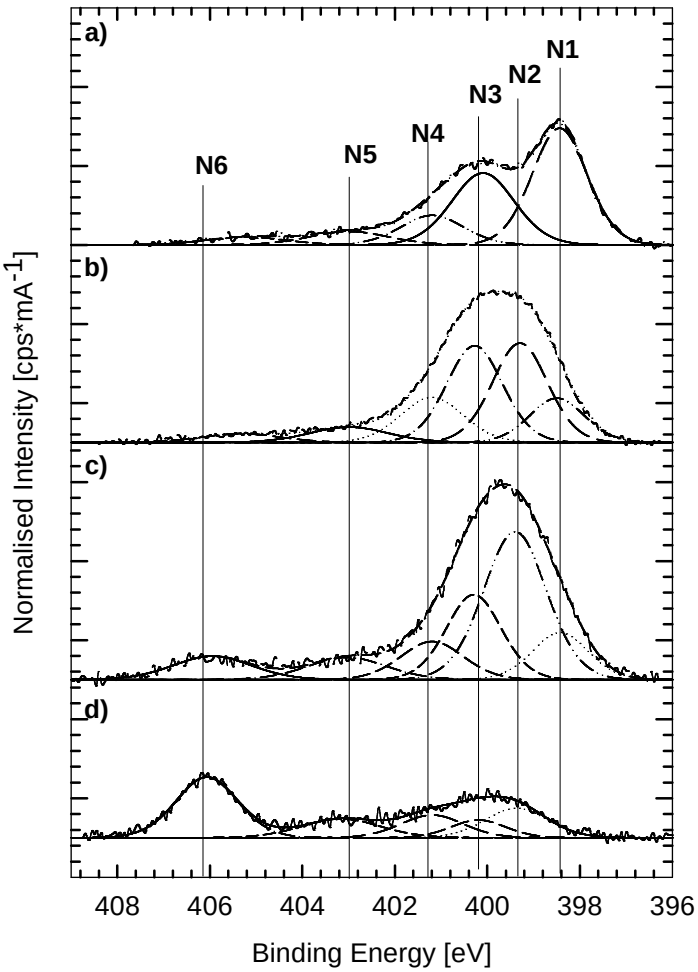

Fig. 4.22: XP N1s spectra: a) NCNF873K; b) NCNF673K; c) NCNF473K; d) CNFox.

XP N1s and O1s core level spectra for all samples are plotted in Fig. 4.22 and Fig. 4.23, respectively. Depending on the treatment temperature, a different overall N1s and O1s peak line shape was observed. The peaks are very broad as consequence of the heterogeneity of the CNFs surface. As described above, a multitude of species coexists in the C1s spectrum having close BE shift in the XP spectrum. The same peak broadening is observed in the N1s and O1s regions.

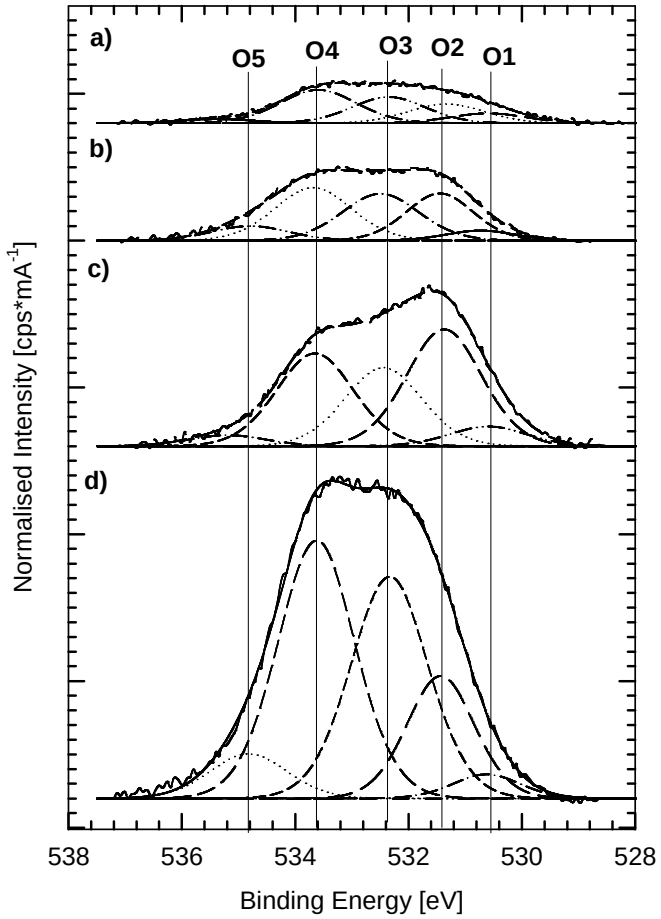

Fig. 4.23: XP O1s spectra of : a) NCNF873K ; b) NCNF673K; c) NCNF473K; d) CNFox.

Accordingly to the difference spectra analysis method reported in the Appendix of this thesis, it seems appropriate to introduce six components in the N1s. The binding energies were as following: N1 (398.4±0.1); N2 (399.4±0.1); N3 (400.1±0.1); N4 (401.1±0. 1); N5 (403±0.1); N6 (406±0.1). The XP O1s core level spectra have been deconvoluted by introduction of five contributions with peak maximum as following: O1 (530.7±0.1); O2 (531.4±0.1); O3 (532.4±0.1); O4 (533.7±0.1); O5 (535±0.1). The N1 species can be identified as the pyridine-like nitrogen, the N2 species is a functionalities containing nitrogen-hydrogen bonds as in amide, the N3 species is referred as N atoms in pyrrol-like configuration, as it is the case for both pyrrol and pyridone functionalities. The N4 is usually referred to any form of quaternary nitrogen[24,153-155,158,159] (N4) including substitutional nitrogen, and quaternary N due to intra or inter-molecular hydrogen bond with pyridine or amine functions. Furthermore, N5 is associated to the pyridine nitrogen-oxide species and N6 to nitro functionalities.

Table 4.4: Summary of XPS data: species abundance is given in atom percentage; in parenthesis the correspondent binding energies ±0.1 eV.

sample	**N1** (398.4)	**N2** (399.4)	**N3** (400.1)	**N4** (401.1)	**N5** (403)	**N6** (406)	**O1** (530.7)	**O2** (531.4)	**O3** (532.4)	**O4** (533.7)	**O5** (535)
CNFox	0	1.3	0.5	0.7	0.8	2	0.8	3.8	8	9.2	1.6
NCNF473K	1.4	5	2.5	1.3	1	1	0.7	4.2	2.9	3.4	0.4
NCNF673K	1.6	6.7	5.4	2.8	1.2	1	0.6	2.9	3.3	3.8	1
NCNF873K	3.5	0	2.5	1	0.6	0.4	0.4	0.7	1	1.2	0.1

In the O1s XP spectrum the components are assigned as following: O1 (530.7±0.1 eV) is an highly conjugated form of carbonyl oxygen such as quinine or pyridone groups[136,158]; O2 (531.4 ±0.1 eV) is assigned to a carbon-oxygen double bond; O3 (532.4 ±0.1eV) is the carbon oxygen single bond in ether-like species; O4 (533.7 ±0.1eV) refers to carbon oxygen single bond in hydroxyl groups. Another feature is present at around 535 ±0.1 eV (O5). Although the assignment is not clear, according to our results (section 4.1.5.1) this feature might be assigned to adsorbed water.

Table 4.4 reports the summary of the XPS species abundance. The amount of pyridine species increase with the functionalization temperature and is the maximum for the sample functionalized at 873 K.

At high functionalization temperature, aromatic cyclic moieties of nitrogen are stabilized at the edge of graphitic domains in carbon materials. Later on in the XP spectrum, the contribution (indicated as N2) and found 1 eV higher than the N1 BE could be due to many functional groups: amino groups attached to aromatic rings, amide groups, nitrile groups have been reported in a interval of BE between 399-400 eV.

The N2 is the main species when the functionalization is carried out at lower temperature. As reported in the previous section, our results strongly support the idea that the functionalization occurs mainly by reaction of NH_3 with those acidic sites that are thermally stable below 973 K, i.e. carboxylic groups. As it is reported in Table 4.3, thermal decomposition of those oxygen species produces a strong decrease of the nitrogen content. The MS profile during the TPD characterization on this sample (NCNF473K) has shown simultaneous detection of *m/z* 27, *m/z* 26 (Fig. 4.4) in a

temperature range reported for amide species. Furthermore, if one considers that the amount of oxygen forming double bond with carbon (O1 and O2 in Table 4.4) is for both CNFox and NCNF473K quite similar, it is quite probable that such kind of oxygen species is retained during the nitrogen functionalization as it is the case for the formation of amide groups. Note that the total amount of O and N are similar in both NCNF473K and NCNF673K, so it is quite likely that for these two samples, nitrogen is present in functionalities accompanied by oxygen, i.e. in amide or lactam species. Nevertheless, the presence of aromatic amine is not unreasonable and cannot be excluded based only on XPS results. Considering that the N2 species is present also on the surface of CNFox, it is hard to accept the existence of amide species on the surface of CNFox. However, it should be mentioned that the N2 species was found at 399.4 eV for the aminated samples while at 399.6 eV for the oxidized sample, thus is also possible that in the two samples, the N2 species has different chemical configuration which have the same BE shift in the XP spectrum.

If the functionalization is done at 673 K the N1s line shape gets less sharp, but broad to the high BE side. This could be explained as an increase in the amount of N3 functionalities with a maximum located at 400.1 eV (1.6 eV higher than N1 BE). According to previous findings on NH_3 treated AC[158] and our recent results on CNTs[24], the N3 species could be an intermediate species such as pyridone or pyrrol groups, resulting in pyridine formation upon heating. Although it is not possible to establish exactly the nature of the species described by the fitting of the N1s, it is evident that the distribution of the different species is affected by the treatment temperature in a trend that follows the pathway of nitrogen insertion already reported in literature and illustrated here in Scheme 4.1.

The amination, in general, produces a strong decrease in the absolute abundance of ether-like C-O single bond (O3) and the hydroxyl species (O4). This reflects a change in the character of the surface from predominantly hydrophilic in the CNFox and NCNF473K to hydrophobic in the NCNF673K and NCNF873K.

In the sample NCNF873K, the small amount of O1 and O2 (oxygen carbon double bound in pyridone groups) with respect to the amount of N3 component (nitrogen in pyridone or pyrrol species) suggests that for this sample the N3 species does not containing O. Thus, for this sample the N3 species is partially due to N in pyrrol-like groups.

In agreement with literature data[141,189,191] , the N6 species is the main species present in the N1s spectrum related to the oxidized CNFs. The oxidative process by nitric acid introduces small amounts of nitrogen in the form of nitro functionalities, probably intermediate species further transformed in oxygenated functionalities. As described in the previous section, the oxidative treatment introduces also not oxidized form of nitrogen species. They may be introduced at the defect sites present on the pristine CNFs surface such as vacancy or pentagon ring. However, the reductive effect of the X-ray beam on the nitro species can be the reason of the presence of N components in the low BE region of the XP spectrum of CNFox.

In spite of some remaining uncertainties in the assignment of some XPS components to a specific structure, the XPS chemical shift analysis is a powerful tool to evaluate the chemical nature of the species generating the signal. Early studies by Shirley[200,201] have dealt with the correlation between the characteristic proton affinity for a series of alcohol and amine and the correspondent O1s and N1s BE. Accordingly, for a series of alkyl-substituted aliphatic amine or alcohol, the final state polarization effects determines the chemical shift in such way that the more stabilized by the surrounding groups the charge on the O or N induced by the photoemission, the more pronounced the BE shift to a lower value. This concept can be applied to the present work by considering the BE shift as a measure of the basicity of the functional groups present on the aminated CNFs. In fact, final state polarization effects in the photoemission process can be compared with the stability of the basic site towards protonation.

Briefly, the lower the BE the more pronounced is the nucleophilic or basic character.

5

Tuning the acid/base properties of CNFs by functionalization with NH_3

In this chapter, the effect of the different thermo-chemical treatment on the surface chemical properties of nitrogen-containing CNFs is reported. The characterization of basic sites on the surface of aminated CNFs is carried out by potentiometric titration and gas-phase micro-calorimetric titration.

The surface chemistry of carbon plays a dominant role in determining its catalytic properties and adsorption capabilities[141]. In fact, the functional groups, usually oxygen or nitrogen, and the delocalized electrons of the graphitic structure define the acid/base and hydrophilic/ hydrophobic character of the carbon surface. The acid/base properties of the carbon surface can be exploited in many catalytic applications and thus they are the key point to be tailored in order to improve the catalytic performance. This work is focused on the characterization of basic sites introduced by the functionalization treatment with NH_3. The characterization techniques which can be applied for this scope are few. Among these, potentiometric titration with strong acid has been extensively applied for the determination of the amount and the strength of the basic sites in carbon material[74,141,202]. Intrinsically, chemical titration does not give information about the molecular structure of the species but conceptually the comparison with the pK_a value of model compounds can be used to derive structural information. As already mentioned, the critical aspect in the characterization of the carbon materials is that due to the high

heterogeneity of the surface species, the experimental techniques often suffer from the impossibility to resolve the individual chemical entities. In fact, the surface of carbon materials is more properly described as a distribution of surface chemical properties characterized by titration curve with not-well defined equivalent point. In some case numerical methods for data deconvolution have been applied[202] to determine qualitatively and quantitatively the number of functionalities being titrated. In the attempt to assign the chemical identity of these species, informations from other characterization techniques are useful. Another critical aspect is that the correlation between the results obtained by different characterization techniques is not always straightforward. This is due to the fact that the functional groups behave flexibly to the characterization environments, i.e. in liquid phase or gas phase, and during the characterization tests they might undergo to changes (sometimes irreversibly). The effect of the dynamic character of the carbon surface is difficult to predict since it depends on a series of factors, such as the experimental set-up and conditions used, and the nature of the samples. This point is highlighted and discussed in this chapter with the critical analysis of the results obtained by the characterization of the surface chemistry of carbon. Further characterization of the surface chemistry of the functionalized carbon is carried on by means of microcalorimetric gas-phase titration using an acidic probe molecule. Such characterization technique widely used for the characterization of basic sites in oxide is rarely applied in the researches for the determination of basic sites in carbon materials[203]. Tentatively, the correlation of the results of basic sites characterization by potentiometric titration and microcalorimetry with the spectroscopic characterization discussed in Chapter 4 is presented with the aim to have a complete picture of the surface chemistry of the CNFs.

5.1 Potentiometric titration with HCl

Typically, the titration curve of a suspension of a carbon materials does not show well separated equivalent-points[202,74]. This fact is usually interpreted as result of the wide varieties of intra and intermolecular interactions between neighboring species, which

alter the original Brønsted acid/base character and produce broadening in the pK_a domains resulting in the overlapping of the equivalent points relative to different species. This was always observed in the potentiometric titration of acidic sites by NaOH[202]. Indeed, potentiometric titration by HCl gives a titration curve characterized by two distinct equivalent points (EQP) as shown in Fig. 5.1. Table 5.1 reports moles of basic site and the pK_a for the two species. The amount of basic sites is of the same order for all samples, with slightly stronger basic character for the samples functionalized at higher temperature. This seems to be in contradiction with expectations based on the total amount of nitrogen detected by XPS or by elemental analysis (Table 4.3 Chapter 4). Before discussing the results from the titration some considerations are necessary.

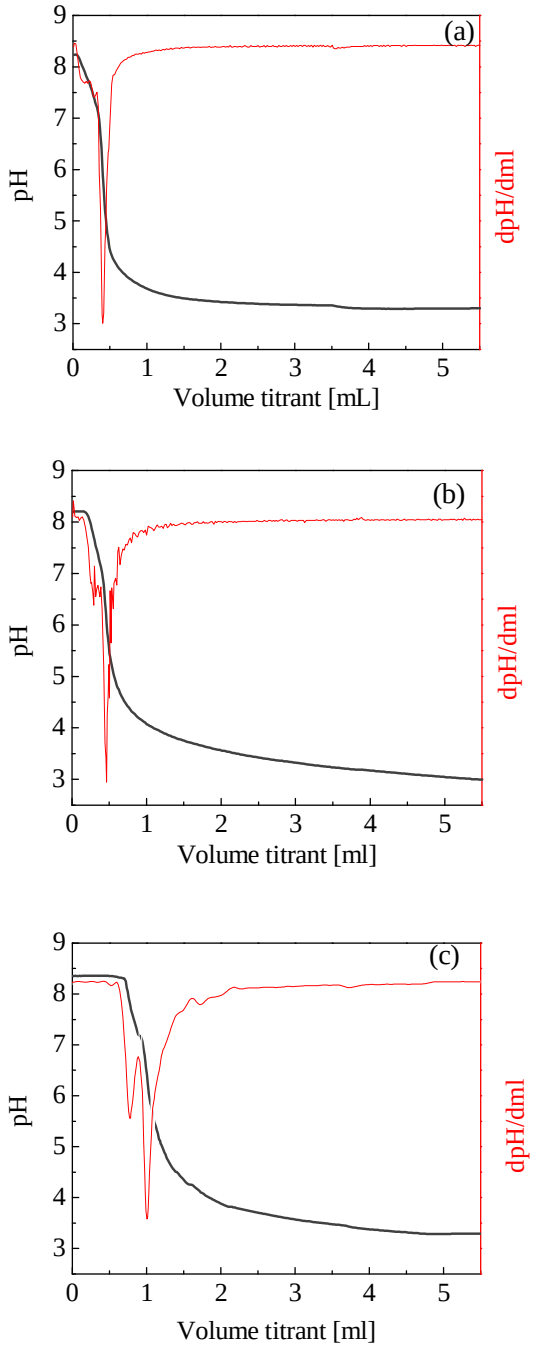

Fig. 5.1: HCl titration curve: (a) NCNF473K; (b) NCNF673K; (c) NCNF873K

We learn from the analysis of the XPS results presented before, that the samples contain a distribution of oxygen and nitrogen functionalities, which is temperature dependent. Thus, each sample presents a distribution of acidic and basic species. Once the samples are immersed in water and left to equilibrate under stirring overnight, acid/base reaction will occur between functional groups and water molecule. The concentration of hydronium generated by reaction of the water with the acidic sites is ruled by the pK_a value of the species, while the concentration of hydroxyl ion by the pK_b value of the basic

sites. Thus, a multitude of acid/base equilibriums coexist. The neutralization of

Table 5.1: Amount of Basic sites determined by potentiometric titration

Sample	mol basic site/g	pK_a
NCNF473K	$4.5*10^{-4}$	7,9; 7.8
NCNF673K	$6*10^{-4}$	8.2; 8
NCNF873K	$1*10^{-3}$	8.35; 8.34

the hydronium ions with the hydroxyl ions results in the final pH of the solution which mirrors the distribution of species on the samples. The final pH of the solution in contact with the carbon sample is in the basic range and it depends on concentration and strength distributions of the original acidic and basic sites of the sample. When the acid titrant is added to the basic CNFs suspension, the hydronium concentration increases and consumes the hydroxyl ions, which shift the base protonation equilibrium toward the right, to form new hydroxyl ions. This will occur until the equivalent point is reached when all the basic sites are consumed. Half of the volume added to the equivalent point corresponds to the condition in which the base is in the protonated form for half of the total concentration according to the following equation for a generic acid HA:

$$pH = pK_a + \log [A^-]/[HA] \quad \textbf{(4)}$$

At this point, the pH value of the solution corresponds to the pK_a of the base. However, one must take into account that the position of the equilibrium for a type of basic sites does not only depend on the solvent used, which act as the acidic counterpart, but also on the acidic sites present on the surface samples investigated. For instance intermolecular and intramolecular hydrogen bond between neighboring species might change the proton affinity for certain functionality. According to XPS analysis, all samples contain different types and amounts of species. In particular, the sample functionalized at 473 K still contains oxygen functionalities with acidic character. During the equilibration time that precedes the titration, the hydronium species generated by the dissociation equilibrium of

the acid species neutralize part of the hydroxyl generated by the protonation equilibrium of the basic species. Thus, for this sample the total volume of acid added is lower compared to the samples functionalized at higher temperature. From other point of view, the strength distribution of basic site is different for the entire set of sample remarking the different distribution of nitrogen functionalities. This is reason for the slight deviation of the pK_a value observed through the samples investigated (Table 5.1).

5.1.1 Correlation of analytical methods with spectroscopic methods: titration vs. XPS

Table 5.2: Dissociation constants of the conjugated acid of base molecules in aqueous solution at 298 K[204]

molecule	pK_a
Ammonia	9.3
n-butylamine	10.77
diethylamine	10.489
piperidine heterocycle aliphatic	11.123
Piperazine	9.83
Benzylamine	9.33
Succinimide	9.6
Aniline	4.63
Pyridine	5.25
Pyridine 2-amino	6.82
Pyridine 4-amino	9.1141
Piridine 2-hydroxy	1) 0.75 2) 11.65 [293 K]
pyridine 2-aldoxime	1) 3.59 2) 10.18
Pyrazine	0.65
quinoline	4.90 [293 K]
isoquinoline	5.42
acridine	5.58
pyrrol	0.40
Naphthylamine	3.92
Benzimidazole	5.532
2-pyridone	11.70[205]
phtalimide	8.3[205]

In order to identify the chemical nature of the species being titrated, correlation with the pK_a value for organic model compounds could be established. However, it is well known from organic chemistry that the pK_a[206] value of certain acid/base specie substituted in the benzene ring is influenced by several factors including the inductive/mesomeric effect of

neighboring species, the number of member of poly-condensed aromatic cycle, the position and eventually the relative position of the nitrogen with other hetero-atoms in the cluster (structural isomer). Some theoretical works aimed at the understanding of the origin of the basicity of the carbon surface are present in literature[75]. In order to justify the strong basicity of carbon, the proposed basic oxygen species structure such as carbonyl or ethers group must be present in conjugated polycyclic pyrone-like structure. In such way the pK_a value of a pyrone species rise dramatically from 5.5 in the case of two condensed pyrone-like rings up to 8-12 for three condensed pyrone-like rings depending on the geometric isomer. This phenomenon is more pronounced for oxygen species than for nitrogen species[75].

Besides chemisorbed species, considered as the main font of the acid/base character of the carbon surface, the π-electron system in graphitic system is also considered as font of weak Lewis basicity. However, changes from sp^2 planar geometry to partial sp^3 hybridization induced by the curvature of the graphene layers produce localized charge accumulation and/or depletion which influence the acid/base character of the carbon surface. At the moment, however, there is not any work in literature aimed to calculate the effect of the structural curvature on the acid/base strength of the carbon surface. Nevertheless, it is interesting to compare the results of the basic sites titration with the structural informations obtained by another characterization technique.

For instance, in spite of some remaining uncertainties in the assignment of some XPS peak components to a specific structure, the XPS chemical shift allows to evaluate the chemical nature of the species generating the signal. The correlation of the XPS with titration data might help in the tentative to assign the chemical structure of these functionalities.

Already in early studies of Shirley[200,201,] the attempt to correlate the variation in proton affinity of an alcohol and amine to the variation in the O1s and N1s BE, was presented. The chemical shift of the BE value observed in the XP spectrum for a certain atom, N or O, in a specified chemical bonding state, sp, sp^2 or sp^3, might be due to initial state effect which depends on the inductive withdrawing (shift to higher BE) or donating (shift to lower BE) exercised by the neighboring atoms and on the mesomeric effect. The inductive effect depends on the electronegativity of neighboring atoms, while the

mesomeric effect depends on the possibility to delocalize electrons through the π-system. It might also be due to final state polarization effect which depends on the capability of the species to stabilize the charge induced by the core-hole created as consequence of the photo-emission process. According to these authors, for aliphatic amine, final state polarization effects determine the chemical shift more markedly than initial state effect, in such way that the better the charge on the O or N is stabilized by the surrounding groups the more pronounced is the BE shift to lower value. In fact the authors explain that the final state polarization effects act as internal solvation, remarking the role that the solvent has in liquid-phase acid/base equilibrium. While performing XPS measurement, depending on the hydrophilic/hydrophobic character of the material, a monolayer of water is present remarking the situation in aqueous phase. In this situation, the protonation of the basic site might occur leading to the shift of the BE to higher value[207]. The concept described above can be applied in the present work by considering the BE shift as a measure of the basicity of the functional groups present on the aminated carbon surface.

Table 5.2 reports the pK_a values of organic bases. In analogy to the pK_a value for the most common organic base compounds reported in Table 5.2, the pK_a values found in this work range between 7.9-8.35 and are in the same magnitude of the aliphatic amine. While correlating the XPS data with those obtained by potentiometric titration in analogy to the pK_a of model compound, a plausible N chemical bonding configuration with similar pK_a is the phtalimide-like structure (pK_a 8.3). This is found in the XP spectrum at 400.9 eV[208] which is close to the value at which we assigned the N4 species. Unfortunately there is no correlation along the sample investigated between the amount of the N4 species and the amount of species giving arises to the first EQP. Indeed, it is interesting to note that the volume of titrant added to the 1st EQP increases with the functionalization temperature, similar to the increasing amount of the pyridine species observed in the N1s XPS (Fig. 4.22). The reported pK_a value for the pyridine is about 5.2 and it differs largely from the pK_a value found ranging 8.3-7.9 which approach the value tabulated for aliphatic amine. Indeed, the NH_2 groups substituted to the aromatic ring, in aniline, has a pK_a of 4.6. Condensed aromatic cycle, as it is in acridine, are characterized by a pK_a of 5.6. Increasing the number of poly-condensed aromatic hetero-cycle

containing N will not lead to a conspicuous increase of the pK_a value[75]. Indeed, the substitution of a basic group, NH_2 i.e. in position 2 or 4 with respect to the pyridine nitrogen, produces a consistent increase of the pK_a value up to 9. However, from the XPS quantification analysis there is no evidence that the coexistence of different functional groups highly conjugated with the pyridine species such as amine or hydroxyl group, would be the reason of the high pK_a value found with respect to the model compound. In fact, there was not any species which would be present in the same amount of pyridine and justifying the trend observed through the samples investigated (Table 4.4). However, the trend observed for the 1st EQP is a clear indication that the pyridine species is involved. And in fact this species is considered the most basic among all the N species introduced according to its lower BE. It should be pointed out that the XPS BE of pyridine in carbon material shift to lower BE if compared to the value for model compound (399 eV) in which pyridine is grafted on the surface of a solid and does not interact electronically (not shown). This is an indication of the stronger basic character of the pyridine in the graphene layer with respect to the model compound. Note that the local partial sp^3 character of the sp^2 graphitic structure induced by the curvature (presence of pentagonal hetero-cycles) produces localized charge accumulation which might explain the increased basicity of the pyridine species. From the XPS characterizations, the species giving arise to the 2nd EQP should be due to amide, lactam species and all the other species found at the higher BE side of the XP spectra. Pyrrol is a very weak base (conjugate acid pK_a=-4). The N lone pair is involved in the π electron aromatic system. Protonation will destroy the aromatic character of the π electron system and this makes the process unfavorable. It is thus unlikely that this functionality will be detected by titration. Amides do not have noticeable acid/base properties in water. This lack of basicity is explained by the electron-withdrawing nature of the carbonyl group where the lone pair of electrons on the nitrogen is delocalized by resonance, thus forming a partial double bond with the carbonyl carbon. Therefore there is more electron density on O than N and under extremely acidic conditions the carbonyl oxygen can become protonated with a pK_a of roughly -1.

However, amide breakdown might occur via amide hydrolysis. Such hydrolysis can occur under basic or acidic conditions. Acidic conditions yield the carboxylic acid and the

ammonium ion. In fact, in the characterization by titration in aqueous solution, amide and lactam are equivalent species and there is not possibility to distinguish them if one considers that in acid environment lactam is susceptible of ring opening to form amide species, which undergoes hydrolysis. The lactam is found in the XPS spectra with BE shift at 400.1 eV (N3). However there is not correlation between XPS and titration results even by summing all the N2 and N3 contributions. This is due to the fact that the chemical treatment in ammonia, not only introduces basic sites with relative amount and strength that are temperature dependent, but also modify the distribution of the original acidic site. In fact conversion of oxygen acid sites in basic sites occurs during the thermal treatment. All those species contribute to define the acid/base character of the carbon surface[75]. According to theoretical calculation oxygen species are more strongly affecting the basic character of carbon surface than nitrogen species. Nevertheless they are influent. The thermal treatment of the CNFox up to 873 K in the absence of NH_3 produces an increase of the basic character of the carbon surface less pronounced that the aminated sample at 873 K[209] (not shown).

5.2 Microcalorimetry titration of basic sites with CO_2 as probe molecule

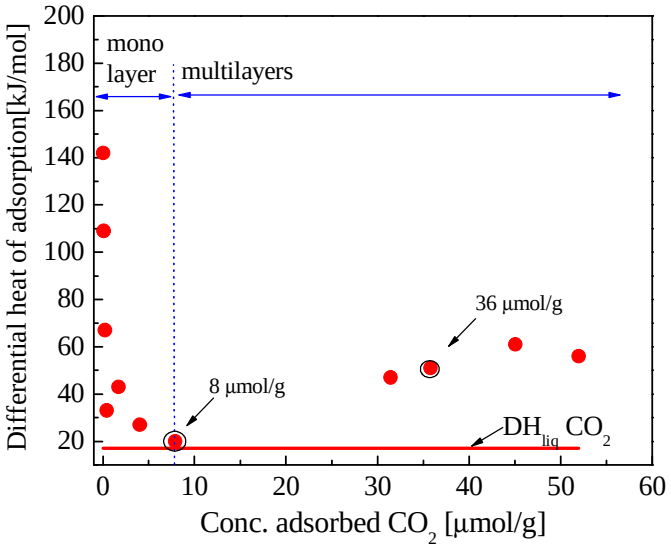

Fig. 5.2: Differential heat of CO_2 adsorption for NCNF873K.

In order to determine the amount and the strength distribution of the basic sites on the carbon surface, the adsorption of CO_2 was studied by microcalorimetry at 313 K. The differential heat of adsorption as function of the CO_2 uptake for the sample NCNF873K is reported in Fig. 5.2. At low CO_2 coverage, the initial differential heat of adsorption is very high and decreases rapidly to reach a plateau with increasing CO_2 pressure. The high values for the initial heat of adsorption and the rapid decreases with increasing coverage demonstrate the presence of heterogeneously distributed and energetically different adsorption sites (basic). Above 8 µmol/g of CO_2 uptake the differential heat of adsorption reach the value of the heat of condensation of CO_2 (-17 kJ/mol) indicating that in this range the monolayer is completed and multilayer adsorption proceeds. Successively, at higher coverage of CO_2, the heat of adsorption increases again indicating that the adsorption of CO_2 is accompanied by secondary exothermic processes may be reaction of CO_2 with the species on the carbon surface. This can be better observed in the integral heat of adsorption recorded as function of time reported here for the sample NCNF873K in Fig. 5.3, Fig. 5.4 and in Fig. 5.5. In Fig. 5.3 is reported the heat signal at low CO_2 coverage (1.7 µmol/g) corresponding to a differential heat of adsorption of 100 kJ/mol (Fig. 5.2). After the adsorption peak, the heat signal reaches the baseline which is an indication of a quasi pure adsorption process.

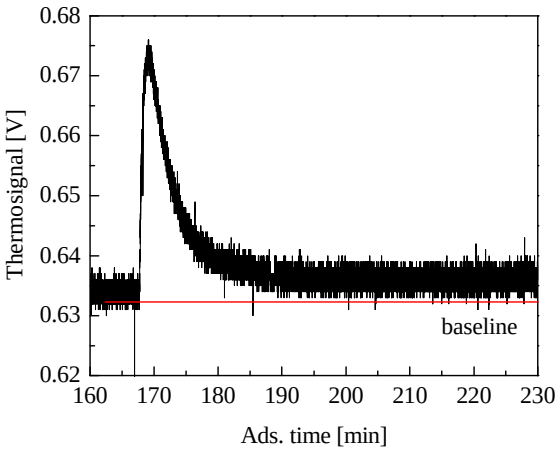

Fig. 5.3: Integral heat signal vs time at 1.7 µmol/g of CO_2 (monolayer region) for NCNF873K.

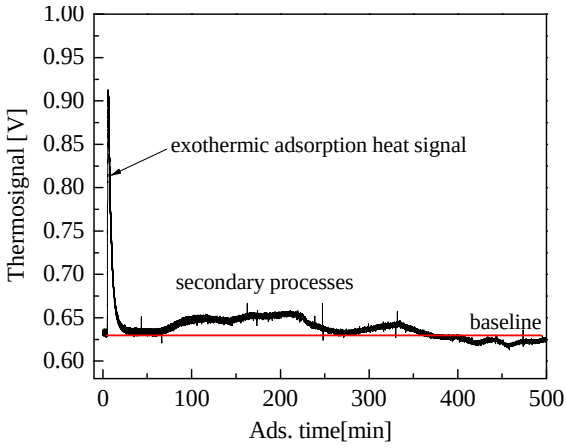

Fig. 5.4: Integral heat signal vs time at 36 µmol/g of CO_2 (multilayer region) for NCNF873K.

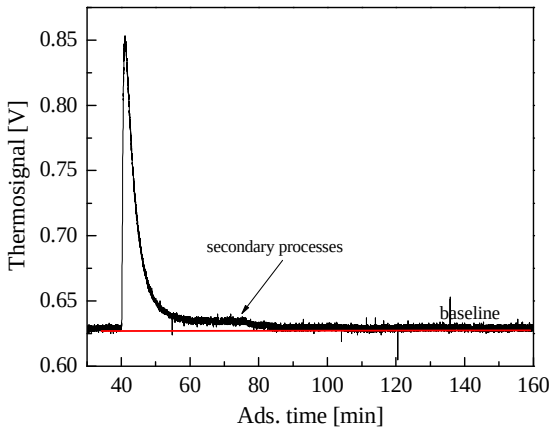

Fig. 5.5: Integral heat signal vs time at 45 μmol/g (multilayer region) of CO_2 for NCNF873K.

With increasing CO_2 coverage (36 μmol/g) corresponding to a differential heat of adsorption of 51 kJ/mol (Fig. 5.2 multilayer region), similarly after the adsorption peak, the heat signal reach the baseline. However after a certain adsorption time, exothermic secondary processes occur as suggested by the increase of the heat signal in Fig. 5.4. At further increase of the CO_2 coverage (45 μmol/g) corresponding to a differential heat of adsorption of 61 kJ/mol (Fig. 5.2), the integral heat signal after the adsorption peak does not reach the baseline and at this condition the secondary processes occur earlier (Fig. 5.5). For the sample NCNF873K, the total amount of integral heat of adsorption measured (-575 mJ) is much higher than the amount of the integral heat of desorption (+138 mJ) indicating the irreversibility of those secondary processes. The differential heat of adsorption in the monolayer region as function of CO_2 uptake for the various samples investigated is shown in Fig. 5.6.

The highest value of differential heat of adsorption, estimated from the first adsorption point, was measured for the sample NCNF873K and it is about 150 kJ/mol. Similar value has been reported for other system such as for hydrotalcite[210], γ-Al_2O_3[211] . In the case of the sample NCNF873K, after the desorption process, the re-adsorption produces a lower amount of differential heat that approach the value found for the sample NCNF473K, which gives arise to an initial heat of adsorption of about 90 kJ/mol (Fig. 5.6a black scatter and Fig. 5.6b). Thus, probably very small amount of very strong basic sites giving arise to the very high initial differential heat are lost during the first run of adsorption due to the reaction with the CO_2.

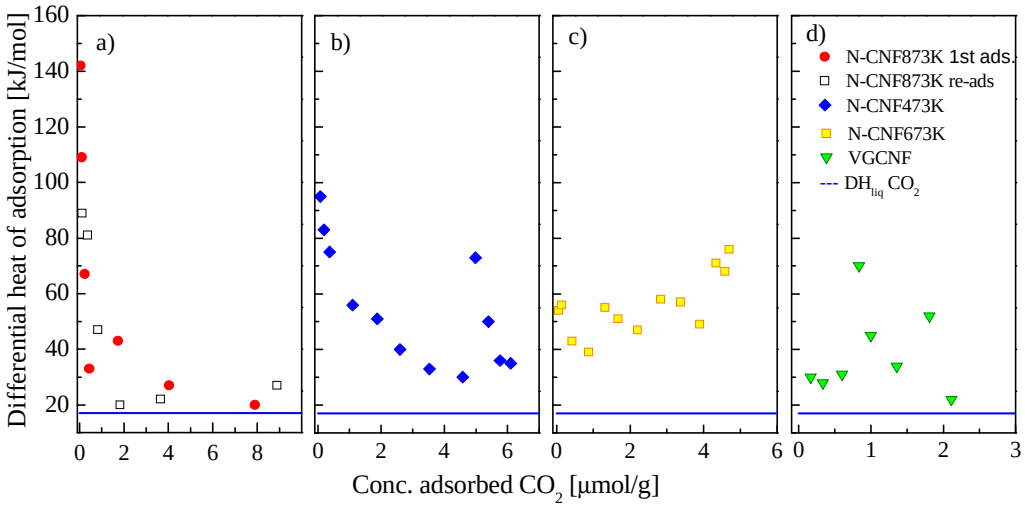

Fig. 5.6: Differential heat of CO_2 versus CO_2 uptake in the monolayer region for the CNFs samples.

A Similar value of differential heat of adsorption measured for the sample NCNF473K is reported in literature[212] for amino groups grafted on SBA-15. At high coverage the curve of the heat of adsorption for the sample NCNF473K almost coincide with that one of the sample NCNF873K. Thus also in this case the monolayer is formed before secondary reactions take place. Following, the sample NCNF673K gives arise to heat of adsorption around 50 kJ/mol. The functionalities on the surface of this sample are highly reactive with respect to the CO_2. In contrary to the other samples, in this sample the secondary reaction occurs before that the monolayer is formed. For this reason, it is not possible to make a precise conclusion on the strength distribution of the basic sites. Interesting to note that the heat of adsorption measured for the commercial VGCNF is very low around 30 kJ/mol, however slightly above the enthalpy of liquefaction of carbon dioxide (ΔH_{liq} 17 kJ/mol)[210-212], thus there is a moderate interaction between the adsorbed carbon dioxide molecules and the VGCNF surface. Also for this sample secondary reactions take place before the formation of a monolayer (the heat of adsorption increase without reaching the value of the enthalpy of liquefaction of CO_2).

The CO_2 isotherms for the samples investigated are reported in Fig. 5.7. The monolayer is completed at < 2 mbar CO_2 for NCNF873K and < 6 mbar for NCNF473K, and above this value is the multilayer region (identified by a frame in Fig. 5.7). In the multilayer

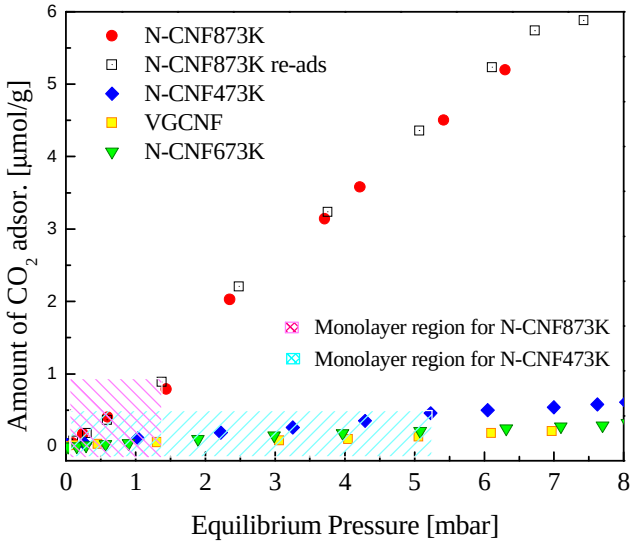

Fig. 5.7: CO_2 adsorption isotherm for the CNFs samples.

region secondary reactions occur. Among the samples investigated, only the sample NCNF873K gives considerable amount of CO_2 adsorbed and for all the others samples the number of basic sites is very low. Since for the samples NCNF473K and NCNF873K the monolayer is formed before secondary reactions takes place, the amount of CO_2 adsorbed to the point at which the monolayer is formed (when the differential heat reaches the enthalpy of CO_2 liquefaction) is indicative of the amount of adsorption sites present on the sample. For the other samples NCNF673K and VGCNF characterized by secondary reactions before the monolayer formation, the quantification of the basic sites is not accurate. For the sample NCNF873K, the amount of basic sites measured in the isotherm of the re-adsorption step is the same as the first adsorption process. It is possible that a chemical modification of the original basic sites is induced by the CO_2 adsorption, i.e. oxidation of the basic site by CO_2 giving arise to the same amount of adsorptive basic sites as in the first run of CO_2 adsorption but with lower basic strength. Another possible explanation is that there is a very small amount of very strong basic sites giving rise to the very high initial differential heat which are lost during the first run of adsorption. The amount of these sites is so small, in comparison with the population of others basic sites that not any differences are observed in the adsorption and re-adsorption isotherm. The CO_2 isotherm for the samples NCNF473K and NCNF873K are analyzed by applying the Langmuir adsorption model in order to calculate the amount of basic sites. For those two

samples the experimental isotherm in the monolayer region fits very well to the theoretical isotherm according to Langmuir model with an order higher than one. The order of the isotherm larger than one matches with the consideration that this is not a pure adsorption process but rather secondary reaction contribute to the differential heat of adsorption. This is specially seen in Fig. 5.6b for the sample NCNF473K (blue spots) where the differential heat of adsorption drastically increases at 5 µmol/g of CO_2 adsorbed. At this point, the differential heat of adsorption is due for 30 kJ/mol to the pure adsorption and 40 kJ/mol is due to the secondary process. The specific surface area calculated by the CO_2 adsorption is of about 2 m^2/g and 1 m^2/g for the samples NCNF873K and NCNF473K, respectively. This value differs largely from that one calculated based on N_2 adsorption which were about 55 m^2/g.

5.2.1 Correlation of potentiometric titration with microcalorimetry data.

The liquid phase titration of basic sites in aqueous solution by means of inorganic acid such as HCl is a way of characterization of the Brønsted basicity intended as affinity of a certain species toward protonation. In gas phase, indeed, the mechanism of acid/base interaction is not the proton transfer, but rather an electron pair is involved, donated from the base to the acid which is an electron deficient species. Thus, gas phase titration is a way of characterizing the basicity according to Lewis definition. In addition, the functional groups must be considered as dynamic entities on a carbon surface and might undergo changes during evaluation. Acid/base reactivity should not be considered as a static property of a material, but rather as a dynamic properties of the carbon surface that respond flexibly (sometimes irreversibly) to its environment. For this reason the two experimental characterization technique should not give necessary consistent results on the same sample. However some correlations might be established.

The summary of the results by microcalorimetry and liquid phase titration are reported in Table 5.3.

Differential heat of adsorption for samples investigated partially correlates with titration data. For the most basic sample (NCNF873K), microcalorimetry measurement evidences few very strong basic sites coexisting with weakly basic sites present in prevalence.

Although, the number of active sites differ in absolute value, this sample was also the most strongly basic one and with the largest amount of basic sites according to the potentiometric titration characterization. The miscorrelation regards the sample NCNF673K, which contains the weakest basic sites according to microcalorimetry. Indeed potentiometric titrations give for this sample a larger amount of basic sites than for the sample NCNF473K.

Table 5.3: Summary of titration and microcalorimetry results of the N-CNFs samples.

Sample	Liquid phase titration		Gas phase Microcalorimetry	
	mol basic site/g	pK_a	Amount of CO_2 (monolayer) mol/g	Initial differential heat of adsorption KJ/mol
NCNF473K	$4.5*10^{-4}$	7,9; 7.8	$5*10^{-6}$	90
NCNF673K	$6*10^{-4}$	8.2; 8	$1.5*10^{-6}$	50
NCNF873K	$1*10^{-3}$	8.35; 8.34	$8*10^{-6}$	150

It was already reported in chapter 4 that the functionalization at 673 K lead to the closing of amide group to form lactam that shows a lower basicity than amide groups due to the involvement of the N electrons in the π-system of the graphitic structure of the CNFs. This was observed by the increase of the intensity to higher BE from the functionalization at 473 K to the functionalization at 673 K. Those species would be characterized by a very low Lewis basicity during CO_2 adsorption by microcalorimetry. Indeed, the lactam bond hydrolysis occurring in water solution to form amide could explain the higher amount of basic sites determined by potentiometric titration with respect to the microcalorimetry experiments. Finally, it must be recognized that the microcalorimetry experiment for the NCNF673K was characterized by secondary process occurring before the monolayer formation which, in fact, hinders the characterization of the strength distribution of the basic sites.

6

Application of N-containing CNFs in heterogeneous catalysis: liquid-phase selective oxidation of benzyl alcohol to benzaldehyde over Pd-based catalysts

In this chapter, the application of N-CNFs as support for Pd nanoparticles and the catalytic performance of the catalysts in the liquid phase oxidation are presented. The study aims at the understanding of the role of the surface chemistry of the CNFs in the reactivity of Pd nanoparticles.

The development of solid catalysts active in the partial oxidation of alcohols has been recently the subject of growing interest[88] due to their central role in the production of fine and specialty chemicals. Among these, the oxidation of benzyl alcohol is the most commonly reported test reaction, since it occurs with good selectivity and yields to benzaldehyde on a large variety of catalysts[213]. In this context, tailoring the "superficial metallic structure"[78] , which is intended as the coordination number between the active metal atoms at the surface, is crucial towards the achievement of very selective and active catalysts. The intrinsic surface activity of a catalyst can be modified by exposing different crystallographic planes or inducing low coordinative defective sites such as kinks and steps. This can be achieved in different way, for instance, by varying the particles size in the range of very small nanoparticles approaching clusters dimensions; by diluting the active species with spectator species, or by inducing metal-support interaction.

Different catalytic system based on noble metal nanoparticles[214,215,216] have been investigated for alcohol oxidation with molecular oxygen or hydrogen peroxide in liquid

phase. Research has traditionally focused on the use of supported noble metal nanoparticles catalysts, such as Pt/C or Pd/C catalysts[217,218].

In the studies reported in literature, the target in the synthesis is searching for a preparation route that can lead to a colloidal solution of metal nanoparticles characterized by narrow size distribution approaching the ideal mono-dispersion. In fact, the size of nanoparticles is considered as the direct controllable parameter related to special structural features that determines the reactivity and the selectivity of the catalyst.

Commercial carbon supports have been used for the macroscopic assembling of the metal nanoparticles[4,145,146], however the influence of the surface chemistry of the carbon support on the adsorption of the metal nanoparticles and the morphology of the wetting particles at the carbon surface was often neglected. In contrary, it is important to elucidate the effect of the surface chemistry of the carbon support in the preparation of immobilized metal nanoparticles.

In order to favor the deposition of the metal nanoparticles at the carbon surface, the surface chemistry of the support in contact with the colloidal solution of the nanoparticles must be tailored in such a way to realize an attractive interaction particles/support.

Furthermore, the nature of the interaction at the metal/support interface influences the catalytic performance of the metal nanoparticles-based catalyst[78].

Weak metal-support interactions (WMSI) stabilize the metal nanoparticles at the defects sites, steps and kinks of graphitic structure preventing the sintering or leaching of the metal nanoparticles into the reaction media. In addition, WMSI are responsible for the peculiar chemical behavior of carbon supported catalyst[231]. The surface chemistry of carbon affects the nature of the metal-support interaction and modify the morphology, the crystallographic metal phase and the electronic structure of the nanoparticles[77,78].

Recently with the boosting of the carbon nanotubes as a new carbon material in heterogeneous catalysis, there is a growing interest in the application of this material in reaction in which carbon materials were historically used either as catalyst itself as well as support for metals[219]. Due to the higher graphitic order of nanostructured carbon materials with respect to AC, which implies higher “inertness”, they can be functionalized in a more selective way preventing the deep changes of the textural properties. It is thus expected that the more defined physic-chemical properties in NC

leads to higher selectivity for the applications in catalysis. In addition, the micropores present in AC have a detrimental effect on mass transport phenomena especially in liquid-phase reactions. This problem is by-passed by using NCs which are characterized by mesoporous texture. In the prospective of rational design of the catalyst, this work aims to establish the role of the surface chemistry of the NCs in the reaction mentioned above.

The screening of CNFs supports with different surface chemical properties (acid/base and hydrophobic/hydrophilic) is used to investigate the influence of those characteristic on the catalytic performance of Pd-based catalyst in the reaction under investigation. Pd was chosen as active species since it shows better performance compared to other metal such as Au, and more poisoning resistant compared to Pt.

Although, only oxidation in the aqueous phase is of practical importance due to safety reason, the catalytic tests have been performed in both solventless and aqueous media in such a way that the influence of the mass transfer of the reactant to the catalysts surface is taken into account. The application of the Pd -CNFs based catalyst in the direct synthesis of H_2O_2 is reported with the aim to corroborate the hypothesis of improved affinity of the Pd nanoparticles towards the O_2 activation induced by a controlled N functionalization of the CNFs.

6.1 Pd on N-containing CNFs

6.1.1 Catalyst preparation

The phenomena regulating the adhesion process of the polymer-wrapped metal nanoparticles onto the carrier surface during the immobilization can have different nature. The pathway in which the process occurs is strictly depending on the chemical properties of the couple support/metal nanoparticles colloidal solution and on the condition in which the immobilization is carried out (with special regard to the pH of the solution). It can occur through electrostatic interaction (Van der Walls interaction, ionic and polar covalent bonding) between the charged surface of the carbon material and the charged surface of the wrapped metal nanoparticles in the colloidal solution. This is the dominant

adsorption mechanism in case of hydrophilic systems. It requires the presence of electron-donating/accepting sites (Lewis acid/base couple) and Brønsted acid/base couple between the carrier surface and the metal nanoparticles surface.

Indeed, dispersive interactions are typical of hydrophobic material. In the case of graphitic material they occur mainly through so called π-stacking interaction.

In order to obtain Pd nanoparticles homogeneously distributed on the surface of CNF, it is important that the particles-support interaction is stronger than particles-particles interaction in the colloidal solution. As the catalytic properties of nanoparticles are "size-dependent", it is necessary that the adhesion of the metal nanoparticles to the CNFs surface occurs through interactions with the protective layer of polymer. The protective agent stabilizes the metal nanoparticles and preserves the metal nanoparticles size by limiting the coalescence. Once the metal nanoparticles are deposited on the surface, the catalyst is washed, owing to remove the excess of protective agent. Since the ions adsorption on a surface occurs by electrostatic interaction[141] between the ionized species on the carbon surface and the ionic species present in the aqueous phase, the catalyst preparation must be optimized in order to realize an attractive interaction. In this context, Zeta potential measurements turn out to be very useful. At pH below the pH_{IEP} the resulting surface charge is positive and the carbon surface attracts anions, while above it is negatively charged and attracts cations.

Fig. 6.1 shows Zeta potential measurements of all the supports and of the Pd-PVA colloidal solution.

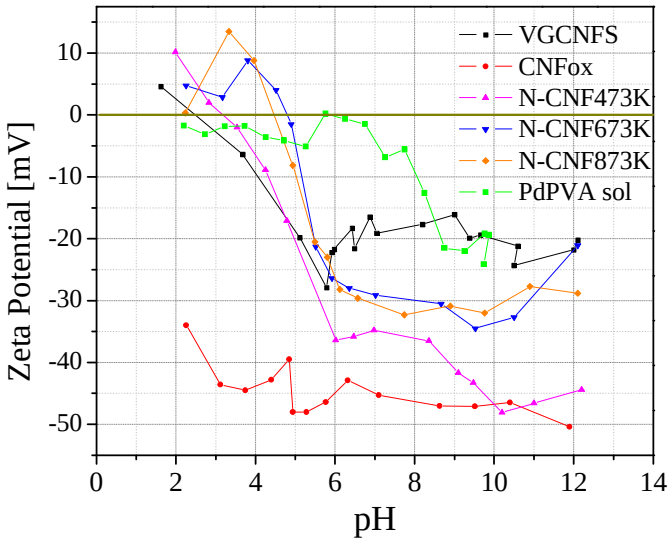

Fig. 6.1: Zeta potential measurements; ■ CNFs ● CNFox▲ NCNF473K▼NCNF673K ◆NCNF873K ■ Pd-PVA sol.

At high pH, around 2, all the supports investigated have a positive charge while the Pd-PVA colloid solution is negatively charged. Thus, by carrying the immobilization at low pH, i.e. 2, the attractive interaction will be realized and at the same time the metal nanoparticles dispersion is preserved. However, the surface chemistry of carbon is heterogeneous. Carbon is characterized by the coexistence of both negatively and positively charged sites, in a given relative amount that depends on the pH of the solution. Furthermore it is always composed by hydrophilic domains, coexisting with hydrophobic domains. Thus, driving force for the metal sol immobilization with different nature than the electrostatic interaction cannot be excluded. It was demonstrated that the adsorption on HSAG (high surface area graphite) occurs through dispersive interaction and after oxidation the adsorption capability is weakened because of the removal of electron from the π-system due to the oxidation[70]. This affects to a greater extent aromatic and unsaturated hydrocarbon and to less extent for alkenes,

In this work, the PVA was used as protective agent because it gives colloidal solution of nanoparticles stable in a large range of pH. In addition when AC is used as the support, it was reported that PVA gives a high metal dispersion, almost maintaining the same particle dimension as in the sol[220]. On the contrary other protective agent such as THPC

gives smaller nanoparticles, but there is some agglomeration of the THPC-protected during the immobilization step[146,220]. This is consistent with the results of our experiment reported in Fig. 6.2 for catalyst preparation using THPC as protective agent. Pd nanoparticles agglomeration is evidenced by the bright part in the BSE image.

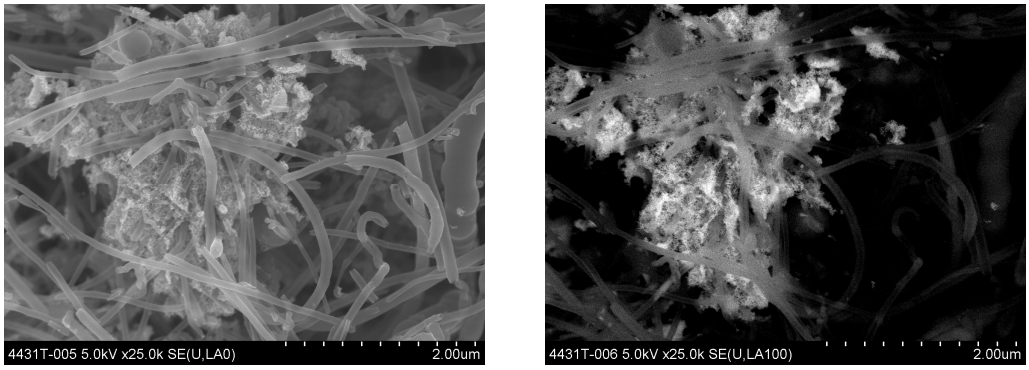

Fig. 6.2: SE (left) and BSE (right) SEM images for the sample Pd-THPC/NCNF473K.

The actual loading of Pd on the CNFs supports determined by XRF is reported in Table 6.1. It is shown that CNFs samples characterized by less hydrophilic surface have higher capability in the metal adsorption. In fact the Pd loading for the samples VGCNFs, NCNF673K and NCNF873K is about 0.7 % in weight, while it is much lower for the most hydrophilic samples CNFox and NCNF473K.

Table 6.1: Pd loading on CNFs samples determined by XRF.

Sample	VGCNFs	CNFox	NCNF473K	NCNF673K	NCNF873K
%wt	0.8	0.35	0.52	0.73	0.77

Characterization and catalytic data related to the system Pd/PVA on CNFs will be reported here following.

6.1.2 Metal nanoparticles characterization by TEM and SEM

The influence of the surface chemistry of the carbon support on the dispersion of Pd PVA-protected nanoparticles has been investigated by SEM and TEM.

Following, some representative pictures of the catalysts are reported. Fig. 6.3 shows SE and BSE images of the sample Pd-PVA/VGCNFs. It is show that the metal

nanoparticles are dispersed over the complete CNFs surface. However from the HRSEM images in Fig. 6.3 it is evident that some tubes present higher particles density as small agglomerate of particles. The same features have been observed for the other samples investigated. The TEM pictures (Fig. 6.4) of the series of catalysts confirm the trend observed in the SEM. Fibres with differently nanoparticles density and nanoparticles agglomeration are present in almost all the sample. It is difficult to judge to which extend this fact occurs as dependence of the surface chemistry of the NC.

The recurrence of metal particles agglomeration on the CNFs surface and the missed deposition of the metal particles in some CNFs could be due to the original heterogeneity of CNFs nanostructure present in the commercial batch used in this work responsible probably of inomogeneous functionalization. Another reason might be related to the immobilization methods of the active species. The low metal loading used in this work and the fast adsorption process might lead to the inhomogeneous wetting of the carbon surface with the Pd colloidal solution.

It should be pointed out that the VGCNFs show metal nanoparticle dispersion similar to that of the other supports, thus the hydrophobic interactions play an important role during immobilization.

In the following paragraphs the results of the catalytic tests and the Cs-corrected HRTEM investigation are presented with the aim to establish a structure activity-correlation. It will be clear how implementation of the microscopy techniques allows the imaging of features relevant in catalysis, which cannot be seen in the conventional HRTEM.

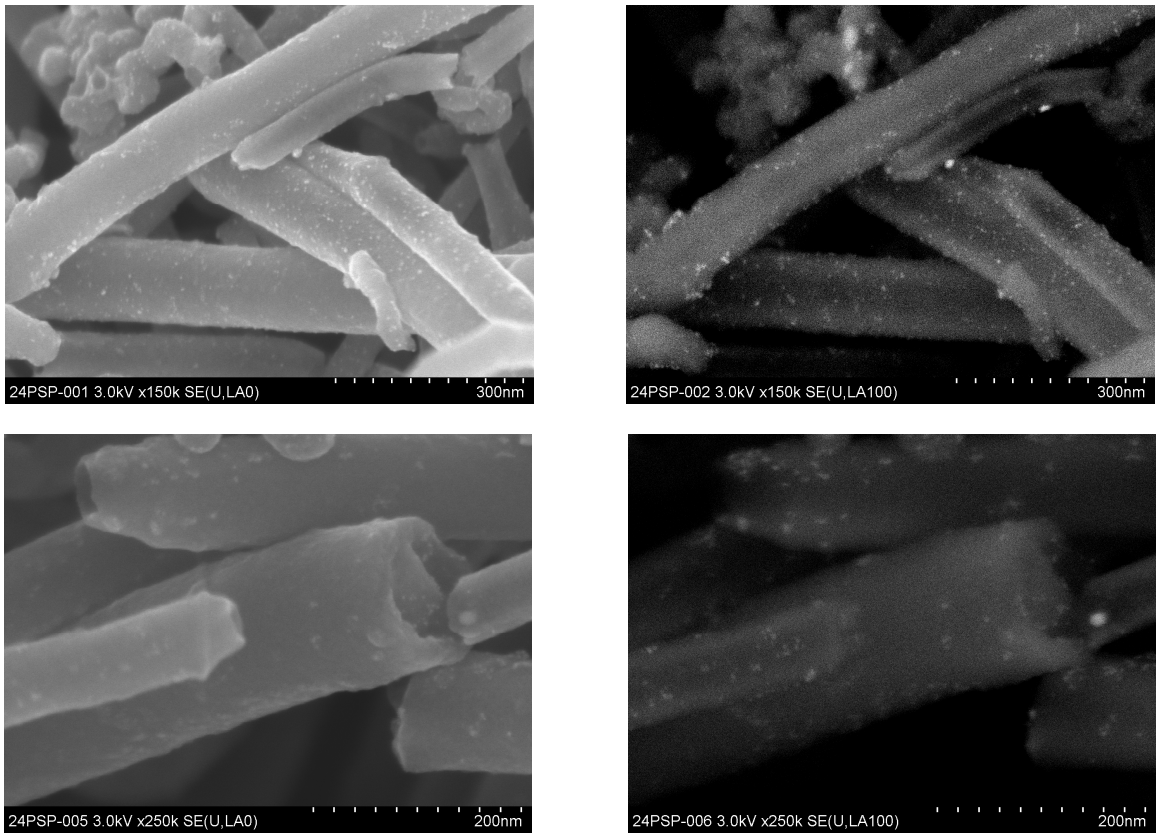

Fig. 6.3: SE (left) and BSE (right) SEM images for the sample Pd-PVA /N-VGCNF.

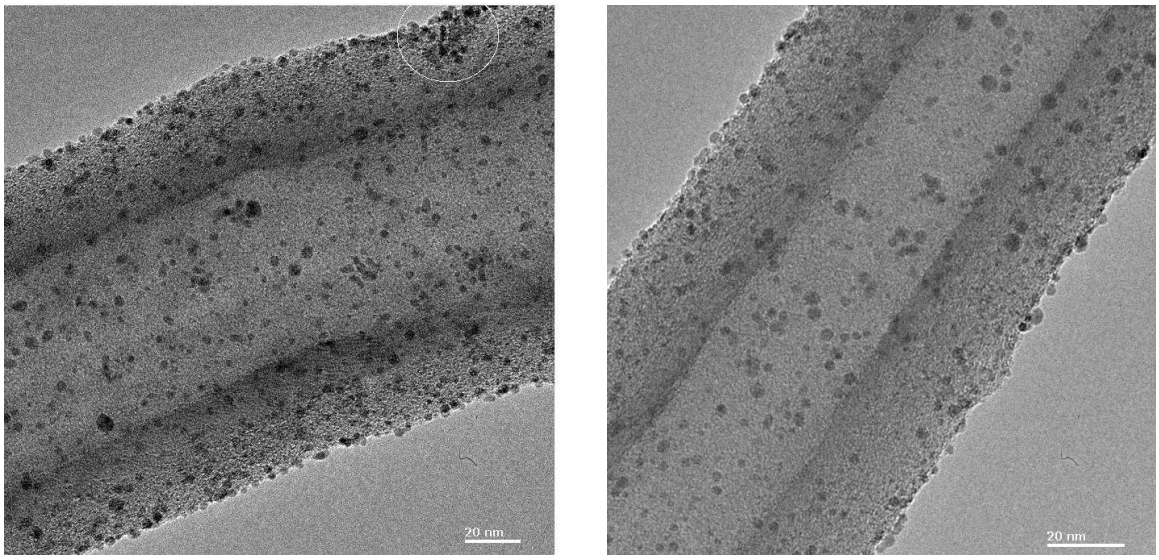

Fig. 6.4: HRTEM images for the sample Pd-PVA/NCNF873K; note different particles density among the CNFs and particular agglomeration of particles in circle in the image on the left side.

6.2 Selective partial oxidation of benzyl alcohol to benzaldehyde by molecular oxygen

The conversion of benzyl alcohol is plotted in Fig. 6.5 versus reaction time for all the catalyst investigated in *solventless* condition.

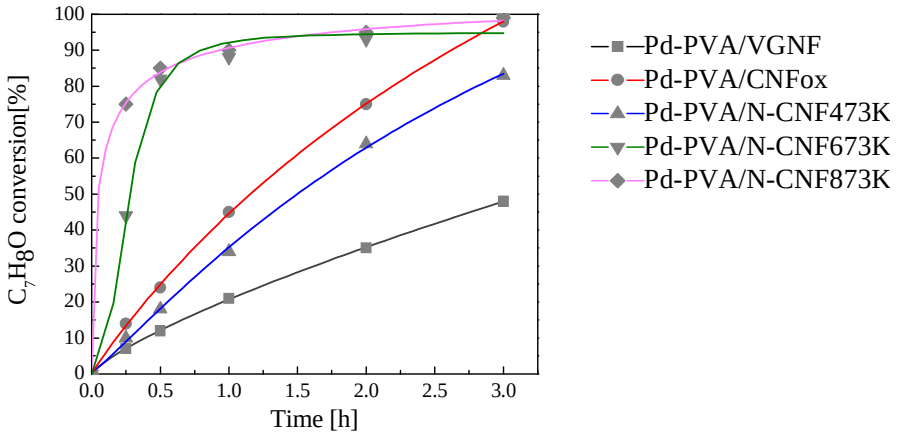

Fig. 6.5: Catalytic data in solventless condition: Conversion *vs* time.

The initial rate of consumption of benzyl alcohol, the initial productivity of benzaldehyde and the selectivity to benzaldehyde in *solventless* condition are reported in Table 6.2.

Table 6.2: Catalytic data in *solventless* condition.

sample	Initial rate of benzyl alcohol consumption [mol/h*g]	Initial rate of benzaldehyde formation [mol/h*g]	Initial instantaneous selectivity to benzaldehyde (%)	Selectivity at max Conversion (%)
Pd/NCNF873K	112	85	76	76 (90%)
Pd/NCNF673K	71	47	66	73.3 (90%)
Pd/NCNF473K	21.74	12.84	60	68.7 (40%)
Pd/CNFox	45.45	33.5	73	75.3 (90%)
Pd/VGCNF	10.2	5	50	74.4 (40%)

The functionalized CNFs supports used as catalyst themselves under the same reaction condition did not lead to a significant benzyl alcohol conversion. However, the functionalization of the surface of the CNFs supports with N or O species leads to better Pd-based catalysts than the Pd-based catalyst on the pristine CNFs. In particular, the N-

functionalization carried out at high temperature leads to a significant enhancement of the catalytic performance. Pd/NCNF873K shows the highest initial rate of benzaldehyde formation. This catalyst reaches almost total conversion after 30 min of reaction and it is the catalyst most active and selective to benzaldehyde. Pd/NCNF673K is also relatively a high active catalyst, however the initial selectivity to benzaldehyde is lower compared to Pd/NCNF873K (75% against 66%). As shown in Table 6.3 the main by-products are toluene and benzene, while benzoic acid and benzyl benzoate are side products formed in a negligible amount. Note that catalysts with higher selectivity to benzene show lower activity. The Pd/CNFox favors the further oxidation of benzaldehyde to benzoic acid and the formation benzyl benzoate.

Table 6.3: Selectivity at maximum conversion in solventless as reported in Fig. 6.5.

Catalyst	Selectivity at maxim conversion [%]					
	Benzene	Toluene	Benzaldehyde	Benzoic acid	Benzyl benzoate	Unknown
Pd/NCNF873K	0.8	18.8	76.0	2.7	1.2	0.5
Pd/NCNF673K	2.4	19.0	73.3	2.9	1.9	0.5
Pd/NCNF473K	5.3	22.8	68.7	1.8	1.4	0.0
Pd/CNFox	3.1	13.1	75.3	3.5	4.4	0.6
Pd/VGCNF	4.3	17.6	74.4	3.2	0.6	0.0

Table 6.4 reports the comparison of the catalytic performance of the Pd-based catalysts after 30 minutes and 2 hours of reaction time in the different media considered in this work (solventless and water). In this way, it is possible to highlight the impact of the mass transfer in the activity and product distribution of the catalysts. In the first 30 min of reaction, the catalysts obtained by immobilization of Pd nanoparticle on NCNFs functionalized at higher temperature lead to higher conversion in *solventless* conditions than in aqueous media. For the catalysts Pd/NCNF473K, the use of diluted aqueous solution of benzyl alcohol has a beneficial effect, in fact in the initial 30 min of reaction, the conversion obtained in aqueous media is much higher than in solventless. Indeed after 2 hours of reaction, the conversion approach similar value in solventless and in aqueous solution for both Pd/NCNF473K and Pd/NCNF873K.

Table 6.4: Catalytic data in solventless *vs* aqueous media.

Sample	Benzyl alcohol conversion after 30min [%]		Productivity of benzaldehyde after 30min reaction [mol*h^{-1}*g^{-1}]		Benzyl alcohol conversion after 2h [%]		Productivity of benzaldehyde after 2h reaction [mol*h^{-1}*g^{-1}]	
	H_2O	SL	H_2O	SL	H_2O	SL	H_2O	SL
Pd/NCNF873K	**46**	**85**	30.5	44	**92**	**95**	15.6	13
Pd/NCNF673K	**35**	**86**	25	45	**90**	**98**	16.8	12
Pd/NCNF473K	**33**	**18**	34	12	**70**	**67**	18.6	13
Pd/CNFox	**25**	**24**	39	28	**34**	**75**	13	23
Pd/VGCNF	**5**	**12**	3.5	3.6	**18**	**38**	3	4.2

The Pd/VGCNF shows the worst catalytic performance regardless the solvent used. In aqueous solution, the Pd/CNFox catalyst, which shows relatively high productivity after 30 min, is almost deactivated as indicated by the low increment of the conversion after 2h (Table 6.4 and Table 6.5). An inversion in the behavior is observed for the sample Pd/NCNF473K which gives higher conversion after 2h of reaction than Pd/CNFox in water, while the opposite situation is observed in *solventless* condition. Those results suggest that the initial course of the reaction depend on the experimental condition used (*solventless* vs. aqueous solution). The availability of the reactants at the catalyst surface influenced by the mass transfer of the reactants and the capability of the catalyst toward the chemisorption of the two reactants determine the productivity and products distribution of the catalyst.

Table 6.5: Catalytic data in aqueous solution.

Catalyst	Time	Conversion	Selectivity			
			Aldehyde	Benzoic acid	Toluene	Benzyl benzoate
Pd/NCNF873K	0.5 h 2 h	46 92	95.6 91.8	3.9 8	0 0	0.5 0.2
Pd/NCNF673K	0.5 h 2 h	35 90	95.4 94.6	3.7 4.8	0 0	0.9 0.6
Pd/NCNF473K	0.5 h 2 h	33 70	96.8 95.7	0.9 3.6	0 0	2.3 0.7
Pd/CNF ox	0.5 h 2 h	25 34	96.2 97.8	0 1.3	3.8 0.9	0 0
Pd/VGCNF	0.5h 2 h	5 18	96.8 93.1	0 6.2	2.1 0.1	1.1 0.6

Under the same reaction condition, while the productivity to benzaldehyde is strongly affected by the surface chemistry of the CNFs support, the selectivity to benzaldehyde is always quite high and similar among the samples investigated compared to the differences observed by using the aqueous solvents (in Table 6.5 the selectivity to benzaldehyde is about 90% in aqueous solution and about 70% in *solventless*). However, regardless the reaction condition, the best catalytic performance is observed for the catalysts Pd/NCNF873K and Pd/NCNF673K in water as well as in *solventless*.

Thus, structural features present in these catalysts must be responsible for the catalytic performance. By evaluating the higher catalytic activity of the catalysts under the same reaction condition (*solventless*), it is clear that the surface chemistry of the support has a strong influence on the activity of the metal nanoparticles. In order to better understand the results from the catalytic tests and to outline some structure-activity correlation, it is necessary to refer to the description of the reaction mechanism reported in literature.

It is well-known that Pd supported on carbon catalyzes different types of reaction in organic synthesis[221]. Several factors influence the selectivity of the benzyl alcohol oxidation. The pH of the solution, the nature of the solvent, the O_2 mass transfer process, the nature and concentration of the chemisorbed oxygen species at the surface of the metal nanoparticles and the strength of the chemisorbed species (reactant or products) at the metal surface determine the selectivity in such a complex network of reactions. Although there is an open debate in the literature concerning the reaction mechanism, in fact, for the selective oxidation of benzyl alcohol to benzaldehyde, an oxidative dehydrogenation mechanism has been generally accepted[222,223,224]:

I. Dehydrogenation of the adsorbed alcohol $RCH_2OH_{ad} \leftrightarrow RCHO_{ad} + 2H_{ad}$
II. Oxygen adsorption $O_2 + 2H_2O \leftrightarrow 4OH_{ad}$
III. Oxidation of adsorbed hydrogen $OH_{ad} + H_{ad} \leftrightarrow H_2O$

In the first step the alcohol deprotonation and the formation of adsorbed alcoholate occur. The adsorbed alcoholate reacts further by β-hydride elimination forming the carbonyl compound. This step is considered the rate-determining step. The hydrogen adsorbed at the metal surface is consumed by the adsorbed O_2 in the last step of the cycle. This step may become rate-determining depending on the chemical structure of the alcohol, on the capability of the metal site towards hydrogen chemisorption and molecular oxygen

adsorption and on the chemisorbed oxygen concentration on the catalyst surface[225]. Under mass transfer limited conditions the oxygen chemisorption at the metal active site could be the rate-determining step.

Fig. 6.6 shows the reaction pathways for the benzyl alcohol oxidation. However, additional reaction pathway cannot be excluded.

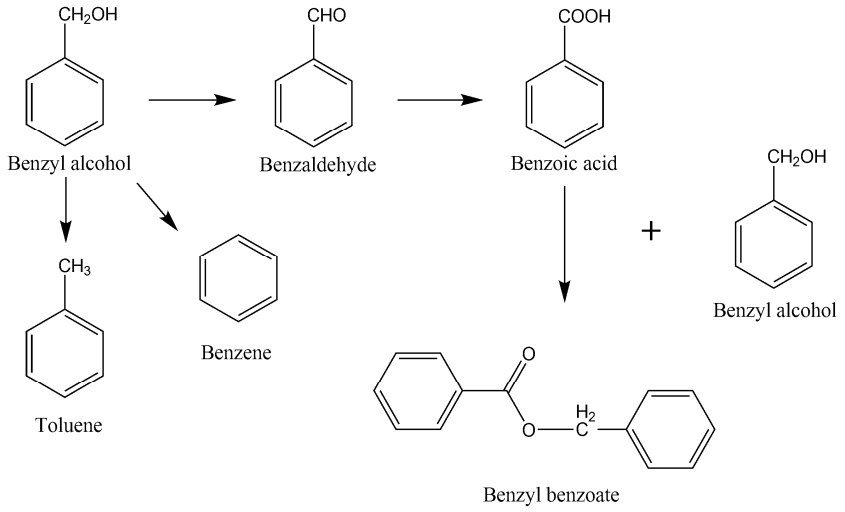

Fig. 6.6: Reaction pathways for the benzyl alcohol oxidation.

As reported in literature[226], Pd clusters catalyze the disproportionation of benzyl alcohol under anaerobic conditions while in presence of O_2 the oxidation of benzyl alcohol to benzaldehyde is favored. The toluene is the co-product of the benzaldehyde obtained through a disproportionation pathway of the benzyl alcohol[227].

It was reported[228] that dehydrogenation of benzyl alcohol to benzaldehyde occurs on reduced Pd even in absence of O_2, through a dehydrogenation pathway which leads to the formation of adsorbed hydrogen. Toluene is formed by hydrogenolysis of the benzyl alcohol which favors the shift of the alcohol-aldehyde equilibrium toward the aldehyde formation. Thus in this case the reactant acts as hydrogen acceptor. In the presence of O_2, the rate of benzaldehyde formation increases due to the fact that the O_2 is a much better hydrogen acceptor than benzyl alcohol.

The side reactions include the successive oxidation of benzaldehyde to benzoic acid and the further esterification reaction to benzyl benzoate. Different reaction pathways have been proposed for the benzoic acid formation[229]. Among these, benzaldehyde

disproportionation to benzoic acid and benzyl alcohol occurs when the concentration of hydroxyl anion on the metal surface is high. The so obtained products might undergo esterification leading to the formation of benzyl benzoate. In addition, the hydration of aldehyde at higher pH promotes the further oxidation of the aldehyde to the correspondent acid. However aromatic alcohols are oxidized to the aldehyde with good yield owing to the stabilizing effect of the aromatic ring[222] which lowers the hydration capacity.

Benzene is obtained through parallel or successive hydrogenolysis reactions involving both the benzyl alcohol and the intermediate products.

One of the possible reactions leading to the formation of Benzene is the decarbonylation of benzaldehyde[221]. This reaction is strongly unwanted because lead to the formation of CO which is cause of catalyst deactivation.

Although the complex reaction network, the products distribution is a clear indication of the existence of two competitive parallel reactions: the oxidative dehydrogenation and the hydrogenolysis, or eventually successive hydrogenolysis of the benzaldehyde.

This might reflect the fact that the O_2 availability at the metal surface and the O_2 activation capability of the catalyst is the crucial point determining the activity and the selectivity to benzaldehyde.

In fact, we have observed that in *solventless* all the catalysts are quite selective to benzaldehyde with a value of selectivity ranging between 70-75%. The main by-product is toluene and in some case benzene in small amount. The lower O_2 availability in *solventless* might be responsible of the disproportionation of the benzyl alcohol to toluene and benzaldehyde. Higher selectivity is obtained with the same catalyst in aqueous solution of benzyl alcohol.

The use of the solvent lower the chemical potential of the benzyl alcohol with respect to the chemical potential of O_2 at the catalyst surface, reduces the amount of hydrogen chemisorbed due to the first dehydrogenation step and thus limits the weight of the hydrogenolysis pathway. This is reflected in the substantial decrease of the selectivity to toluene (Table 6.5).

The higher catalytic activity observed for the Pd/NCNF873K with respect to the Pd/NCNF673K and Pd/NCNF473K is indicative of higher affinity of the Pd/NCNF873K towards the O_2 chemisorption than other catalysts.

On the other hand, catalysts favoring the hydrogenolysis reaction characterized by higher selectivity to benzene (Pd/NCNF473, Pd/CNFox and Pd/VGCNF) show lower catalytic activity. The strong chemisorption of by-product such as the CO, formed by hydrogenolysis of benzaldehyde, is poison for the metal catalyst and this can be the reason that the catalysts show low activity.

The data reported here shows that the catalytic activity of the metal nanoparticles is influenced by the surface chemistry of the CNFs support. This is probably due to the capability of the metal toward the oxygen chemisorption which serves as scavenger for hydrogen chemisorbed. The hydrogen chemisorption process may also play a role in determining the catalytic performance of the catalysts. However, further experiments aimed at the determination of the nature and the amount of active sites are necessary to elucidate the influence of the surface chemistry of the support on the amount of active sites at the metal surface or rather the intrinsic activity of the active sites.

6.3 Structure-activity relationship

In order to understand the catalytic properties of a catalyst, it is necessary to establish a structure-activity correlation. This is a fundamental step for catalyst design. Tailoring the "superficial metallic structure"[78] , which is intended to optimize the coordinative under saturation of the active metal atoms at the surface, is crucial for obtaining selective and active catalysts. The intrinsic surface activity of a catalyst can be modified by exposing different crystallographic planes or inducing low coordinative defective sites such as kinks and steps. This can be achieved by: 1) varying the particles size in the range of very small nanoparticles which approach clusters dimensions; 2) diluting the active species with spectator species; 3) inducing metal-support interaction. A part of the second point which is not considered in this work, the above mentioned factors might co-participate to determine the final activity of the supported metal nanoparticles catalysts used here. This can be explained in terms of the effect of the metal-support interaction on the metal particle size and morphology, which is an observable parameter of great importance for adsorption and catalytic properties because it precludes a certain surface electronic structure of the metal nanoparticles.

6.3.1 Metal-support interaction

Most of the studies present in literature have dealt with the understanding of the metal/oxide interface interaction and correlation with the properties of those materials for both catalysis and nanotechnology[230]. However there are experimental evidences for weak metal-support interaction WMSI[231] in carbon support which are responsible of the peculiar behavior of carbon supported catalyst. The strength of the metal support interaction are determined by the nature of the bond (dispersive and Van der Walls interaction, ionic and polar covalent bonding) at the interface metal/support which depends on the physic-chemical properties of the support on one side and, on the electronegativity of the metal and the particle size on the other side. The metal/support interaction originates from charge transfer between metal and support and produces a perturbation of the electronic structure of the metal catalyst with charge redistribution on

the metal surface (according to image charge model[77,78]). Secondly the metal/support interactions are responsible of inducing specific crystallographic plane, defect and low coordinative sites on the metal surface. Yet strong metal-support interaction, typical the case of oxide, might lead to metal encapsulation by the support or atoms inter-diffusion at the metal-support interface. However the extend of those effects becomes of relevance only for very small metal particles. Indeed any charges induced on the metal of large size would be shared among hundreds atoms and would not produce conspicuous alteration of the superficial metal structure.

Differently than oxide in which SMSI takes place, in carbon material WMSI is expected to interfere with the valence band (VB) of the metal nanoparticles and to modify the geometric coordination of the metal atoms. The nature of the interaction and the resulting effect on the superficial metal structure depends on the carbon surface chemistry. In analogy to oxide, the interaction of the metal particles with local acid cites (Lewis or Brønsted) at the support surface, extensively studies on the case of sulphated zirconia and zeolite[77], produce an electron deficit on the metal surface. In the case of the couple metal particles/proton of a Brønsted acid site, the term of "collapsed bifunctional site" was coined[77]. In such adduct the metal becomes less metallic, whereas the proton becomes less acidic. In the case of basic systems, such as in hydrotalcites, the interaction of basic sites with the metal cluster was found to induce negative charging of the metal surface and at the same time weakening of the basic sites. This discussion can be extended to the case of basic carbons. When the support is characterized by no pronounced acidity or basicity, usually neutral metal particles are formed. In theory, carbon materials are usually considered as neutral carrier and they weakly interact through the π-electron system.

However the presence of defects, i.e. functionalities, curvature and vacancies induce surface charging that stabilizes metal species with unexpected activity. It was found that metal nanoparticles are stabilized in the steps and kinks of graphite where localized charges are expected[231].

An important characteristic of supported metal nanoparticles is the particle shape which is influenced by the strength of the metal support interaction and on the size of the metal nanoparticles. It is appropriate to consider flat particles spread over the support surface as

result of quite strong metal-support interaction, while particles with well-defined shape and less wetting with the surface are characterized by a weaker interaction with the support.

Formation of raft metal structure has been found together with spherical particles in system such as Pd/C catalyst[231].

Theoretical calculations[77] for the system Ni/SiO_2 revealed strong distortion of the spherical particle shape occurring while in contact with the support due to the capability of the metal atoms to diffuse on the support surface to find energetically preferable adsorption sites. This distortion results in a lower average coordination number compared with thermodynamically stable condition for stable isolated metal particles. Increase in the interatomic distance for small particles was also calculated. Experimentally it is indeed more difficult to evaluate the crystallographic structure of the supported metal particles. Therefore, usually the relationship between the overall shape of the metal particles (flat, hemispherical, etc.) and the catalytic performance is analyzed without discriminating the contributions of the different crystallographic planes.

6.3.1.1 Metal-support interaction: HRTEM investigation

Transmission electron microscopy is one of the most powerful tools for studying the metal/support interaction. Compared with conventional HRTEM, the use of Cs-corrected HRTEM offers new opportunities for atomic-scale investigations of materials with extension of point-to-point resolution, clear images of surfaces/interfaces border and

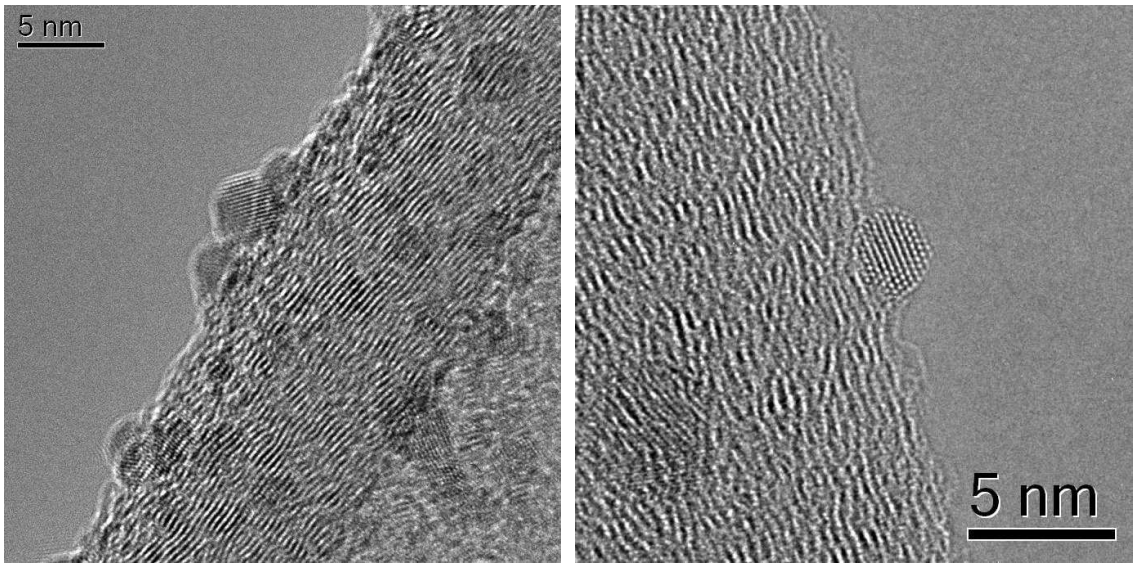

Fig. 6.7: HRTEM image by FEG(left image) and by Cs-corrected TEM (right image).

better resolution of metal lattice planes. Fig. 6.7 displays HRTEM image of Pd/NCNF873K and compared with CS-corrected image. Note the clear structure at the metal surface compared with the conventional TEM image. The higher resolution achieved with CS-corrected TEM allow to visualize details which cannot be interpreted by means of conventional HRTEM. The left image in Fig. 6.7 reveal a feature encountered in these catalysts investigated: in case of low degree of surface wetting, the particles are encapsulated in an organic layer of the PVA used as protective agent; otherwise the particles are imbibed with the PVA at the interface support/metal, while the exposed metal particles are not completely covered and there is part in which the naked metal surface is exposed. The structure of small palladium particles was investigated in literature by HRTEM with the aim to know if structural metal variations could explain some of the size effects encountered in heterogeneous catalysis[232]. However, the particles

nanostructure is not easy to recognize at the HRTEM images due to the different orientation of the particles with respect to the electron beam. For the interpretation of the EM images of metal nanoparticles computer simulation has been performed[233] .

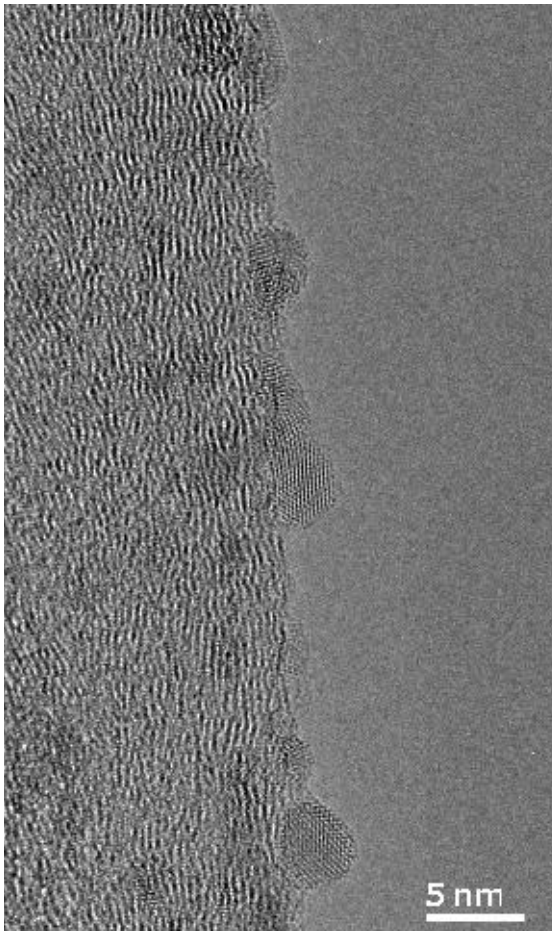

Fig. 6.8: HRTEM image for the sample Pd/NCNF873K.

From these studies is well known that Pd nanoparticles might exist with a broad distribution of morphologies and polydispersity of the size distribution[234,235,236]. The Pd nanoparticles can be imagined as formed by simple fcc tetrahedrons connected to each other by sharing of {111} planes. This type of morphology is referred as multiply twinned particles (MTPs).

A decahedral nanoparticle is made up of 10 face-sharing tetrahedrons while an icosahedral nanoparticle is made up of 20 face-sharing tetrahedrons. Truncated decahedron forms have been found too and they are referred as Marks decahedron, cuboctahedron, star decahedron and round decahedron.

Distortion of the tetrahedron from the fcc structure occurs too.

Fig. 6.8 shows HRTEM image of the sample Pd/NCNF873K in which it is possible to distinguish particles with different sizes, morphology and wetting with the carbon surface. Note the very small particles which approach cluster dimension, the 5-fold orientation decahedron particle and coalesced particles. As mentioned in section 3.2 the nanoparticles size distribution during the synthesis of the nanoparticles colloidal solution is determined by the nature of the protective agent (PVA) and the reductive agent used ($NaBH_4$). However, after the immobilization of the colloidal solution of the metal nanoparticles on the carbon surface, if the interaction at the carbon support is not strong

enough, during the successive washing and drying the removal of the capping layer of PVA might occur leading the particles to undergo coalescence and overgrowth. In fact, the aim is to stabilize the particles at the carbon surface by enhancing the interaction with the carbon surface. When the nanoparticles are supported on the CNFs, they accommodate on the surface with a certain wetting degree which depends on the strength of the metal/support interaction.

Fig. 6.9 shows the 5-fold decahedron particle well imbibed on the surface of CNFs for the sample Pd/NCNF873K(right image) and the overgrown icosahedrons particles less wetted with the surface of CNFs for the sample Pd/VGCNFs (left image).

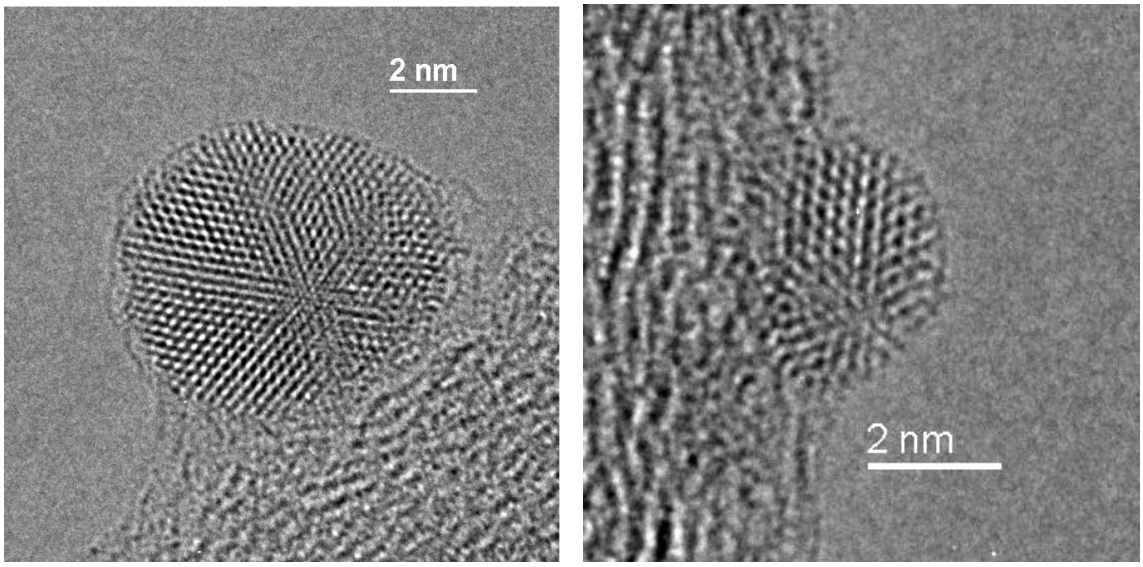

Fig. 6.9: HRTEM image for sample Pd/VGCNFs (left image) and Pd/NCNF873K (right image).

Other feature observed often is the elongation of the particles in the direction of the wetting with the surface reported in Fig. 6.10 for the sample Pd/NCNF873K. Yet, Fig. 6.11 show in the cycle the particular of low coordinated site of the metal atom arrangement on the surface of the metal nanoparticles for the samples Pd/NCNF673K. Fig. 6.12 shows an atom dislocation for the sample Pd/NCNF673K. Fig. 6.13 shows a particular of step on the surface of a Pd particle coalesced with another particles for the sample Pd/NCNF673K. Those step sites are expected to be highly reactive site.

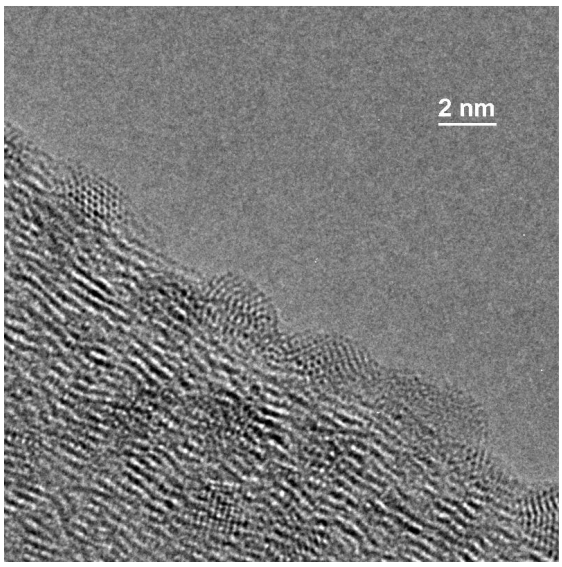

Fig. 6.10: Elongated particles in Pd/N CNF873K.

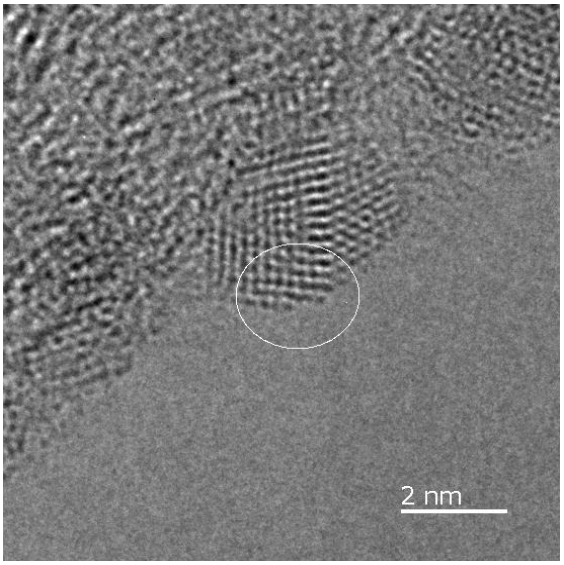

Fig. 6.11 Low coordinated site in Pd/NCNF673K.

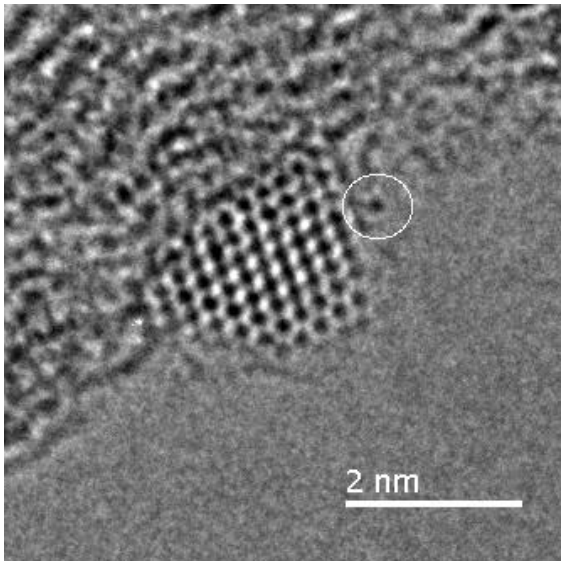

Fig. 6.12: Atom in disequilibrium position in Pd/NCNF673K.

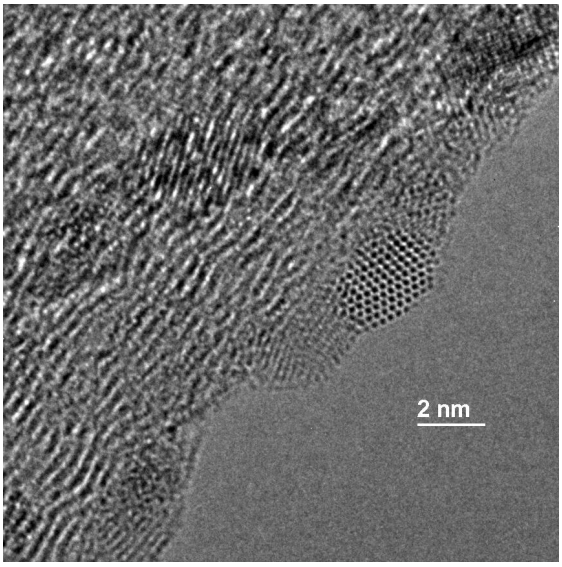

Fig. 6.13: Steps in Pd/NCNF673K.

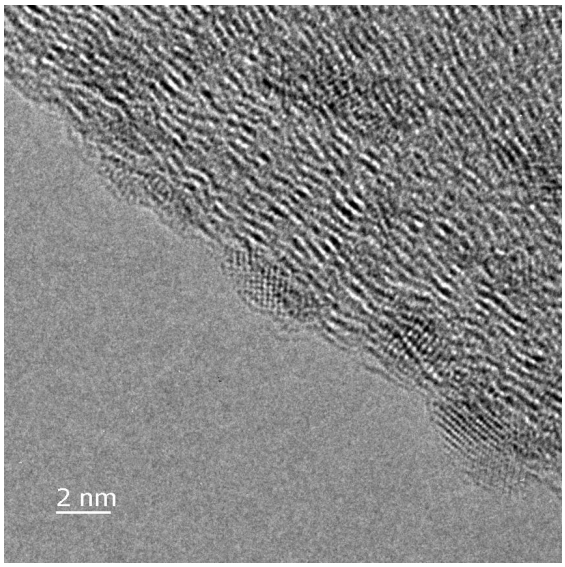

Fig. 6.14: "raft" particles in Pd/NCNF873K.

Following the Fig. 6.14 shows the so called "raft" particle similar to a multilayer of metal. We attribute all these features to the stronger metal support interaction which stabilize the metal nanoparticles at the defective sites of the CNFs surface. All this observed changes in the morphology are more pronounced for small particles, while the bigger ones maintain the round shape. The small nanoparticles are less thermodynamically stable thus characterized by high mobility of the atoms which might diffuse on the carbon surface to reach more stable position. In analogy to the Pd complex with N-heterocyclic carbenes (NHC) ligand used in homogeneous oxidation catalysis[237], the presence of atomically dispersed Pd atoms cannot be excluded and must be the subject of further investigation.

In order to define numerically the entity of the metal support interaction, statistic measurements of the aspect ratio of the particles on the carbon supports have been measured. For non spherical particle it is convenient to refer to the particle aspect ratio, intended as the ratio between the length and the height of the particle. The aspect ratio gives numerical information about the divergence of the particle shape from the spherical situation which is defined by an aspect ratio equal to 1. For the statistical counting of the particles size, "raft" particle have not been taken into account because of the difficulties in determining the two dimensional lengths. However we do believe that those particles are of relevance for catalysis.

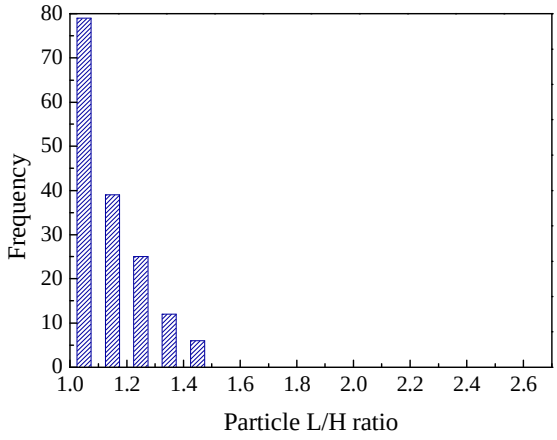

Fig. 6.15: Aspect ratio frequency for Pd/CNFox.

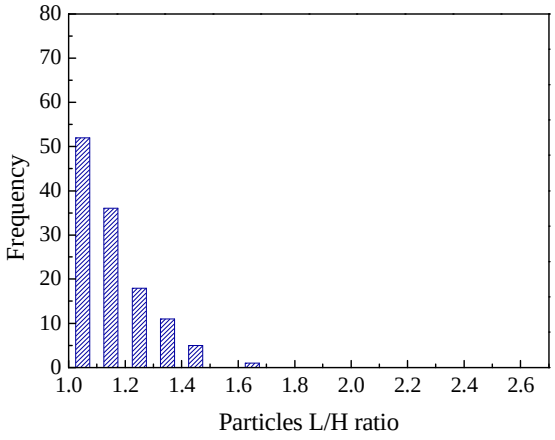

Fig. 6.16: Aspect ratio frequency for Pd/VGCNF.

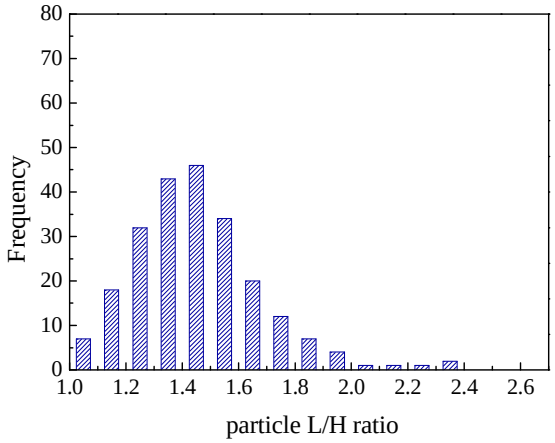

Fig. 6.17: Aspect ratio frequency for Pd/NCNF673K.

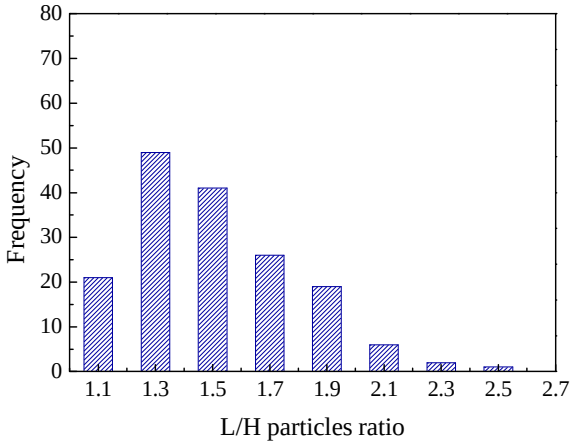

Fig. 6.18: Aspect ratio frequency for Pd/NCNF873K.

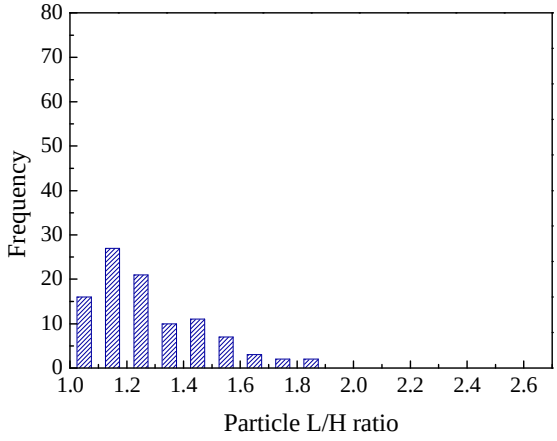

Fig. 6.19: Aspect ratio frequency for Pd/NCNF473K.

The statistical measurements are displayed in Fig.6.15-6.19 for the sample Pd/CNFox, Pd/VGCNF, Pd/NCNF673K, Pd/NCNF873K and Pd/NCNF473K, respectively.

The correlation of the HRTEM investigation with the catalytic data shows that the samples with higher activity are also characterized by a higher population of particles with higher aspect ratio above 1.4. It is thus proved the surface chemistry of NC through interaction with metal is responsible of the particles elongation and induces defectiveness on the metal surface which might have a role in the catalytic activity. As reported in literature, we have found that the originally basicity of the support decrease after metal nanoparticles immobilization as consequence of the metal support interaction[77]. Macroscopically, the wetting phenomenon can be explained in term of the Pd/CNFs interfacial surface free energy. The higher coordinative capability of localized charged in the graphitic layer (Lewis basic site)induced by the ammonia treatment at 673 K and 873 K give arise to stronger metal/C bond at the interface which lower the surface tension and favor the wettability[238]. The statistic measurements of the aspect ration have highlighted the tendency of the nanoparticles to undergo structural modification at the surface of the carbon support depending on the surface chemistry of the carbon support. In analogy to the high catalytic activity of Pd N-heterocyclic carbenes ligand complex for the liquid phase selective oxidation catalysis, the presence of such N-heterocyclic moieties on the surface of the carbon support might stabilize Pd clusters with high catalytic activity.

6.3.1.2 Catalytic activity in the liquid phase synthesis of H_2O_2

The series of Pd supported on CNFs catalyst have been used for the direct synthesis of H_2O_2 from O_2 and H_2. The catalytic test have been carried out in CO_2 expanded methanol in order to improve O_2 and H_2 solubility with respect to water as a solvent and thus the H_2O_2 productivity and selectivity[239].

The results obtained in batch conditions are shown in Fig. 6.20.

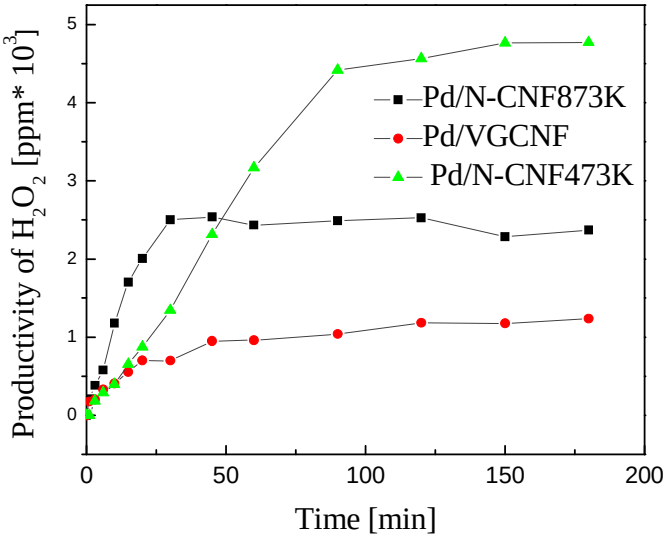

Fig. 6.20: H_2O_2 synthesis on Pd-based CNF catalysts.

At room temperature and 6.5 bar total pressure, the catalyst based on Pd nanoparticles immobilized on N-containing CNFs lead in about 2 hours reaction time to H_2O_2 productivities of 5000 ppm/gPd and a stable selectivity of about 60%. Pd nanoparticles on the N-free CNFs give productivities of about one fifth with respect to Pd /NCNFs based catalysts in the same experimental conditions. The initial H_2O_2 productivity observed along the samples investigated remark the trend observed for the initial benzaldehyde productivity in the benzyl alcohol oxidation reported before. This fact corroborates the hypothesis of the improved reductive oxygen adsorption capability of the Pd nanoparticles induced by the metal support interaction.

7

Conclusion and outlook

This thesis aims to evaluate and exploit the chemical properties of CNFs in heterogeneous catalysis. Due to its incomparable feasibility towards chemical functionalization, NC represents an ideal organic substrate whose surface chemistry can be tailored according to specific needs. This is an interesting aspect in view of the application of NCs as support for metal nanoparticles. An important goal in the preparation of highly active metal particles supported on carbon is the enhancement of the metal support interaction which favors the metal wetting and lead to more stable catalysts. The metal support interaction influence the metal reactivity by inducing defective sites on the metal nanoparticle surface. In this work, the influence of N and O functionalization of the carbon support on the structure of the Pd nanoparticles is studied. The selective liquid phase oxidation of benzyl alcohol to benzaldehyde is presented as test reaction to evaluate the catalytic activity of Pd-based CNF catalysts. In order to establish a structure-activity relationship, the emphasis was placed on a detailed characterization of support and catalysts. N-functionalization of VGCNFs was carried out via amination reaction. This synthetic route includes an oxidation step of CNFs by HNO_3, followed by thermal treatment in NH_3 at different temperature. In this way it was possible to tune the surface chemistry of the starting VGCNFs. The chemical nature of the functionalities present on the carbon surface after the thermo-chemical treatments was investigated by XPS and TPD. The impact of the functionalization route on the surface acid/base properties was investigated by liquid phase potentiometric titration and gas

phase microcalorimetric adsorption of CO_2. The surface of the functionalized CNFs is characterized by the coexistence of energetically different acidic and basic sites. The population of O and N acidic and basic sites is temperature dependent. At 473 K acid oxygen functionalities coexist with basic N and O sites. With increasing the functionalization temperature (673 K), the most acidic site are thermally decomposed and the surface arrangement of nitrogen and oxygen species to form hetero-cycle moieties results in the enhancement of the hydrophobic character of the surface. A further increase in the functionalization temperature up to 873 K produces a surface with the stronger basic character. Pd metal nanoparticles from a PVA-protected colloidal solution have been immobilized on the surface of the CNFs samples.

The screening of the catalysts under different experimental condition (*solventless* and aqueous solution) has lead to the conclusion that the surface chemistry of the carbon surface and the experimental condition play a role in addressing the selectivity of the reaction, quite probably by influencing the chemical potential of the reactants at the catalyst surface. However, the comparison of the catalytic performance of the Pd-based catalysts under the same condition has evidenced the different catalytic activity of the Pd nanoparticles depending on the surface chemistry of the support. Indeed, the results presented here give indications for the role of the surface chemistry of carbon in affecting the metallic structure through metal-support interaction. By means of Cs-corrected HRTEM investigation, it was possible to establish a correlation between the catalytic activity and the observable structural parameter that is the aspect ratio of the metal particles. Catalyst with metal nanoparticles characterized by higher aspect ratio (average above 1.4) shows the best catalytic performance. Although the aspect ratio is an observable parameter which does not describe the structure of the metal nanoparticles, it is still an indication of the strength of the metal-support interaction. The stronger the metal support interaction the more pronounced is the elongation of the nanoparticles along one direction. HRTEM investigations have highlighted the presence of metal cluster on the surface of CNF, formation of “raft” metal particles with under-coordinated site on the metal surface. Thus, the surface chemistry of the CNFs play a crucial role in the resulting metal support interaction and thus in the formation of highly active metal sites. The catalytic data show that the catalyst obtained by immobilization of the metal

nanoparticles on the most basic and hydrophobic support give rise to the best catalytic performance. Those catalyst (NCNF673K and NCNF873K) are characterised by the presence of nitrogen hetero-cyclic moieties on the surface which produce charge localization on the graphitic surface acting as Lewis basic site. Microscopically, for small nanoparticles, in analogy to the homogeneous catalyst based on N-heterocyclic carbenes used as ligands for Pd complex, it is possible to imagine high metal coordinative capability on the defective N-containing sites of the carbon surface. The presence of such kind of N species in heterocyclic moieties on the carbon surface favor the spreading of the metal nanoparticles on the carbon surface as observed by the increse of the nanoparticles aspect ratio. This produces reorganization of the metal atoms at the surface of the nanoparticles, with generation of under-coordinated Pd sites as obsedved by the EM investigation. Macroscopically, this can be explained in terms of decreasing of the metal/support interface free energy due to the stronger metal/support bond which increases the metal wettability. The higher population of spread particles on Pd/NCNF673K and Pd/NCNF873K is reflected in the higher catalytic activity of these catalysts in the liquid phase selective oxidation.

In the framework of ELCASS and IDECAT, the catalysts Pd/VGCNF, Pd/NCNF473K and Pd/NCNF873K have been tested in the liquid phase synthesis of H_2O_2. This work was performed at the University of Messina. It is interesting to note that with respect to the Pd/VGCNF both the Pd/N-CNT873K and Pd/NCNF473K shows better catalytic performance in the H_2O_2 synthesis. The investigations of the catalytic performance of these catalysts in the direct synthesis of H_2O_2 allow us to corroborate the idea that the presence of N in hetero-cycle moieties on the carbon surface induces, by means of nanoparticles/support interactions, special structural feature of the metal nanoparticles with improvement on the reductive adsorption of O_2. It is noticeable that the higher initial productivity of H_2O_2 in the case of the Pd/NCNF873K with respect to the Pd/NCNF473K correlate perfectly with the higher catalytic activity observed in the liquid phase oxidation of benzyl alcohol to benzaldehyde for the Pd/NCNF873K. Instead in the synthesis of H_2O_2, the catalyst Pd/NCNF473K presents an induction time. As the surface is highly hydrophilic, it is probably highly covered by ions which hinder the O_2 adsorption leading to the observed induction time. This is not dramatic in the H_2O_2 synthesis, became a

limiting factor in the benzyl alcohol oxidation. The low initial concentration of chemisorbed oxygen species, probably superoxide species, may lead to secondary pathway such as disproportionation or decarbonylation of the benzaldehyde to benzene which is poison for the catalyst. The concentration of superoxide species is the controlling factor of the reactivity and the selectivity. In fact, we have observed different selectivity in H_2O solution (higher to benzaldehyde) where the chemical potential of the two reactants at the catalyst surface is different than in *solventless* and less benzyl alcohol is available. This was the reason of the large amount of toluene obtained as co-product together with benzaldehyde by the disproportionation of benzyl alcohol. At present, our results show that Pd-based NCNF catalysts have significant potential for selective oxidation reaction. Although these are promising catalyst for the application in liquid phase selective oxidation, in order to have a practical impact at the commercial level, it is necessary to improve the long-term stability and performance of the catalyst. In this work the role of the PVA covering the nanoparticles surface was not investigated, although it may have an important role, besides protecting the metal nanoparticles. Other preparation techniques which do not include the use of protective agent are of interest because they lead to a more exposed metallic surface. Furthermore the absence of the interlayer of protective agent allows a better study of the metal support interaction. In the view of a rational design of the catalyst, the systematic study of the influence of the singular nitrogen functionalities on the catalytic behavior of Pd on CNFs based catalyst represents one of the points in the outlook. This point was not possible to address here due to the broad distribution of nitrogen species introduced by this synthetic route on the support surface.

Further experiment aimed at the understanding of the impact of the surface chemistry of the carbon support on the nature and the Pd exposure are the main outlook of this work.

A

Appendix

A.1 Fitting parameters

Different methods have been reported in literature to resolve the N1s and O1s envelopes[134,135]. When the spectrum is very broad without well resolved features, a mathematical analysis of the XPS data, e.g. derivative or difference spectra method[134, 135], or PCA (principal component analysis if an extended data set is available), can be used to determine the appropriate number of peaks to fit the XP spectrum. The temperature programmed XPS was used as strategy to produce modification of species distribution present on the sample surface that can be used to separate the XPS spectra in the individual components. The data were, thus, mathematically treated by means of the difference method. The difference between two spectra recorded sequentially results in the component which is lost (positive Y value) or formed (negative Y value) during the thermal desorption experiments.

A.1.1 N1s

The temperature programmed XPS on the N-CNT873K is reported as first example to describe the parameter used to fit the N1s core level spectra. The spectra recorded at the

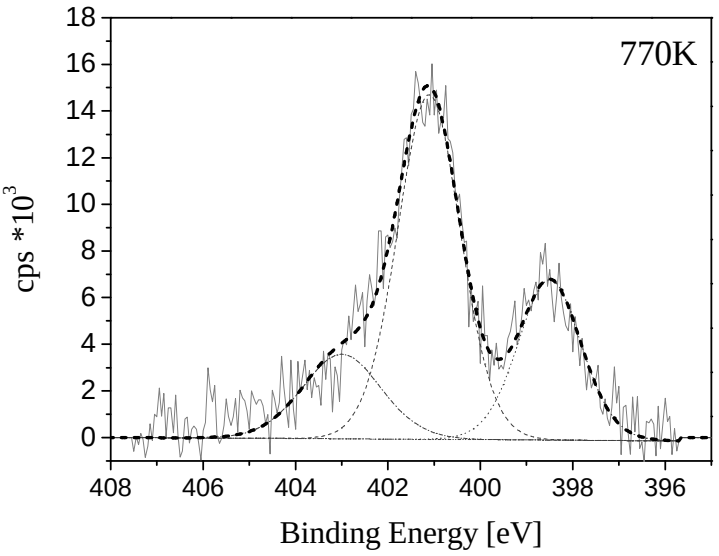

Fig. A.1: N1s at 770 K for sample NCNF873K

higher temperature (Fig. A.1) shows well separated peaks located at 398.5 eV and 401 eV, easily fitted with a mixed G-L function (GL30) and with FWHM of 1.5 after linear background subtraction.

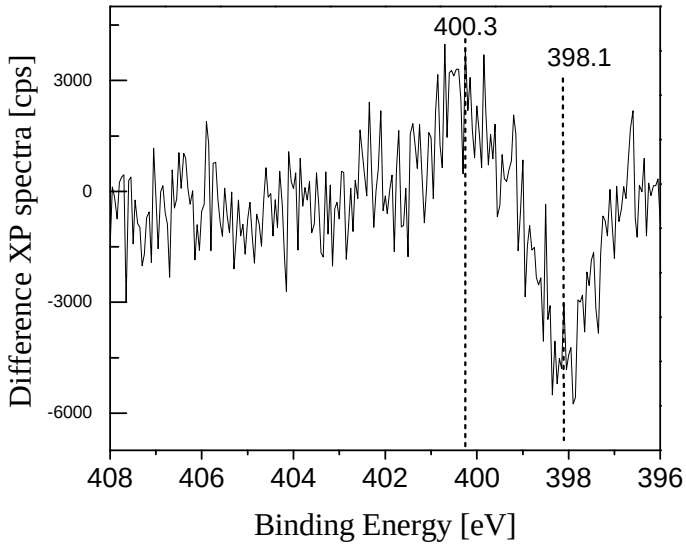

Fig. A.2 Difference spectra from 329 K to 360 K for sample NCNF873K

Fig. A.2 reports the difference of spectra recorded stepwise while heating from 329 K to 360 K. This graph shows formation of a peak at about 398.1 eV (positive ordinate value) and vanishing peak at 400.3 eV (negative ordinate value). In fact, the BE values which

better fit the original spectrum (Fig. A.1) are slightly different from these ones obtained in the difference spectra (Fig. A.2). This is due to the fact that the two peaks overlap in the middle region of the N1s spectrum and then the peaks originated by the difference function (peak maximum and the FWHM) are not the same. However, this spectrum highlights the presence of another species in the N1s at about 400.1 eV. The analysis of the temperature programmed XPS on the N-CNT473K is reported as second example. The N1s spectrum for the N-CNT473K is broader than the N-CNT873K spectrum. Other peaks should be taken into account for a good fitting. Between 645 K and 672 K the surface modification of the nitrogen functionalities allows the detection of another species located at around 399.4 eV (Fig. A.3).

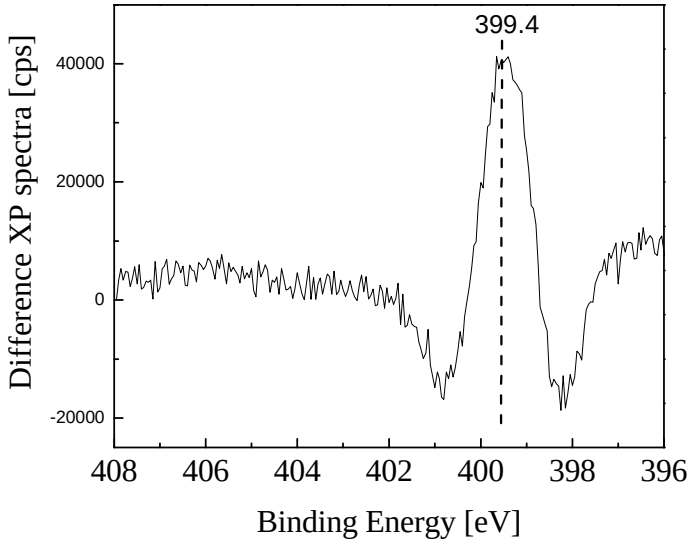

Fig. A.3: Difference spectra from 645 K to 672 K for sample NCNF473K

As shown in the Fig. A.4, it is necessary to introduce other two peaks located at about 406 and 403 eV in the fitting of the N1s.

The reproducibility and the valuability of the experimental methods were verified by the mathematical treatments of the data resulting from different TP-XPS measurement on the same sample and the comparison with the results from the different sample. High number of spectra has been analyzed by mean of the XPS casa software. In fact, the data are consistent each other concerning the number of peaks and the line shape, however among the different sample and the different runs the absolute value of peak maximum and

FWHM slightly vary within ±0.1 eV. The deconvolution of the XP spectra was done according to the following specifications: after Shirley background subtraction, six peaks have been introduced for the deconvolution of all the spectra, adjusting the fitting in such a way to get a standard deviation (STD) value around 1. For the spectra with low amount of N a linear background was subtracted. The six contributions have peak maximum as following: 398.4±0.1 (N1); 399.4±0.1 (N2); 400.1±0.1 (N3); 401.1±0. 1 (N4); 403.5 ±0.1 (N5); 406±0.1(N6).

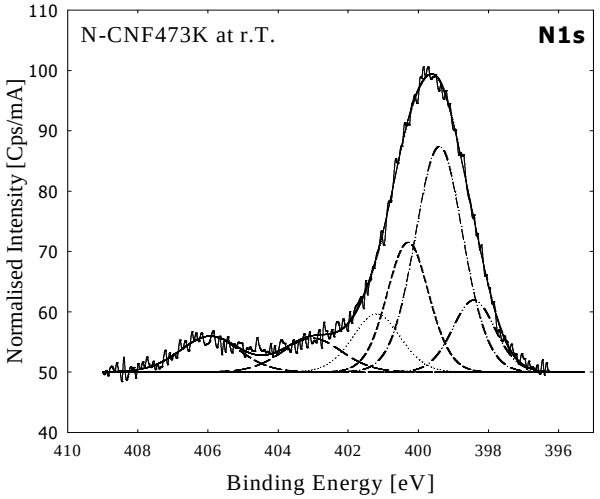

Fig. A.4: N1s spectrum recorded at room temperature for sample NCNF473K.

The BE to which correspond the maximum of the peak was fixed with interval of freedom within ±0.1 eV and a FWHM within 1.35 and 1.6 eV, which were the value of the scattering between different samples a/o measurements. For instance, it must be pointed out that for the N1 species the FWHM vary from 1.35 at room temperature up to 1.5 at 770 K. However, even this small variation in FWHM results in different number of species needed to fit the experimental curve. This emphasizes the complexity of the analysis of the XP N1s and O1s spectrum. Thus, here peaks with a BE that were common to all the samples have been used with a FWHM ranging from 1.35-1.6 eV.

A.1.2 O1s

If in the case of the N1s, the difference of spectra recorded sequentially during heating show some positive peaks and negative peaks, due to the lost of some species and the creation of new one, with the overlapping in the middle region that make the peak shape determination less obvious, this is rarely observed in the case of the O1s. In this case a more precise determination of the peak shape, FWHM and BE, was possible. Fig. A.5 shows the difference of the O1s spectra recorded at room temperature and 412K for the sample N-CNT473K. The curve was fitted with a Gaussian curve with maximum at 532.4 eV and a FWHM of about 1.85 eV.

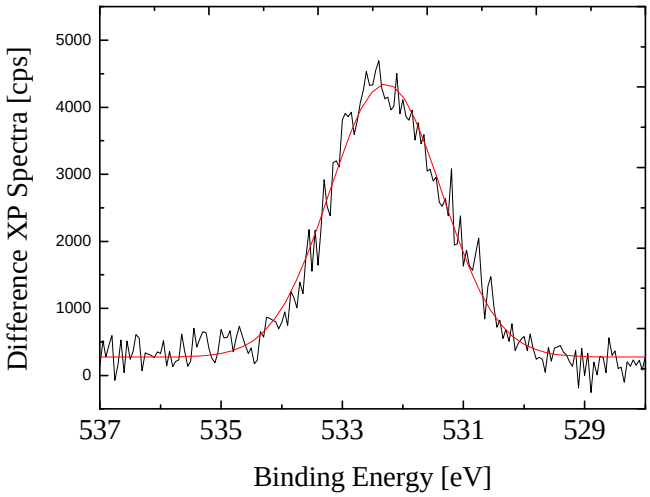

Fig. A.5: Difference between spectra recorded at r. T. and 412 K for the sample NCNF473K.

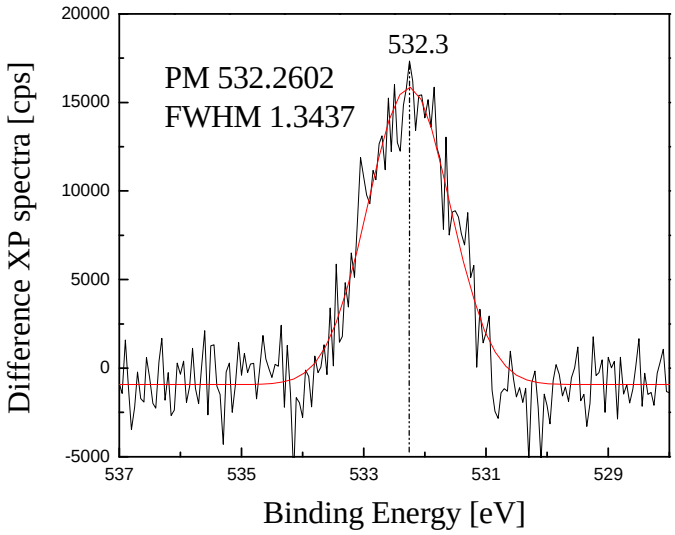

Fig. A.6: Difference spectra recorded at 479 K and 698 K for the sample NCNF473K.

Fig. A.6 shows the difference of the spectrum recorded at 479 K and 698 K for the sample N-CNT473K. The curve was fitted by a Gaussian with maximum at 532.3 eV and a FWHM of about 1.35 eV. From 712 K to 736 K (Fig. A.7) there is loss of the species at 531.3 eV (FWHM 1.52) and another species at 533.6 eV with FWHM 1.56 fitted with Gaussian curve.

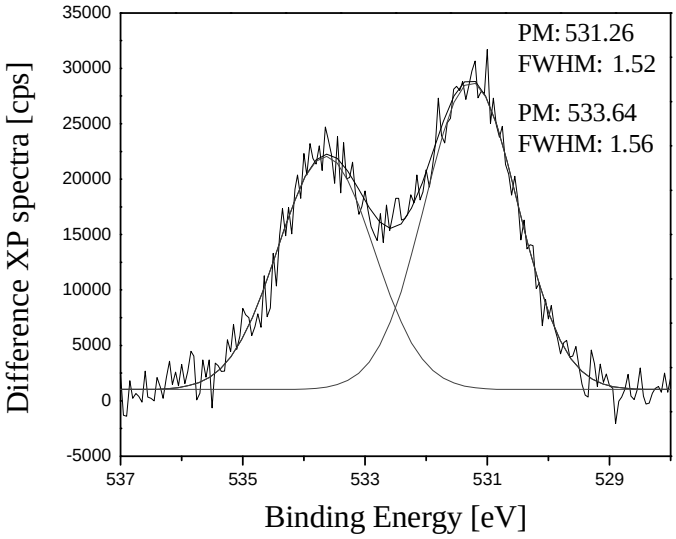

Fig. A.7: Difference spectra recorded at 712 K and 736 K for the sample NCNF473K

The same species was observed for the CNTox (Fig. A.8). From room temperature to 398 K the peak located at 532.4 eV is lost while from 398 K to 447 K a slightly shifted peak at 532.9 eV is removed by heating (Fig. A.9).

From 717 K to 838 K two new features appear centered at 531.3 eV and 533.5 eV (Fig. A.10)

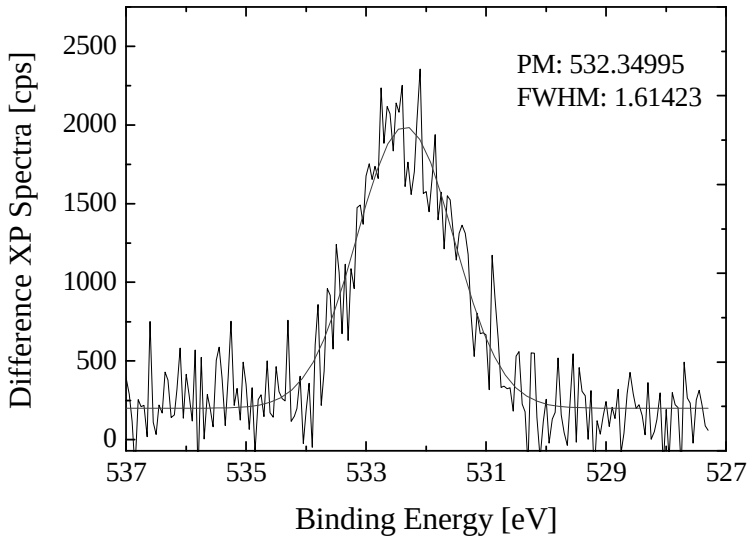

Fig. A.8: Difference between spectra recorded at r.T and 398 K for sample CNFox.

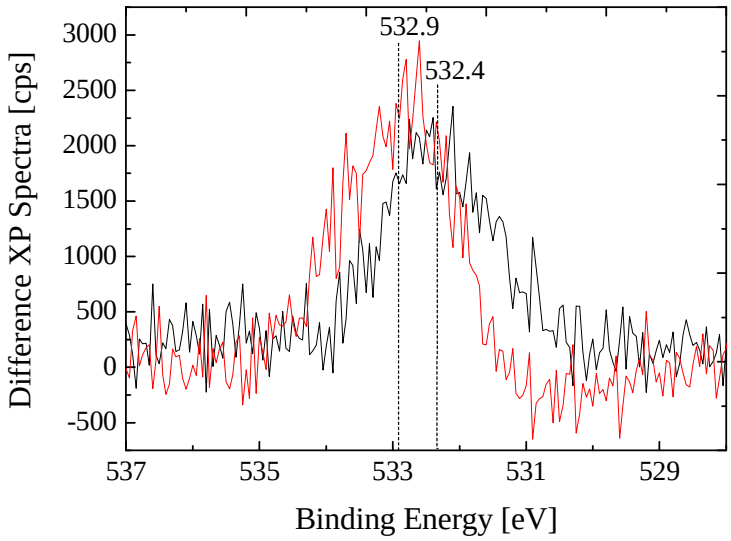

Fig. A.9: Difference between spectra recorded at r.T and 398 K for sample CNFox(black curve) and from 398 K to 477 K (red curve).

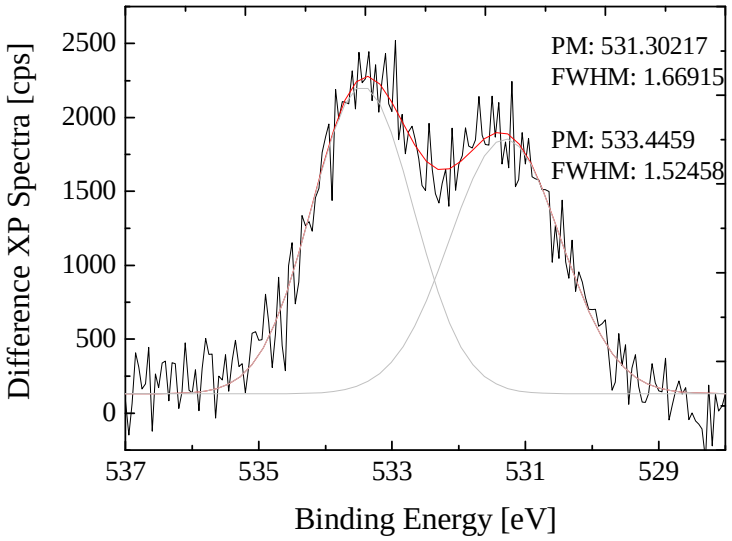

Fig. A.10: Difference between spectra recorded at 717 K and 838 K for sample CNFox.

At 838 K (Fig. A.11) the 532.5 eV is totally gone and the spectra is mainly composed by the peak at 533.6 eV, 0.1 eV shifted with respect the feature observed during the initial thermal desorption (Fig. A.10). Another peak located at 530.7 eV is visible.

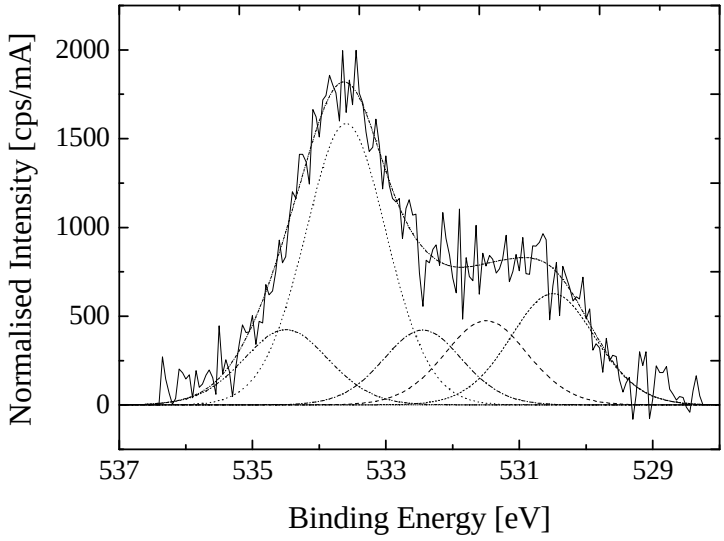

Fig. A.11: O1s spectrum recorded at 838 K for sample CNFox.

Fig. A.12 reports the O1s for the sample CNFox measured at room temperature. For the fitting of this spectrum it is necessary to introduce a small peak at about 535 eV. This is a common feature for all the samples investigated.

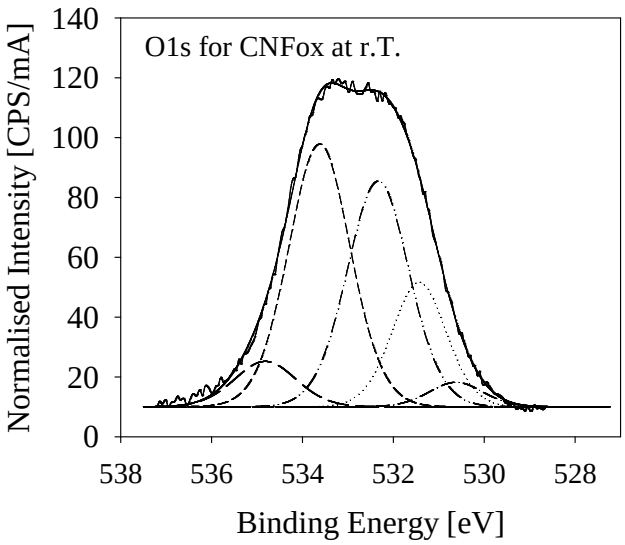

Fig. A.12: O1s spectrum recorded at room temperature for sample CNFox**.**

The fitting of all the O1s spectra relative to the sample investigated have been done according to the results of the difference method data treatment described here. Five GL 30 peaks have been used with BE maximum which can slightly vary ±0.1 eV, which was the scattered value observed through all the spectra recorded.

Furthermore, in order to reach a STD 1 a FWHM about 1.4-1.6 was required. The FWHM was considered the same for all the peaks. In contrary if one wants to use a narrower FWHM a higher number of peaks should be considered. The O1s core level spectra have been deconvolved after Shirley background subtraction by introduction of five contributions with peak maximum as following: 530.7±0.1 (O1); 531.4±0.1 (O2); 532.4±0.1 (O3); 533.7±0.1 (O4); 535 (O5). When necessary a linear background was subtracted.

Deconvolution of the C1s core level spectra was omitted in this work considering that the presence of both O and N would make the analysis very complicated and not leading to a meaningful understanding. In conclusion, the components used to fit the N1s and O1s spectra match with those reported in literature (Table 4.1).

Bibliography

[1] J. W. Hassler, *AC* Chemical publishing Company, New York, **1963**

[2] J. Zhang, D. Su, A. Zhang, D. Wang, R. Schlögl, and C. Hébert, "Nanocarbon as Robust Catalyst: Mechanistic Insight into Carbon-mediated Catalysis", *Angewandte Chemie International Edition*, Volume 46, Issue 38 (**2007**) 7319-7323.

[3] D. S. Cameron, S. J. Cooper, I. L. Dodgson, B. Harrison and J. W. Jenkins, "Carbons as Supports for Precious Metal Catalysts", *Catalysis Today* 7 (**1990**) 113-137.

[4] N. Dimitratos, C. Messi, F. Porta, L. Prati, A. Villa, "Investigation on the Behavior of Pt(0)/Carbon and Pt(0),Au(0)/Carbon Catalysts Employed in the Oxidation of Glycerol with Molecular Oxygen in Water", *Journal of Molecular Catalysis A: Chemical* 256 (**2006**) 21-28.

[5] S. Demirel, K. Lehnert, M. Lucas, P. Claus, "Use of Renewables for the Production of Chemicals: Glycerol Oxidation over Carbon Supported Gold Catalysts", *Applied Catalysis B: Environmental* 70 (**2007**) 637-643.

[6] I. Martin-Gullon , J. Vera, J. A. Conesa, J. L. González, C. Merino, "Differences between Carbon Nanofibers Produced Using Fe and Ni Catalysts in a Floating Catalyst Reactor", *Carbon* 44 (**2006**) 1572–1580.

[7] T. W. Pechar, S. Kim, B. Vaughan, E. Marand, M. Tsapatsis, H. K. Jeong and Chris J. Cornelius, "Fabrication and Characterization of Polyimide-Zeolite L Mixed Matrix Membranes for Gas Separations", *Journal of Membrane Science* 277, Issues 1-2 (**2006**) 195-202.

[8] G. P. Knowles, J. V. Graham, S. W. Delaney and A. L. Chaffee, "Aminopropyl-functionalized Mesoporous Silica as CO_2 Adsorbents", *Fuel Processing Technology* 86, Issues 14-15(**2005**) 1435-1448.

[9] A. M. Chippindale and R. I. Walton, "[C9H20N][Al2(HPO4)2(PO4)]: An Aluminium Phosphate with a New Layer Topology", *Journal of Solid State Chemistry* 145 (**1999**) 731-738.

[10] J. Gascon, U. Aktay, M. D. Hernandez-Alonso, G. P.M. van Klink, F. Kapteijn, "Amino-based Metal-organic Frameworks as Stable, Highly Active Basic Catalysts", *Journal of Catalysis* 261, Issue 1 (**2009**) 75-87.

[11] R. J. J. Jansen and H. van Bekkum, "Amination and Ammoxidation of Activated Carbons", *Carbon* 32 (**1995**) 1507-1517.

[12] B. Stöhr, H. P. Boehm and R. Schlögl, "Enhancement of the Catalytic Activity of Activated Carbons in Oxidation Reactions by Thermal Treatment with Ammonia or Hydrogen Cyanide and Observation of a Superoxide Species as a Possible Intermediate", *Carbon* 29, Issue 6 (**1991**) 707–720.

[13] E. R. Rideal and W. M. Wright, "Low Temperature Oxidation at Charcoal Surfaces. Part II. The Behaviour of Charcoal in the Presence of Promoters", *Journal of the Chemical Society* (**1926**) 1813–1820.

[14] K. Li , L. Ling, C. Lu, W. Qiao, Z. Liu, L. Liu and I. Mochida, "Catalytic Removal of SO_2 over Ammonia-AC Fibers", *Carbon* 39, Issue 12 (**2001**) 1803-1808.

[15] A. Arenillas, F. Rubiera, and J. J. Pis, "Nitric Oxide Reduction in Coal Combustion: Role of Char Surface Complexes in Heterogeneous Reactions", *Environmental Science and Technology* 36**,** Issue 24 (**2002**) 5498–5503.

[16] S. Matzner and H. P. Boehm, "Influence of Nitrogen Doping on the Adsorption and Reduction of Nitric Oxide by Activated Carbons", *Carbon* 36, Issue 11 (**1998**) 1697-1709.

[17] J. L. Figureido and M. F. Pereira, "carbon as Catalyst", *Carbon Materials for Catalysis* edited by P. Serp and J. L. Figueiredo, WILEY-VCH (**2009**) 177-217.

[18] V. V. Strelko, V. S. Kutsa and P. A. Thrower, "On the Mechanism of Possible Influence of Heteroatoms of Nitrogen, Boron and Phosphorus in a Carbon Matrix on the Catalytic Activity of Carbons in Electron Transfer Reactions", *Carbon* 38 (**2000**) 1499-1524.

[19] V. V. Strelko, N. T. Kartel, I. N. Dukhno; V. S. Kuts, R. B. Clarkson, B. M. Odintsov, "Mechanism of Reductive Oxygen Adsorption on Active Carbons with Various Surface Chemistry", *Surface science* 548 (**2004**) 281-290.

[20] K. Gong, F. Du, Z. Xia, M. Durstock, L. Dai, "Nitrogen-doped Carbon Nanotube Arrays with High Electrocatalytic Activities for Oxygen Reduction", *Science* 323 (**2009**) 760-764.

[21] P. H. Matter, L. Zhang and U. S. Ozkan, "The Role of Nanostructure in Nitrogen-containing Carbon Catalysts for the Oxygen Reduction Reaction", *Journal of Catalysis* 239 (**2006**) 83-96.

[22] A. Guerrero-Ruiz and I. Rodríguez-Ramos, "Hydrodesulfurization and Hydrogenation Activities of Carbon Supported Bimetallic Catalysts", *Reaction Kinetic Catalysis Letter* 41 (**1990**) 167-173.

[23] X. Li, Y. Liu , L. Fu, L. Cao, D. Wei, G. Yu and D. Zhu, "Direct Route to High-density and Uniform Assembly of Au Nanoparticles on Carbon Nanotubes", *Carbon* 44 (**2006**) 3139-3142.

[24] R. Arrigo M. Hävecker, R. Schlögl and D. Su, "Dynamic Surface Rearrangement and Thermal Stability of Nitrogen Functional Groups on Carbon Nanotubes", *Chemical Communication* (**2008**) 4891-4893.

[25] J. Biscoe and B. E. warren, "An X-ray Study of Carbon Black", *Journal of Applied Physic* 13 (**1942**) 364-371.

[26] T. J. Bandosz, M. J. Biggs, K. E. Gubbins, Y. Hattori, T. Liyiama, K. Kaneko, J. Pikunic, K. T. Thomson, *Chemistry and Physics of Carbon* 28 edited by L. R. Radovic, MDInc. (**2003**).

[27] O. Zhou , R. M. Fleming, D. W. Murphy, C. H. Chen, R. C. Haddon, A. P. Ramirez, and S. H. Glarum," Defects in Carbon Nanotubes", *Science* 263 (**1994**) 1744 -1747.

[28] A. Oberlin, M. Endo, T. Koyama "Filamentous Growth of Carbon through Benzene Decomposition", *Journal of Crystal Growth* 32 (**1976**) 335—349.

[29] S. Iijima, "Helical Microtubules of Graphitic Carbon**",** *Nature* 354 (**1991**) 56–58.

[30] S. Iijima and T. Ichihashi, "Single-Shell Carbon Nanotubes of 1-nm Diameter", *Nature* 363 (**1993**) 603–605.

[31] M. Terrones, A. Jorio, M. Endo, A. M. Rao, Y. A. Kim, T. Hayashi, H. Terrones, J. C. Charlier, G. Dresselhaus and M. S. Dresselhaus, "New Direction in Nanotubes Science", *Materials Today* (**2004**) October,30–45.

[32]A. Rochefort, Ph. Avouris, F. Lesage, D. R. Salahub, "Electrical and Mechanical Properties of Distorted Carbon Nanotubes", *Physical Review B* 60, Issue19 (**1999**) 13824-13829.

[33] A. R. Rocha, M. Rossi, A. Fazzio and A. J. R. da Silva, "Designing Real Nanotube-Based Gas Sensors", *Physical Review Letter* 100 (**2008**) 176803.

[34] M. W. Zhao, Y. Y. Xia, J. P. Lewis, R. Q. Zhang, "First-principles Calculations for Nitrogen-containing Single-walled Carbon Nanotubes", *Journal of Applied Physics* 94, Issue 4 (**2003**) 2398-2402.

[35] J. Chen, A. M. Rao, S. Lyuksyutov, M. E. Itkis, M. A. Hamon, H. Hu, R. W. Cohn, P. C. Eklund, D. T. Colbert, R. E. Smalley, R. C. Haddon, "Dissolution of Full-length Single-walled Carbon Nanotubes", *Journal of Physical Chemistry B* 105 (**2001**) 2525-2528.

[36] S. Reich, C. Thomsen, J. Maultzsch, "*Carbon Nanotubes: Basic Concepts and Physical Properties*", WILEY-VCH, **2004**.

[37] Q. B. Wen, L. Qiao, W. T. Zheng, Y. Zeng, C. Q. Qu, S. S. Yu, Q. Jiang, "Theoretical Investigation on Different Effects of Nitrogen and Boron Substitutional Impurities on the Structures and field Emission Properties for Carbon Nanotubes", *Physica* E 40 (**2008**) 890–893.

[38] J. P. Tessonnier, A. Villa, O. Majoulet, D. Su, R. Schlögl, *Angewante Chemie* submitted

[39] M. Sasaki, T. Yokono, M. Satou, and Y. Sanada, "Fractionation of Coal-tar Pitch with Iodine", *Energy Fuel* 5, issue 1 (**1991**) 122-125.

[40] P. J. F. Harris, "Impact of the Discovery of Fullerene on Carbon Science" in *Chemistry and Physics of Carbon* 28, edited by L. R. Radovic, MDInc. (**2003**) 1-39.

[41] J. Robertson, "Diamond-like Amorphous Carbon", *Materials Science and Engineering* R 37 (**2002**) 129-281.

[42] J. Robertson, "Amorphous and Non-crystalline Carbons" in *Graphite and Precursor* edited by Pierrè Delhaes (**2001**) 264-273.

[43] F. Buonocore, "Doping Effects on Metallic and Semiconductor Single-wall Carbon Nanotubes", *Philosophical magazine* 87, Issue 7 (**2007**) 1097-1105.

[44] A. H. Nevidomskyy, G. Csányi, M. C. Payne, "Chemically active substitutional nitrogen impurity in carbon nanotubes", *Physical Review Lett*er 91 (**2003**) 105502.

[45] J. M. Carlsson, "Curvature and chirality dependence of the properties of point defects in nanotubes", *Physic State Solid* 243, Issue 13 (**2006**) 3452-3457.

[46] R. Saito, G. Dresselhaus, M. S. Dresselhaus, "Physics of CNTs", Imperial College Press, **1998.**

[47] M. S. Dresselhaus, G. Dresselhaus, L. H. Avouris, "Carbon nanotubes", *Topic in Applied Physics* 80 (**2001)**.

[48] P. R. Wallace, "The band theory of graphite", *Physical Review* 71, Issue 9 (**1947**) 622-634.

[49] A. K. Geim and K. S. Novoselov, "The rise of graphene", *Nature Materials* 6 (**2007**) 183 -191.

[50] B. Partoens and F. M. Peeters, "From graphene to graphite: electronic structure around the K point", *Physical Review B* 74 (**2006**) 075404.

[51] O. Gülseren, T. Yildirim and S. Ciraci "Systematic *ab initio* study of curvature effects in carbon nanotubes", *Physical Review B* 65 (**2002**) 153405.

[52]A. Rochefort, D. R. Salahub and P. Avouris, "The effect of structural distortions on the electronic structure of carbon nanotubes", *Chemical Physics Letters* 297 (**1998**) 45–50.

[53] P. J. Britto, K. S. V. Santhanam, A. Rubio, J. A. Alonso and P. M. Ajayan, "Improved charge transfer at carbon nanotube electrodes", *Advanced Materials* 11, Issue 2 (**1999**) 154-157.

[54] T. Hertel, R. Martel and Ph. Avouris, "Manipulation of Individual Carbon Nanotubes and Their Interaction with Surfaces", *Journal of Physical Chemistry B* 102 (**1998**) 910-915.

[55] T. Hertel, R. Walkup and Ph. Avouris, "Deformation of Carbon Nanotubes by Surface Van der Waals Forces", *Physical Review* B 58 (**1998**) 13870-13873.

[56] H. J. Choi, J. Ihm, S. G. Louie and M. L. Cohen, "Defects, Quasibound States, and Quantum Conductance in Metallic Carbon Nanotubes"**,** *Physical Review Letters* 84, Issue13 (**2000**) 2917-2920.

[57] D. Kang, N. Park, J. H. Ko, E. Bae and W. Park, "Oxygen-induced p-type Doping of a Long Individual Single-Walled Carbon Nanotube", *Nanotechnology* 16 (**2005**) 1048–1052.

[58] J. M. Carlsson and M. Scheffler, "Structural, Electronic, and Chemical Properties of Nanoporous Carbon", *Physical Review Letters* 96 (**2006**) 0468061-4.

[59] J. I. Paredes, A. Martinez-Alonso, and J. .M. D. Tascon, "Comparative Study of the Air and Oxygen Plasma Oxidation of Highly Oriented Pyrolitic Graphite: a Scanning Tunneling and Atomic Force Microscopy Investigation", *Carbon* 38 (**2000**) 1183-1197.

[60] Y. Miyamoto, M. L. Cohen, S. G. Louie, "Theoretical Investigation of Graphitic Carbon Nitride and Possible Tubule Forms", *Solid state communications* 102 (**1997**) 605-608.

[61] M. C. dos Santos and F. Alvarez, "Nitrogen Substitution of Carbon in Graphite: Structure Evolution Toward Molecular Forms", *Physical Review* B 58, Issue 20 (**1998**) 13918-13924.

[62] B. G. Sumpter, J. Huang, V. Meunier, J. M. Romo-Herrera, E. Cruz-Silva, H. Terrones, M. Terrones , "Theoretical and Experimental Study on Manipulating the Structure and Properties of Carbon Nanotubes Using Substitutional Dopants", *International Journal of Quantum Chemistry* 109, Issue 1 (**2009**) 97-118.

[63] R. Czerw, M. Terrones, J. C. Charlier, X. Blase, B. Foley, R. Kamalakaran, N. Grobert, H. Terrones, D. Tekleab, P. M. Ajayan, W. Blau, M. Rühle, D. L. Carroll, "Identification of Electron Donor States in *N*-Doped Carbon Nanotubes", *Nanoletters* (**2001**) 457-460.

[64] M. Terrones, P. M. Ajayan, F. Banhart *et al.*, "N-doping and Coalescence of Carbon Nanotubes: Synthesis and Electronic Properties", *Applied Physics A 74* (**2002**) 355-361.

[65] M. Rossi, A. Fazzio, A. J. R. da Silva on-line avaiable cond-mat/0701602.

[66] E. D. Lavrinenko-Ometsinskaya, I. V. Repyakh, N. T. Kartel, V. V. Strelko, "States of a Heteroatom in Graphite-like Structures of Nitrogen-containing Carbons", *Teoreticheskaya I eksperimental'naya khimiya* 18, Issue 2 (**1982**) 224-227.

[67] E. D. Larinenko-Ometsinskaya, K. A. Kazdobin, V. V. Strelko, "Quantum-Chemical Evaluation of Electron-Donor Properties of Ordinary and Modified Carbon Sorbent", *teoreticheskaya I eksperimental´naya khimiya* 25, Issue 6 (**1989**) 723-727.

[68] J. Robertson and C. A. Davis, "Nitrogen Doping of Tetrahedral Amorphous Carbon", *Diamond and Related Materials* 4 (**1995**) 441-444.

[69] F. J. Owens, "Effect of Functionalization and Boron and Nitrogen Substitution on some Properties of Carbon Nanotubes", *Material Letter* 61, Issue 10 (**2007**) 1997-1999.

[70] M. R. Cuervo, E. Asedegbega-Nieto, E. Díaz, S. Ordóñez, A. Vega, A. B. Dongil and I. Rodríguez-Ramos**,** "Modification of the Adsorption Properties of High Surface Area Graphites by Oxygen Functional Groups", *Carbon* 46 (**2008**) 2096-2106.

[71] D. Tasis, N. Tagmatarchis, A. Bianco and M. Prato, "Chemistry of Carbon Nanotubes", *Chemical Review*106 (**2006**) 1105–1136.

[72]J. M. Carlsson, F. Hanke, S. Linic and M. Scheffler, "Two-step mechanism for low temperature oxidation of vacancies in graphene", *Physical review letter* 102 (**2009**)166104 .

[73] H. P. Boehm, "Catalytic Properties of Nitrogen-Containing Carbons" in *Carbon Materials for Catalysis* edited by P. Serp and J. L. Figueiredo, WILEY-VCH (**2009**) 219-265.

[74] R. Schlögl, "Carbons" in *Handbook of Heterogeneous Catalysis* edited by G. Ertl, H. Knözinger, F. Schüth and J. Weitkamp , WILEY-VCH (**2008**) 357-427.

[75] M. A. Montes-Morán, D. Suárez , J.A. Menéndez , E. Fuente, "On the Nature of Basic Sites on Carbon Surfaces: an Overview", *Carbon* 42 (**2004**) 1219–1225.

[76] T. J. Bandosz "Surface Chemistry of Carbons Materials" in *Carbon Materials for Catalysis* edited by P. Serp and J. L. Figueiredo, WILEY-VCH (**2009**) 45-92.

[77] A. Y. Stakheev and L. M. Kustov, "Effects of Support on the Morphology and Electronic Properties of Supported Metal Clusters: Modern Concepts and Progress in 1990s", *Applied Catalysis A: General* 188 (**1999**) 3-35.

[78] B. Coq, F. Figueras, "Structure–activity Relationships in Catalysis by Metals: some Aspects of Particle Size, Bimetallic and Supports Effects", *Coordination Chemistry reviews* 178-180 (**1998**) 1753-1783.

[79] J. Zhang, X. Liu, R. Blume, A. Zhang, R. Schlögl, D. Su, "Surface-Modified Carbon Nanotubes Catalyze Oxidative Dehydrogenation of n-Butane", *Science* 322 (**2008**) 73-77.

[80] E. Raymundo-Piñero, D. Cazorla-Amorós, C. Salinas-Martinez de Lecea and A. Linares-Solano, "Factors Controlling the SO_2 Removal by Porous Carbons: Relevance of SO_2 Oxidation Step", *Carbon* 38, Issue 3 (**2000**) 335-344.

[81] E. Raymundo-Piñero, D. Cazorla-Amorós, A. Linares-Solano, "The Role of Different Nitrogen Functional Groups on the Removal of SO_2 from Flue Gases by N-doped Activated Carbon Powders and Fibres", *Carbon* 41, Issue 10 (**2003**) 1925-1932.

[82] E. Raymundo-Piñero, D. Cazorla-Amorós, A. Linares-Solano "Temperature Programmed Desorption Study on the Mechanism of SO_2 Oxidation by Activated Carbon and Activated Carbon Fibres", *Carbon* 39 (**2001**) 231-242.

[83] L. Singoredjo, F. Kapteijn, J. Moulijn, J. Martínez and H. Boehm "Modified AC for the Selective Catalytic Reaction of NO with NH_3", *Carbon* 31 (**1993**) 213–222.

[84] J. L. Figureido and M. F. Pereira, "Carbon as Catalyst", *Carbon Materials for Catalysis* edited by P. Serp and J. L. Figueiredo, WILEY-VCH (**2009**) 177-217.

[85] S. Bashkova, F. S. Baker, X. Wu, T. R. Armstrong, V. Schwartz, "AC Catalyst for Selective Oxidation of Hydrogen Sulphide: On the Influence of Pore Structure, Surface Characteristics, and Catalytically-Active Nitrogen" *Carbon* 45, Issue 6 (**2007**) 1354-1363.

[86] L. B. Khalil, B. S. Girgis, T. A. M. Tawfik, "Decomposition of H_2O_2 on AC Obtained from Olive Stones" *Journal of Chemical Technology and Biotechnology* 76 (**2001**) 1132-1140.

[87] J-M Nhut, L. Pesant, J-P. Tessonnier, G. Winé, J. Guille, C. Pham-Huu and M-J. Ledoux "Mesoporous Carbon Nanotubes for Use as Support in Catalysis and as

Nanosized Reactors for One-dimensional Inorganic Material Synthesis", *Applied Catalysis A: General* 254, Issue 2 (**2003**) 345-363.

[88] T. Mallat and A. Baiker "Oxidation of Alcohols with Molecular Oxygen on Solid Catalysts" *Chemical Review* 104 (**2004**) 3037-3058.

[89] L. Calvillo, M. Gangeri, S. Perathoner, G. Centi, R. Molinera, M. J. Lázaro, "Effect of the support properties on the preparation and performance of platinum catalysts supported on carbon nanofibers" *Journal of Power Sources* (**2009**) *In press*

[90] M. Gangeri, S. Perathoner, G. Centi "Synthesis and performances of carbon-supported noble metal nanoclusters as electrodes for polymer electrolyte membrane fuel cells" *Inorganica Chimica Acta* 359, Issue 15 (**2006**) 4828-4832.

[91] M. Gangeri, G. Centi, A. La Malfa, S. Perathoner, R. Vieira, C. Pham-Huu, M.J. Ledoux "Electrocatalytic performances of nanostructured platinum–carbon materials" *Catalysis Today* 102-103 (**2005**) 50-57.

[92] M. Gangeri, S. Perathoner, S. Caudo, G. Centi, J. Amadou, D. Bégin , C. Pham-Huu, M. .J. Ledoux, J.-P. Tessonnier, D. S. Su, R. Schlögl, "Fe and Pt carbon nanotubes for the electrocatalytic conversion of carbon dioxide to oxygenates" *Catalysis Today* 143 (**2009**) 57–63.

[93] F. Winter, V. Koot, A. Jos van Dillen, J W. Geus and K. P. de Jong, "Hydrotalcites supported on carbon nanofibers as solid base catalysts for the synthesis of MIBK", *Journal of Catalysis* 236, Issue 1 (**2005**) 91-100.

[94] J. Zhang, M. Comotti, F. Schüth, R. Schlögl and D. Su, "Commercial Fe or Co containing carbon nanotubes as catalysts for NH_3 decomposition", *Chemical Communication* (**2007**) 1916–1918.

[95] J. L. Faria and W. Wang, "Carbon Materials in Photocatalysis" in *Carbon Materials for Catalysis* edited by P. Serp and J. L. Figueiredo, WILEY-VCH (**2009**) 481-506.

[96] K. A. Ahrendt, C. J. Borths, and D. W. C. MacMillan "New Strategies for Organic Catalysis: The First Highly Enantioselective Organocatalytic Diels-Alder Reaction", *Journal of American Chemical Society* 122, Issue 17 (**2000**) 4243-4244.

[97] C. Chandler, P. Galzerano, A. Michrowska, B. List "The Proline-Catalyzed Double Mannich Reaction of Acetaldehyde with N-Boc Imines", *Angewandte Chemie International Edition* 48, Issue 11 (**2009**) 1978-1980.

[98] Several examples are reported in this review: S. Das, G. W. Brudvig and R. H. Crabtree, "Molecular recognition in homogeneous transition metal catalysis: a biomimetic strategy for high selectivity", *Chemical Communication* (**2008**) 413-424.

[99] Y. Ono, "Solid Base Catalysts for the Synthesis of Fine Chemicals", *Journal of Catalysis* 216 (**2003**) 406-415.

[100] J. M. Fraile, J. I. García, J. A. Mayoral, "Basic Solid in the Oxidation of Organics", *Catalysis Today* 57 (**2000**) 3-16.

[101] Y. Kayaki, M. Yamamoto, and T. Ikariya, "N-Heterocyclic Carbenes as Efficient Organocatalysts for CO_2 Fixation Reactions", *Angewandte Chemie International Edition* 48 (**2009**) 1-5.

[102] K. Suenaga, M.P. Johansson, N. Hellgren, E. Broitman, L.R. Wallenberg and C. Colliex, J-E. Sundgren and L. Hultman"Carbon nitride nanotubulite-densely-packed and well-aligned tubular nanostructures", *Chemical Physic Letter* 300 (**1999**) 695–700.

[103] N. Hellgren, M.P. Johansson, E. Broitman, L. Hultman and J.E. Sundgren, "Role of Nitrogen in the Formation of Hard and Elastic CN_x Thin Films by Reactive Magnetron Sputtering", *Physical Review B* 59, Issue 7 (**1999**) 5162–5169.

[104] F. Le Normand, J. Hommet, T. Szörényi, C. Fuchs and E. Fogarassy, "XPS Study of Pulsed Laser Deposited CNx Films", *Physical Review B* 64 (**2001**) 2354161-2354176.

[105] J. Hu, P. Yang and C. M. Lieber, "Nitrogen-driven sp^3 to sp^2 transformation in carbon nitride materials", *Physical Review B* 57, Issue 6 (**1998**) 3185–3188.

[106] A. G. Kudashov, A. V. Okotrub, L. G. Bulusheva, I. P. Asanov, Y. V. Shubin and N. F. Yudanov, "Influence of Ni−Co Catalyst Composition on Nitrogen Content in Carbon Nanotubes", *Journal of Physical Chemistry B* 108 (**2004**) 9048–9053.

[107] H. C. Choi, J. Park and B. Kim, "Distribution and Structure of N Atoms in Multiwalled Carbon Nanotubes Using Variable-Energy X-Ray Photoelectron Spectroscopy", *Journal of Physical Chemistry B* 109 (**2005**) 4333–4340.

[108] S. van Dommele, K.P. de Jong and J.H. Bitter, "Nitrogen-containing Carbon Nanotubes as Solid Base Catalysts", *Chemical Communication* (**2006**) 4859–4861.

[109] M. Terrones, P. Redlich, N. Grobert, S. Trasobares, W.K. Hsu and H. Terrones, "Carbon Nitride Nanocomposites: Formation of Aligned C_xN_y Nanofibers", *Advanced Material* 11, Issue 8 (**1999**) 655–658.

[110] J. Amadou K. Chizari, M. Houllé**,** I. Janowska, O. Ersen, D. Bégin and C. Pham-Huu**, "**N-doped Carbon Nanotubes for Liquid-phase C-C Bond Hydrogenation"**,** *Catalysis Today* 138, Issues 1-2, (**2008**) 62-68.

[111] S. Van Dommele, A. Ramera-Izquirdo, R. Brydson, K. P. De Jong, J. H. Bitter, "Tuning Nitrogen Functionalities in Catalytically Grown Nitrogen-containing Carbon Nanotubes", *Carbon* 46 (**2008**) 138-148.

[112] R. Sen, B. C. Satishkumar, A. Govindaraj, K. R. Harikumar, G. Raina, J-P Zhang, A. K. Cheetham and C. N. R. Rao, "B–C–N, C–N and B–N Nanotubes Produced by the

Pyrolysis of Precursor Molecules over Co Catalysts", *Chemical Physics Letter* 287 (**1998**) 671-676

[113] M. Terrones, R. Kamalakaran, T. Seeger, M. Rühle, "Novel Nanoscale Gas Containers: Encapsulation of N_2 in CNx Nanotubes", *Chemical Communications* 23 (**2000**) 2335-2336.

[114] H. Terrones and M. Terrones, "Curved nanostructured materials", *New Journal of Physics* 5 (**2003**) 126.1–126.37.

[115] H. C. Choi, S. Y. Bae, J. Park, K. Seo, C. Kim and B. Kim *et al.*, "Experimental and theoretical studies on the structure of N-doped carbon nanotubes: possibility of intercalated molecular N_2", *Applied Physic Letter* 85, Issue 23 (**2004**) 5742–5744.

[116] J. Su, R. Kamalakaran, T. Seeger and M. Rühle, "Aligned Array of N_2-encapsulated Multilevel Branched Carbon Nanotubes", *Applied Physic A* 90 (**2008**) 135–139.

[117] C. Tang, Y. Bando, D. Golberg and F. Xu, "Structure and Nitrogen Incorporation of Carbon Nanotubes Synthesized by Catalytic Pyrolysis of Dimethylformamide", *Carbon* 42 (**2004**) 2625–2633.

[118] D. Tasis, N. Tagmatarchis, A. Bianco and M. Prato, "Chemistry of Carbon Nanotubes", *Chemical Review* 106 (**2006)** 1105–1136.

[119] J-P Tessonnier, D. Rosenthal, T. W. Hansen, C. Hess, M. E. Schuster, R. Blume, F. Girgsdies, N. Pfänder, O. Timpe, D. Su, R. Schlögl, "Analysis of the Structure and Chemical Properties of some Commercial Carbon Nanostructures", *Carbon* 47, Issue 7 (**2009**) 1779-1798.

[120] H. P. Boehm, "Some Aspects of the Surface Chemistry of Carbon Black and other Carbon", *Carbon* 32, Issue 5 (**1994**) 759-769.

[121] M. Domingo-García, A. J. Groszek, F. J. López-Garzón and M. Pérez-Mendoza, "Dynamic Adsorption of Ammonia on Activated Carbons Measured by Flow Microcalorimetry", *Applied Catalysis A: General* 233, Issues 1-2 (**2002**) 141-150.

[122] H.P. Bohem, "Chemical Identification of surface groups", *Advances in Catalysis* 16 (**1966**) 179-274.

[123] R. C. Bansal, J-B Donnet and F. Stoeckli, "Surface Chemical Structures on Active Carbons" in *Active carbon*, Marcel Dekker Inc. New York (**1988)** 27-118.

[124]J-O. Müller, "Investigation on Environmental carbons", PhD thesis, Berlin **2005.**

[125] J. A Brandes, G. D. Cody, D. Rumble, P. Haberstroh, S. Wirick, Y. Gelinas, "K-edge XANES Spectromicroscopy of Natural Graphite", *Carbon* 46 (**2008**) 1424-1434.

[126] J. H. Yang, B. J. Kim, Y. H. Kim, Y. J. Lee, B. H. Ha, Y. S. Shin, S. Y. Park, H. S. Kim, and C-Y. Park, **"**Nitrogen-incorporated Multiwalled Carbon Nanotubes Grown by Direct Current Plasma-enhanced Chemical Vapor Deposition", *Journal of Vacuum Science and Technology B* 23, issue 3 (**2005**) 930-933.

[127] C. A. Davis, D. R. McKenzie, Y. Yin, E. Kravtchinskaia, G. A. J. Amaratunga and V. S. Veerasamy, "Substitutional nitrogen doping of tetrahedral amorphous carbon", *Philosophical Magazine Part B* 69, Issue 6 (**1994**) 1133-1140.

[128] R. R. Deshmukh, A. R. Shetty, "Comparison of Surface Energies Using Various Approaches and Their Suitability", *Journal of Applied Polymer Science* 107 (**2008**) 3707–3717.

[129] M. Hävecker, F. Senf, W. Eberhardt, R. Schlögl, in preparation

[130] R. Follath and F. Senf, "New Plane–grating Monochromators for Third Generation Synchrotron Radiation Light Sources", *Nuclear Instruments and Methods in Physics Research A* 390 (**1997**) 388–394.

[131] K. J. S. Sawhney, F. Senf, M. Scheer, F. Scheer, F. Schäfers, J. Bahrdt, A. Gaupp and W. Gudat, "A Novel Undulator-based PGM Beamline for Circularly Polarised Synchrotron Radiation at BESSY II", *Nuclear Instruments and Methods in Physics Research A* 390 (**1997**) 395-402.

[132] D. A. Shirley, "High-resolution X-ray photoemission spectrum of the valence bands of Gold", *Physic Review B: Solid State* 5, Issue 12 (**1972**) 4709-4714.

[133]http://www.casaxps.com.

[134] A. Proctor, P. M. A. Sherwood, "X-ray Photoelectron Spectroscopic Studies of Carbon Fibre Surfaces", *Journal of electron spectroscopy and related phenomena* 27 (**1982**) 39-56.

[135] A. Proctor, P. M. A. Sherwood, "Data Analysis Techniques in X-ray Photoelectron Spectroscopy**",** *Analytical Chemistry* 54 (**1982**)13-19.

[136] J. Lahaye G Nanse P. Fioux, A. Bagreev, A. Broshnik, V. Strelko, "Chemical Transformation During the Carbonisation in Air and the Pyrolysis under Argon of a Vinylpyridine–divinylbenzene Copolymer by X-ray Photoelectron Spectroscopy", *Applied Surface Science* 147(**1999**)153-174.

[137] J. J Yeh, I. Lindau, Atomic Data and Nucl. Tables 32 (**1985**) 1-155.

[138] S. Brunauer, P. Emmet, and E. Teller, "Adsorption of Gases in Multimolecular Layers", *Journal of American Chemical Society* 60 (**1938**) 309-319.

[139] E. P. Barrett, L. G. Joyner, P. P. Halenda, "The Determination of Pore Volume and Area Distributions in Porous Substances. I. Computations from Nitrogen Isotherms", *Journal of American Chemical Society* 73 (**1951**) 373–380.

[140] E. N. Coker, C. Jia, H. G. Karge, "Adsorption of Benzene and Benzene Derivatives onto Zeolite H-Y Studied by Microcalorimetry", *Langmuir* 16 (**2000**) 1205-1210.

[141] L. R. Radovic, I. F. Silva, J. I. Ume, J. A. Menéndez, C. A. Leon Y Leon and A. W. Scaroni, "An experimental and theoretical study of the adsorption of aromatics possessing electron-withdrawing and electron-donating functional groups by chemically modified activated carbons", *Carbon* 35 (**1997**) 1339-1348.

[142] G. C. Bond, "Active Phase-Support Interaction" in *Handbook of Heterogeneous Catalysis* 2 edited by E. Gerhard, H. Knözinger, F. Schüth, J. Weitkamp, (**2008**) Wiley-WCH, 752-770.

[143] H. Bönnemann and R. M. Richards, "Nanoscopic Metal Particles-Synthetic Methods and Potential Applications", *European Journal of Inorganic Chemistry* (**2001**) 2455-2480.

[144] L. Prati and F. Porta, "Oxidation of alcohols and sugars using Au/C catalysts: Part 1. Alcohols", *Applied Catalysis A: General* 291 (**2005**) 199-203.

[145] F. Porta, L. Prati, M. Rossi, G. Scari, "New Au(0) Sols as Precursors for Heterogeneous Liquid-Phase Oxidation Catalysts", *Journal of Catalysis* 211 (**2002**) 464-469.

[146] F. Porta, L. Prati, M. Rossi, S. Coluccia, G. Martra, "Metal Sols as a Useful Tool for Heterogeneous Gold Catalyst Preparation: Reinvestigation of a Liquid Phase Oxidation", *Catalysis Today* 61(**2000**) 165-172.

[147] D. B. Williams and C. Barry Carter, "Transmission Electron Microscopy", Springer (**2004**).

[148] C. Kozlowski, P. M. A. Sherwood, "X-ray photoelectron-spectroscopic studies of carbon-fibre surfaces" *Journal of Chemical Society Faraday transition* 81 (**1985**) 2745-2756.

[149] E. Desimoni, G. I. Casella, A. Morone, A. M. Salvi, "XPS Determination of Oxygen-Containing Functional Groups on Carbon Fibres Surfaces and the Cleaning of these Surfaces", *Surface and Interface Analysis* 15, Issue 10 (**1990**) 627-634.

[150] D. T. Clark, H. R. Thomas, "Applications of ESCA to Polymer Chemistry. XVII. Systematic Investigation of the Core Levels of Simple Homopolymers", *Journal of Polimer Science: Polymer Chemistry Edition* 16 (**1978**) 791-820.

[151] A. Proctor, P. M. A. Sherwood, "X-ray Photoelectron Spectroscopic Studies of Carbon Fibre Surfaces. III Industrially Treated Fibres and the Effect of Heat and Exposure to Oxygen", *Surface and Interface Analysis* 4, Issue 5 (**1982**) 212-219.

[152] L. G. Bulusheva, A.V. Okotrub, A.G. Kudashov, I. P. Asanov, and O. G. Abrosimov, "Electronic State of Nitrogen Incorporated into CNx Nanotubes", *European Physical Journal D* 34 (**2005**) 271–274.

[153] J. P. Boudou, M. Chehimi, E. Broniek, T. Siemieniewska and J. Bimer**,** "Adsorption of H_2S or SO_2 on an Activated Carbon Cloth Modified by Ammonia Treatment", *Carbon* 41 (**2003**) 1999-2007.

[154] F. Kapteijn, J. A. Moulijn, S. Matzner, H. P. Boehm, "The Development of Nitrogen Functionality in Model Chars During Gasification in CO_2 and O_2", *Carbon* 37 (**1999**)1143-1150.

[155] T. Belz, A. Bauer, J. Find, M. Gunter, D. Herein, H. Mockel, N. Pfander, H. Sauer, G. Schulz; J. Schutze O. Timpe, U. Wild; R. Schlogl „Structural and Chemical Characterization of N-doped Nanocarbons", *Carbon* 36, Issue 11 (**1997**) 731-741.

[156] K. Staczyk, R. Dziembaj, Z. Piwowarska and S. Witkowski, "Transformation of Nitrogen Structures in Carbonization of Model Compounds Determined by XPS", *Carbon* 33 (**1995**) 1383-1392.

[157] R. J. J. Jansen and H. van Bekkum, "XPS of Nitrogen-containing Functional Groups on Activated Carbon**",** *Carbon* 33 (**1995**) 1021-1027.

[158] J. R. Pels, F. Kapteijn, J. A. Moulijn, Q. Zhu and K. M. Thomas, "Evolution of Nitrogen Functionalities in Carbonaceous Materials During Pyrolysis", *Carbon* 33 (**1995**) 1641-1653.

[159] A. N. Buckley "Nitrogen Functionality in Coals and Coal-tar Pitch Determined by X-ray Photoelectron Spectroscopy", *Fuel Processing Technology* 38 (**1994**) 165-179.

[160] S. R. Kelemen, M. L. Gorbaty, P. J. Kwiatek, "Quantification of Nitrogen Forms in Argonne Premium Coals", *Energy Fuels* 8 (**1994**) 896-906.

[161] G. Gabriel, G. Sauthier, J. Fraxedas, M. Moreno-Mañas, M. T. Martínez, C. Miravitlles, J. Casabó, "Preparation and Characterization of Single-walled Carbon Nanotubes Functionalized with Amines", *Carbon* 44 (**2006**) 1891–1897.

[162] N. I. Kovtyukhova. and T. E. Mallouk, "Ultrathin Anisotropic Films Assembled from Individual Single-Walled Carbon Nanotubes and Amine Polymers", *Journal of physical Chemistry B* 109, Issue 7 (**2005**) 2540-2545.

[163] C. D. Batich, D. S. Donald, "X-ray Photoelectron Spectroscopy of Nitroso Compounds: Relative Ionicity of the Closed and Open Forms", *Journal of American Chemical Society* 106 (**1984**) 2758-2761.

[164] R. Graupner, J. Abraham, A. Vencelova, T. Seyller, F. Hennrich, M. M. Kappes, A. Hirsch, L. Ley, "Doping of Single-Walled Carbon Nanotube Bundles by Brønsted Acids", *Physical Chemistry Chemical Physics* 5 (**2003**) 5472–5476.

[165] N. Keller, N. I. Maksimova, V. V. Roddatis, M. Schur, G. Mestl, Y. V. Butenko, V. L. Kuznetsov and R. Schlögl, „The Catalytic Use of Onion-like Carbon Materials for Styrene Synthesis by Oxidative Dehydrogenation of Ethylbenzene", *Angewandte Chemie International Edition* 41, Issue11, (**2002**)1885–1888.

[166] T. I. T. Okpalugo, P. Papakonstantinou, H. Murphy, J. McLaughlin, N. M. D. Brown, High Resolution XPS Characterization of Chemical Functionalized MWCNTs and SWCNTs" *Carbon* 43 (**2005**) 153-161.

[167] J. A. Maciá-Agulló, D. Cazorla-Amorós, A. Linares-Solano, U. Wild, D.S. Su and R. Schlögl**,** "Oxygen functional groups involved in the styrene production reaction detected by quasi in situ XPS", *Catalysis Today* 102-103 (**2005**) 248-253.

[168] M. Walczyk, A. Swiatkowski, M. Pakula, S. Biniak, "Electrochemical Studies of the Interaction between a Modified Activated Carbon Surface and Heavy Metal Ions", *Journal of applied electrochemistry* 35 (**2005**) 123-130.

[169] J. L. Figuereido, M. F. R. Pereira, M. M. A. Freitas, J. J. M. Orfao, "Modification of the Surface Chemistry of Activated Carbons", *Carbon* 37 (**1999**) 1379-1389.

[170] B. Marchon, J. Carrazza, H. Heinemann, G. A. Somorjai, "TPD and XPS Studies of O_2, CO_2, and H_2O Adsorption on Clean Polycrystalline Graphite", *Carbon* 26**,** Issue 4 (**1988**) 507-514.

[171] E. Desimoni, G. I. Casella, T. R. I. Cataldi, A. M. Salvi, T. Rotunno, E. Di Croce, "Remarks on the Surface Characterization of Carbon Fibres", *Surface and Interface Analysis* 18 (**1992**) 623-630.

[172] C. Ozlowsk, P. M. A. Sherwood, "X-ray Photoelectron-Spectroscopic Studies of Carbon-Fibre Surfaces. Part 5-The Effect of pH on Surface Oxidation", *Journal of American Chemical Society Faraday Transition* 81 (**1985**) 2745-2756.

[173] R. Schlögl, G. Loose and M. Wesemann, "On the mechanism of the oxidation of graphite by molecular oxygen", *Solid State Ionics* 43 (**1990**) 183-192.

[174] J. Casanovas, J. M. Ricart, J. Rubio, F. Illas, J. M. Jiménez- Mateos, "Origin of the Large N 1s BE in X-ray Photoelectron Spectra of Calcined Carbonaceous Materials", *Journal of American Chemical Society* 118 (**1996**) 8071-8076.

[175] J. P. Boutique, "3,5,11,13-Tetraazacycl[3.3.3]Azine: Theoretical (ab initio) and Experimental (X-ray and Ultraviolet Photoelectron Spectroscopy) Studies of the Electronic Structure", *Journal of American Chemical Society* 106 (**1984**)4374-4378.

[176] C. A. Faustin, R. Gouttebaron, C. De Nadaï, R. Caudano, F. Zerbetto, D. A. Leigh, P. Rudolf, "Photoemission study of pristine and potassium intercalated benzylic amide [2]catenane films", *Surface Science* 404 (**2001**)37-46.

[177] B. Henschke, H. Schubert, J. Blöcker, F. Atamny, R. Schlögl, "Mechanistic aspects of the reaction between carbon and oxygen", *Thermochimica acta* 234 (**1994**) 53-83.

[178] J. Surygała, R. Wandas E. Śliwka, „Oxygen Elimination in the Process of Non-Catalytic Liquefaction of Brown Coal", *Fuel* 72 (**1993**) 409-411.

[179] W. W. Wendlandt, J. A. Hoiberg, "A differential Thermal Analysis (DTA) and Thermogravimetric Analysis (TGA) study of some organics acids 2", *Analytica Chimica Acta* 29, Issue 6 (**1963**) 539-544.

[180] W. W. Wendlandt, JA Hoiberg " A Differential Thermal Analysis Study of some Organic Acid 1", *Analytica Chimica Acta* 28, Issue 6 (**1963**) 506-511.

[181] M. Wesolowski, T. Konarski, "Studies on the Thermal Decomposition of Benzoic Acid and its Derivatives", *Journal of Thermal Analysis and Calorimetry* 55 (**1999**) 995-1002.

[182] J. H. Zhou, Z. J. Sui, J. Zhu, P. Li, D. Chen, Y-C. Dai and W-K. Yuan, "Characterization of Surface Oxygen Complexes on Carbon Nanofibers by TPD, XPS and FT-IR", *Carbon* 45 (**2007**) 785-796.

[183] C. Moreno-Castilla, F. Carrasco-Marin, F.J. Maldonado-Hodar, J. Rivera-Utrilla, "Effects of Non-Oxidant and Oxidant Acid Treatments on the Surface Properties of an Activated Carbon with Very Low Ash Content", *Carbon* 36, Issue 1-2 (**1998**) 145-151.

[184] H. F. Gorgulho, J. P. Mesquita, F. Gonçalves, M. Fernando R. Pereira and J. L. Figueiredo, "Characterization of the Surface Chemistry of Carbon Materials by Potentiometric Titrations and Temperature-Programmed Desorption", *Carbon* 46, Issue 12 (**2008**) 1544-1555.

[185] G. de la Puentea, J.J. Pis, J.A. Menéndez and P. Grange, "Thermal Stability of Oxygenated Functions in Activated Carbons", *Journal of Analytical and Applied Pyrolysis* 43, Issue 2 (**1997**) 125-138.

[186] L. J. Lemus-Yegres, I. Such-Basáñez, M. C. Román-Martínez and C. Salinas-Martínez de Lecea, "Catalytic Properties of a Rh–diamine Complex Anchored on Activated Carbon: Effect of Different Surface Oxygen Groups", *Applied Catalysis A: General* 331 (**2007**) 26-33.

[187] J. A. Moulijn and P. J. J. Tromp, "Coal Pyrolysis", in Carbon and Coal Gasification edited by J. L. Figueiredo and J. A. Moulijn , Series E: Applied Science 105 (**1986**) 455-507.

[188] J. P. Boudou, Ph. Parent, F. Suárez-García, S. Villar-Rodil, A. Martínez-Alonso, J. M. D. Tascón, "Nitrogen in Aramid-based Activated Carbon Fibers by TPD, XPS and XANES", *Carbon* 44 (**2006**) 2452-2462.

[189] C-M. Yang, D. Y. Kim, and Y. H. Lee, "Formation of Densely Packed Single-Walled Carbon Nanotube Assembly", *Chemical Materials* 17, Issue 25 (**2005**) 6422-6429.

[190] J. Zawadski, "IR Spectroscopic Investigations of the Mechanism of Oxidation of Carbonaceous Films with HNO_3 Solution", *Carbon* 18, Issue 4 (**1980**) 281-285.

[191] R. Pietrzak' and H. Wachowska, "The Influence of Oxidation with HNO_3 on the Surface Composition of High-Sulphur Coals: XPS Study", *Fuel Processing Technology* 87 (**2006**) 1021–1029.

[192] D. R. Mehandjiev, R. N. Nickolov, R. B. Ioncheva, "Determination of Nitrogen Structures on Activated Carbon Surfaces by a Chemical Method", *Fuel* 76, Issue 5 (1997) 381-384.

[193] P. M. Th. M. van Attekum and G. K. Wertheim, "Excitonic Effects in Core-Hole Screening", *Physical Review Letter* 43, Issue 25 (**1979**) 1896 - 1898.

[194] G. Speranza, L. Minati, „ The Surface and Bulk Core Lines in Crystalline and Disordered Polycrystalline Graphite", *Surface Science* 600, (**2006**) 4438-4444.

[195] D.-Q. yang, E. sacher, „s-p Hybridization in Hyghly Oriented Pyrolityc Graphite and ist Change on the Surface Modification, as Studied by X-ray Photoelectron and Raman Spectroscopy", Surface Science 504 (**2002**) 125-137.

[196] H. Werner, D. Herein, J. Blöcker, B. Henschke, U. Tegtmeyer, Th. Schedel-Niedrig, M. Keil, A.M. Bradshaw and R. Schlögl, "Spectroscopic and Chemical Characterization of Fullerene Black", *Chemical Physics Letters* 134, Issue 1,2 (**1992**) 62-66.

[197]F. Atamny, J. Bloecker, B. Henschke, R. Schloegl, T. Schedel-Niedrig, M. Keil, and A. M. Bradshaw, "The Reaction of Oxygen with Graphite: X-Ray Absorption Spectroscopy of Carbonaceous Materials", *Journal of Physical Chemistry* 96, Issue 11, (**1992**) 4522-4526.

[198] U. Wild, N. Pfànder, R. Schloegl, "Species Analysis of Automotive Carbon Particles: Application of XPS for integral analysis of filter Samples", *Fresenius Journal of Analytical Chemistry* 357, Issue 4 (**1997**) 420-428.

[199] P. M. A. Sherwood, "Surface Analysis of Carbon and Carbon Fibers for Composites", *Journal of Electron Spectroscopy and Related Phenomena* 81 (**1996**) 319.

[200] D. A. Schirley, "Esca. Results Versus Other Physical and Chemical Data", *Journal of Electron Spectroscopy and Related Phenomena* 5, Issue 1 (**1974**) 135-148.

[201] R. L. Martin and D. A. Shirley. "Relation of core-level BE shifts to proton affinity and Lewis basicity", *Journal of American Chemical Society* 96, Issue17 (**1974**) 5299–5304.

[202] A. Contescu, C. Contescu, K. Putyera and J. A. Schwarz, "Surface Acidity of Carbons Characterized by Their Continuous p*K* Distribution and Boehm Titration", *Carbon* 35, Issue 1 (**1997**) 83-94.

[203] F. Xie, J. Phillips, I. F. Silva, M. C. Palma and J. A. Menéndez, "Microcalorimetric Study of Acid Sites on Ammonia- and Acid-pretreated Activated Carbon", *Carbon 38*, Issue 5 (**2000**) 691-700.

[204] David R. Lide, "Handbook of Chemistry and Physics", CRC press.

[205] http://www.chemaxon.com/test/marvin/help/calculations/pKa.html.

[206] A. Borowiak-Resterna, J. Szymanowski, A. Voelkel, "Structure and Nitrogen Basicity of Pyridine Metal Extractants", *Journal of Radioanalytical and Nuclear Chemistry* 208, Issue 1 (**1996**) 75-76.

[207] J. M. Martin, C. Grossiord, T. Le Mogne, J. Igarashi, "Role of Nitrogen in Tribochemical Interaction between Zndtp and Succinimide in Boundary Lubrication", *Tribology International* 33 (**2000**) 453-459.

[208] A. Chenite, A. Selmani, "Cr/Phthalimide System: XPS Study of Interfacial Reactions", *Surface Science* 301, Issue 1-3 (**1994**) 197-202.

[209] J. - P. Tessonnier, D. Rosenthal, J. Amadou, D. Bégin, C. Pham-Huu, D. Su and R. Schlögl, "Influence of the Graphitization of Carbon Nanotubes on their Functionalization and Subsequent Filling with Metal Nanoparticles", submitted to *Chemical Communication*.

[210] W. Winter, X. Xia, B. P. C. Hereijgers, J. H. Bitter, A. J. van Dillen, M. Muhler, and K. P. de Jong, "On the Nature and Accessibility of the Brønsted-Base Sites in Activated Hydrotalcite Catalysts", *Journal of Physical Chemistry B* 110 (**2006**) 9211-9218.

[211] J. Shen, R. D. Cortright, Y. Chen and J. A. Dumesic, "Microcalorimetric and Infrared Spectroscopic Studies ofγ-Al_2O_3 Modified by Tin Oxides" *Catalysis Letter* 26 (**1994**) 247-257.

[212]C. Knöfel, J. Descarpentries, A. Benzaouia, V. Zeleňák, S. Mornet, P.L. Llewellyn and V. Hornebecq**,** "Functionalized Micro-/Mesoporous Silica for the Adsorption of Carbon Dioxide", *Microporous and Mesoporous Materials* 99 (**2007**) 79–85.

[213] J. Muzart, "Palladium-catalyzed oxidation of primary and secondary alcohols", *Tetrahedron* 59 (**2003**) 5789-5816.

[214] J. S. Rafelt and J. H. Clark, "Recent Advances in the Partial Oxidation of Organic Molecules Using Heterogeneous Catalysis", *Catalysis Today* 57, Issue1-2 (**2000**) 33-44.

[215] J. H. J. Kluytmans, A. P. Markusse, M.B. F. Kuster, G. B. Marin, J. C. Schouten, "Engineering Aspects of the Aqueous Noble Metal Catalyzed Alcohol Oxidation", *Catalysis Today* 57 , Issue 1-2 (**2000**) 143-155.

[216] V. R. Gangwal, J. van der Schaaf, B. F. M. Kuster and J. C. Schouten, "Noble-Metal-Catalyzed Aqueous Alcohol Oxidation: Reaction Start-up and Catalyst Deactivation and Reactivation", *Journal of Catalysis* 232, Issue 2 (**2005**) 432-443.

[217] G. J. Hutchings, S. Carrettin, P. Landon, J. K. Edwards, D. Enache, D. W. Knight, Y-J Xu and A. F. Carley , "New Approaches to Designing Selective Oxidation Catalysts: Au/C a Versatile Catalyst", *Topics in Catalysis* 38, Issue 4 (**2006**) 223-230.

[218] G. J. ten Brink, I. W. C. E. Arends, R. A. Sheldon," Green, Catalytic Oxidation of Alcohols in Water", *Science* 287, Issue 5458 (**2000**) 1636-1639.

[219] J. W. Nicoletti, G. M. Whitesides, "Liquid-phase oxidation of 2-propanol to acetone by dioxygen using supported platinum catalysts"**,** *Journal of Physical Chemistry* 93, Issue 2 (**1989**) 759-767.

[220] S. Biella, F. Porta, L. Prati and M. Rossi, "Surfactant-Protected Gold Particles: New Challenge for Gold-on-Carbon Catalysts" *Catalysis letter* 90, Issue 1-2 (**2003**) 23-29.

[221] K. Ohno and J. Tsuji, "Organic Syntheses by Means of Noble Metal Compounds. XXXV. Novel Decarbonylation Reactions of Aldehydes and Acyl Halides Using Rhodium Complexes"**,** *Journal of the American Chemical Society* 90, Issue 1 (**1968**) 99–107.

[222] C. Brönnimann, Z. Bodnar, R. Aeschimann, T. Mallat, and A. Baiker, "Localized Basification of Catalytic Surfaces enhances the Selective Oxidation of L-Sorbose over Supported Pt Catalysts modified with Tertiary Amines", *Journal of Catalysis* 161 (**1996**) 720–729

[223] T. Mallat and A. Baiker, "Oxidation of alcohols with molecular oxygen on platinum metal catalysts in aqueous solutions", *Catalysis Today* 19 (**1994**)247-283.

[224] M. Besson, P. Gallezot, "Selective Oxidation of Alcohols and Aldehydes on Metal Catalysts", *Catalysis Today* 57 (**2000**) 127–141.

[225] Z. Opre, J.-D. Grunwaldt, T. Mallat and A. Baiker, "Selective Oxidation of Alcohols with Oxygen on Ru–Co-hydroxyapatite: A Mechanistic Study", *Journal of Molecular Catalysis A: Chemical* 242, Issues 1-2 (**2005**) 224-232.

[226] S. S. Hladyi, M. K. Starchevsky, Yuriy A. Pazdersky, M. N. Vargaftik and I. I. Moiseev, **"**Oxidative and Anaerobic Reactions of Benzyl Alcohol Catalysed by a Pd-561 Giant Cluster", *Mendeleev Communications* 12, Issue 2 (**2002**) 45-46.

[227] S. Mathew, C. Shiva Kumara, N. Nagaraju, "Influence of Nature of Support on the Catalytic Activity of Supported Molybdenum-oxo Species in Benzyl Alcohol Conversion", *Journal of Molecular Catalysis A: Chemical* 255 (**2006**) 243–248.

[228] C. Keresszegi, D. Ferri, T. Mallat, and A. Baiker, "Unraveling the Surface Reactions during Liquid-Phase Oxidation of Benzyl Alcohol on Pd/Al2O3: an in Situ ATR-IR Study", *Journal of Physical Chemistry B* 109 (**2005**) 958-967

[229] I. S. Kislina, G. G. Bikbaeva and M. I. Vinnik, "Kinetics of benzaldehyde disproportionation in aqueous KOH solutions", *Russian Chemical Bulletin* 25, Issue 12 (**1976**) 2475-2478.

[230] Q. Fu, T. Wagner, "Interaction of Nanostructured Metal Overlayers with Oxide Surfaces", *Surface science reports* 62 (**2007**) 431-498.

[231] L. R. Radovic and F. Rodriguez-Reinoso in *Chemistry and Physics of Carbon* 25, edithed by P. A. Thrower, Marcel Dekker Inc. **1997**.

[232] C. R. Henry, C. Chapon, J.M. Penisson, and G. Nihoul, "Structure of Small Palladium Particles studied by HRTEM", *Zeitschrift für Physik D Atoms, Molecules and Cluster* 12, Issue 1-4 (**1989**) I45-148.

[233] C. Altenhein, S. Giorgio, J. Urban and K. Weiss, "Structure of Supported Palladium, Silver and Gold Clusters", *Zeitschrift für Physik D Atoms, Molecules and Cluster* 19, Issue 4 (**1991**) 303-306.

[234] A. Renou and J. M. Penisson, "Direct Atomic Imaging in Small Multiply Twinned Palladium Particles", *Journal of Crystal Growth* 78, Issue 2, (**1986**) 357-368.

[235] H. Wu, Y. Yu, K. E. Gonsalves, M. J. Yacaman, "Incorporation of Polyhedral Oligosilsesquioxane in Chemically Amplified Resists to Improve their Reactive Ion Etching Resistance", *Journal of Vacuum Science Technologies B* 19 (**2001**) 851-855.

[236] Q. Zhang, J. Xie, J. Yang and J. Yang Lee, "Monodisperse Icosahedral Ag, Au, and Pd Nanoparticles: Size Control Strategy and Superlattice Formation", *ACS Nano* 3, Issue 1 (**2009**) 139–148.

[237] T. Strassner, "The Role of NHC Ligands in Oxidation Catalysis", *Topic in Organometallic Chemistry* 22 (**2007**) 125-148

[238] J. R. M. Humenik and W. D. Kingery, "Metal-Ceramic Interactions: III, Surface Tension and Wettability of Metal-Ceramic Systems", *Journal of the American Ceramic Society* 37, Issue 1(**2006**)18-23.

[239] V. Cortés Corberán, F. Cavani, G. Centi, S. Perathoner, G. Mestl and P. Ruiz, "Innovation in Selective Oxidation (ISO 2007), Turku, Finland, 26-31 August, 2007, *Catalysis Today* 141, Issues 3-4 (**2009**) 243-244.

Acknowledgements

At the end of the PhD the list of people to thank is very long.
Some colleagues have been sharing the working experience, transferring to me their knowledge, while some other have been sharing the friendship. Both are necessary support for getting the PhD to the end. I would like to dedicate these last pages for mentioning all the important people who contributed to the realization of this work.
I would like to express my special gratitude to *Prof. Robert Schlögl* for the opportunity to work within the department of Inorganic Chemistry at the Fritz Haber Institute. Under his teaching, project guidance and support, I improved my scientific knowledge.
The assessment of this thesis by the Technischen Universität Berlin is gratefully acknowledged: in particular I would like to thank Prof. Reinhard Schomäcker and the committee members of my doctorial board.
I would, also, like to thank my supervisors, *Dr. Dangsheng Su* for his advice and assistance during the development of the scientific work.
All the members of my group, "Microstructure", deserve special thanks for giving both a scientific contribution and moral support to the development of the project and the assessment of thesis.
In particular I thank *Dr. Di Wang* for performing the TEM investigations on the samples under study. I would like to thank him for the friendly welcome when I joined the group, for sharing the office in a comfortable atmosphere, the prompt help in any matter of the scientific discussion and practical TEM use.
I thank *Dr. Bernd Kubias* for the development and the maintaince of the laboratory set-up and the prompt technical support in the laboratory set-up.
I thank *Gisela Weinberg* for performing the SEM investigations on numerous samples and for teaching me how to operate the SEM with much patient and clarity.
I thank the members of the Surface Analysis group, especially *Dr. Axel Knop-Gericke* for allowing to measure at the Berliner Elektronenspeicherring-Gesellschaft für Synchrotronstrahlung and *Dr. Michael Hävecker,* for his help in measuring, teaching and assisting me in the analysis procedure of the data obtained.

I thank *Edith Kitzelmann* and *Dr. Raoul Naumann d´Alnoncourt* for teaching how to operate the TG machine, for discussion and for the special treatment they reserve to me in allowing the free use of the set up in the Thermo-analysis laboratory.

I thank *Dr. Sabine Wrabetz* for the prompt help in providing the calorimetry data and the clear discussion any time I needed.

I thank *Gisela Lorenz* for measuring the surface areas of the carbon samples.

I thank *Achim Klein-Hoffmann* for providing the XRF measurements and for his prompt help any time I have asked for.

In addition, I would like to thank some people for the contribution they gave to improving my knowledge by means of constructive discussion and criticism: *Dr. JP Tessonnier, Dr. Raoul Blume, Dr. Dirk Rosenthal, Dr. Jian Zhang, Dr. Olaf Timpfe, Dr. Johan Carlsson, Dr. Detre Techner, Prof. Manfred Bearns, Ali Rinaldi, Dr. Xi Liu and Dr. Xiaowei Chen.*

I thank *Prof. Laura Prati* for giving me the opportunity to perform some experiments in her laboratory at the University of Milano.

Dr. Alberto Villa for the collaboration and the experimental support in the part of the thesis dedicated to the catalytic application of the materials under investigation.

Within the ELCASS network, I would like to thank *Dr. Salvo Abate* and *Dr. Simona Caudo* for performing catalytic test on the samples prepared.

I am in debt with *Manfred E. Schuster* who has supported and helped me in the final assessment of the thesis and for "catching the mistake" and *Tom Cotter* and *Dr. Thomas Hansen* for help in improving the English style in some chapter of the thesis.

I would like to thank *Prof. Gabriele Centi* and *Prof. Siglinda Perathoner* at the University of Messina. They support and encourage me in this experience. I would like to thanks all the colleagues-friends at the FHI for their suggestions and support in matter of research, and also for the funny time we spent together.

Personal financial support and development programs from the International Max Planck Research School are also gratefully acknowledged.

The last words I want to dedicate to my family and specially my son. His patient and strength supported me along the way.